Behavior of Fiber-Reinforced Polymer Composite Piles Under Vertical Loads

PUBLICATION NO. FHWA-HRT-04-107

AUGUST 2006

U.S. Department of Transportation
Federal Highway Administration

Research, Development, and Technology
Turner-Fairbank Highway Research Center
6300 Georgetown Pike
McLean, VA 22101-2296

FOREWORD

A full-scale experiment on fiber-reinforced polymer (FRP) piles, including static and dynamic load tests, was conducted at a site provided by the Port Authority of New York and New Jersey at its Port of Elizabeth facility in New Jersey, with the cooperation and support of its engineering department and the New York State Department of Transportation. The engineering use of FRP-bearing piles required field performance assessment and development and evaluation of reliable testing procedures and design methods to assess short-term composite material properties, load-settlement response and axial-bearing capacity, drivability and constructability of composite piling, soil-pile interaction and load transfer along the installed piling, and creep behavior of FRP composite piles under vertical loads.

Gary L. Henderson
Director, Office of Infrastructure
Research and Development

NOTICE

QUALITY ASSURANCE STATEMENT

The Federal Highway Administration (FHWA) provides high-quality information to serve Government, industry, and the public in a manner that promotes public understanding. Standards and policies are used to ensure and maximize the quality, objectivity, utility, and integrity of its information. FHWA periodically reviews quality issues and adjusts its programs and processes to ensure continuous quality improvement.

Technical Report Documentation Page

1. Report No. FHWA-HRT-04-107	2. Government Accession No.	3. Recipient's Catalog No.
4. Title and Subtitle BEHAVIOR OF FIBER-REINFORCED POLYMER (FRP) COMPOSITE PILES UNDER VERTICAL LOADS		5. Report Date August 2006 6. Performing Organization Code
7. Author(s) Ilan Juran and Uri Komornik		8. Performing Organization Report No.
9. Performing Organization Name and Address Urban Utility Center Polytechnic University 6 Metrotech Center Brooklyn, NY 11201		10. Work Unit No. 11. Contract or Grant No. DTFH61-99-X-00024
12. Sponsoring Agency Name and Address Office of Infrastructure Research and Development Federal Highway Administration 6300 Georgetown Pike McLean, VA 22101-2296		13. Type of Report and Period Covered Final Report 2000-2003 14. Sponsoring Agency Code
15. Supplementary Notes Contracting Officer's Technical Representative (COTR): Carl Ealy, HRDI-06		

16. Abstract

Composite piles have been used primarily for fender piles, waterfront barriers, and bearing piles for light structures. In 1998, the Empire State Development Corporation (ESDC) undertook a waterfront rehabilitation project known as Hudson River Park. The project is expected to involve replacing up to 100,000 bearing piles for lightweight structures. The corrosion of steel, deterioration of concrete, and vulnerability of timber piles has led ESDC to consider composite materials, such as fiber-reinforced polymers (FRP), as a replacement for piling made of timber, concrete, or steel. Concurrently, the Federal Highway Administration (FHWA) initiated a research project on the use of FRP composite piles as vertical load-bearing piles.

A full-scale experiment, including dynamic and static load tests (SLT) on FRP piles was conducted at a site provided by the Port Authority of New York and New Jersey (PANY&NJ) at its Port of Elizabeth facility in New Jersey, with the cooperation and support of its engineering department and the New York State Department of Transportation (NYSDOT). The engineering use of FRP-bearing piles required field performance assessment and development and evaluation of reliable testing procedures and design methods to assess short-term composite material properties, load-settlement response and axial-bearing capacity, drivability and constructability of composite piling, soil-pile interaction and load transfer along the installed piling, and creep behavior of FRP composite piles under vertical loads.

This project includes:

- Development and experimental evaluation of an engineering analysis approach to establish the equivalent mechanical properties of the composite material. The properties include elastic modulus for the initial loading quasilinear phase, axial compression strength, inertia moment, and critical buckling load. The composite material used in this study consisted of recycled plastic reinforced by fiberglass rebar (SEAPILE™ composite marine piles), recycled plastic reinforced by steel bars, and recycled plastic reinforced with randomly distributed fiberglass (Trimax), manufactured respectively by Seaward International Inc., Plastic Piling, Inc., and U.S. Plastic Lumber.
- Static load tests on instrumented FRP piles. The instrumentation schemes were specifically designed for strain measurements. The experimental results were compared with current design codes as well as with the methods commonly used for evaluating the ultimate capacity, end bearing capacity, and shaft frictional resistance along the piles. As a result, preliminary recommendations for the design of FRP piles are proposed.
- Analysis of Pile Driving Analyzer® (PDA) and Pile Integrity Tester (PIT) test results using the Case Pile Wave Analysis Program (CAPWAP)[1] and the GRL Wave Equation Analysis of Piles program GRLWEAP[2] to establish the dynamic properties of the FRP piles. The PDA also was used to evaluate the feasibility of installing FRP piles using standard pile driving equipment. Pile bearing capacities were assessed using the CAPWAP program with the dynamic data measured by the PDA, and the calculated pile capacities were compared to the results of static load tests performed on the four FRP piles.

The dynamic and static loading test on instrumented FRP piles conducted in this project demonstrated that these piles can be used as an alternative engineering solution for deep foundations. The engineering analysis of the laboratory and field test results provided initial data basis for evaluating testing methods to establish the dynamic properties of FRP piles and evaluating their integrity and drivability. Design criteria for allowable compression and tension stresses in the FRP piles were developed considering the equation of the axial force equilibrium for the composite material and assuming no delamination between its basic components. However, the widespread engineering use of FRP piles will require further site testing and full-scale experiment to establish a relevant performance database for the development and evaluation of reliable testing procedure and design methods.

17. Key Words	18. Distribution Statement
Piles, fiber-reinforced polymers, static load tests, dynamic load tests	No restrictions. This document is available to the public through the National Technical Information Service, Springfield, VA 22161.

19. Security Classif. (of this report)	20. Security Classif. (of this page)	21. No. of Pages	22. Price
Unclassified	Unclassified	97	

Form DOT F 1700.7 (8-72) **Reproduction of completed pages authorized**

SI* (MODERN METRIC) CONVERSION FACTORS

APPROXIMATE CONVERSIONS TO SI UNITS

Symbol	When You Know	Multiply By	To Find	Symbol
		LENGTH		
in	inches	25.4	millimeters	mm
ft	feet	0.305	meters	m
yd	yards	0.914	meters	m
mi	miles	1.61	kilometers	km
		AREA		
in^2	square inches	645.2	square millimeters	mm^2
ft^2	square feet	0.093	square meters	m^2
yd^2	square yard	0.836	square meters	m^2
ac	acres	0.405	hectares	ha
mi^2	square miles	2.59	square kilometers	km^2
		VOLUME		
fl oz	fluid ounces	29.57	milliliters	mL
gal	gallons	3.785	liters	L
ft^3	cubic feet	0.028	cubic meters	m^3
yd^3	cubic yards	0.765	cubic meters	m^3
		NOTE: volumes greater than 1000 L shall be shown in m^3		
		MASS		
oz	ounces	28.35	grams	g
lb	pounds	0.454	kilograms	kg
T	short tons (2000 lb)	0.907	megagrams (or "metric ton")	Mg (or "t")
		TEMPERATURE (exact degrees)		
^oF	Fahrenheit	5 (F-32)/9 or (F-32)/1.8	Celsius	^oC
		ILLUMINATION		
fc	foot-candles	10.76	lux	lx
fl	foot-Lamberts	3.426	$candela/m^2$	cd/m^2
		FORCE and PRESSURE or STRESS		
lbf	poundforce	4.45	newtons	N
lbf/in^2	poundforce per square inch	6.89	kilopascals	kPa

APPROXIMATE CONVERSIONS FROM SI UNITS

Symbol	When You Know	Multiply By	To Find	Symbol
		LENGTH		
mm	millimeters	0.039	inches	in
m	meters	3.28	feet	ft
m	meters	1.09	yards	yd
km	kilometers	0.621	miles	mi
		AREA		
mm^2	square millimeters	0.0016	square inches	in^2
m^2	square meters	10.764	square feet	ft^2
m^2	square meters	1.195	square yards	yd^2
ha	hectares	2.47	acres	ac
km^2	square kilometers	0.386	square miles	mi^2
		VOLUME		
mL	milliliters	0.034	fluid ounces	fl oz
L	liters	0.264	gallons	gal
m^3	cubic meters	35.314	cubic feet	ft^3
m^3	cubic meters	1.307	cubic yards	yd^3
		MASS		
g	grams	0.035	ounces	oz
kg	kilograms	2.202	pounds	lb
Mg (or "t")	megagrams (or "metric ton")	1.103	short tons (2000 lb)	T
		TEMPERATURE (exact degrees)		
^oC	Celsius	1.8C+32	Fahrenheit	^oF
		ILLUMINATION		
lx	lux	0.0929	foot-candles	fc
cd/m^2	$candela/m^2$	0.2919	foot-Lamberts	fl
		FORCE and PRESSURE or STRESS		
N	newtons	0.225	poundforce	lbf
kPa	kilopascals	0.145	poundforce per square inch	lbf/in^2

*SI is the symbol for the International System of Units. Appropriate rounding should be made to comply with Section 4 of ASTM E380.
(Revised March 2003)

TABLE OF CONTENTS

LIST OF FIGURES

LIST OF TABLES

CHAPTER 1. INTRODUCTION

Piles are mainly used to support structures under lateral and vertical loads. Vertical load-bearing capacity of piles depends mainly on site conditions, soil properties, pile material properties, pile dimensions, and method of pile installation. Pile types can be divided into two categories, according to their method of installation.[3] The first category consists of driven piles, which displace and disturb the soil, and the second category consists of piles that are installed without soil displacement. Steel, precast concrete, wood, and fiber-reinforced polymer piles belong to the first category. In the second category, soil is removed by drilling, and concrete is cast in the borehole to form the pile.

Analytical methods[4] and several design codes[5,6,7] can be used to evaluate the axial pile capacity, end bearing, and shaft friction along the pile. Dynamic methods, based on pile driving measurements, can be used to predict the axial static capacity of driven piles and assess the drivability and durability of piles during installation.[8] However, before dynamic testing is conducted, several material properties and data must be determined; these include the pile length, cross-sectional area, specific weight, wave speed, and dynamic elastic modulus. The evaluation of the dynamic methods for predicting the load-set response and the ultimate static capacity of piles must be obtained by comparing the dynamic method analysis results and static load test (SLT) results. Considering the engineering use of fiber-reinforced composite piles, it is essential to perform the above-mentioned engineering testing procedure to evaluate the behavior of these piles under axial loads and to develop reliable design methods to assess the short- and long-term behavior of fiber reinforced polymer (FRP) composite piles.

In 1998, a waterfront rehabilitation project known as the Hudson River Park began. One goal was the replacement of up to 100,000 bearing piles for lightweight structures. The corrosion of steel, deterioration of concrete, and vulnerability of timber piles to the marine environment led the developer to consider composite materials with high degradation resistance, such as FRPs, as a replacement for pilings made of timber, concrete, or steel.

Concurrently, in 1998, the Federal Highway Administration (FHWA), with a long-term interest in the application of polymers in infrastructure, initiated a research project on the use of FRP pilings,

The main purpose of this current research was to address the need for a feasibility assessment of FRP composite bearing piles for highway and related facilities substructures, replacing traditional materials such as timber, concrete, or steel, specifically in the construction of waterfront structures in hostile marine environments. The engineering application of FRP may present competitive alternatives to conventional pile materials, due to the accelerated degradation of these conventional materials in aggressive environments (figures 1 and 2). Further, chemical treatment of wood pilings has become more difficult, due to the toxic nature of typical chemical treatments. State departments of transportation (DOT) facing major rehabilitation projects also have become interested in assessing the feasibility of using FRP composite bearing piles for infrastructure applications. To assess the feasibility of using FRP composite piles as vertical

load-bearing piles, laboratory tests and a full-scale experiment, including dynamic and static load tests on FRP piles were conducted.

Figure 1. Photo. Marine borers (Limnoria) attacking untreated timber piles that support many of New York's highways and harbor piers.[9]

Figure 2. Photo. Complete corrosion of steel H piles supporting a harbor pier (recently installed retrofit channels are already corroding).[9]

CURRENT STATE OF PRACTICE

Research on the engineering behavior of FRP piles has primarily been focused on these piles' performance under lateral loading as fender piles. In general, current research and applications of FRP piles have addressed:

- Mechanical behavior of FRP piles.
- Field observations and experimental demonstration projects on the engineering performance of FRP piles.

Mechanical Behavior of FRP Piles

The research conducted thus far has involved primarily laboratory tests on the mechanical behavior, flexural behavior, and buckling resistance of FRP pile materials.

Laboratory tests were performed on the Plastic Piling, Inc. (PPI), pile to determine the lateral flexural stiffness. The tested pile had a 38.7-centimeter (cm)- (15.25-inch-) diameter, and the steel reinforcement consisted of 16 25.4-millimeter (mm)- (1-inch-) diameter bars connected with a spiral. The free span between the two supports at both pile ends was 5.8 meters (m) (19 feet (ft)). During the testing, the load was applied cyclically at the middle of the free span. The test results show that loads exceeding 222 kilonewtons (kN) (50 kips) caused permanent deflections in the pile. At these loads, yielding of the steel bars was initiated, inducing slippage in the recycled plastic. The ultimate lateral load-bearing capacity was 311 kN (70 kips), at which point the pile underwent fully plastic behavior. Further, the pile's response was ductile up to this load, and the recycled plastic did not appear to crack during loading.

Two axial laboratory tests were performed to obtain the buckling loads of Lancaster Composite, Inc., piles.[10] The pile samples had diameters of 25.4 and 30.5 cm (10 and 12 inches) and lengths of 9 and 11 m (29.52 and 36.08 ft), respectively. Two loading cycles were applied to the 30.5-cm- (12-inch-) diameter pile sample to a maximum load of 2113 kN (475 kips) and 2228 kN (501 kips); the latter load caused the sample to experience failure. A third applied loading cycle caused this pile sample to buckle at 1841 kN (414 kips). The maximum applied load on the 25.4-cm- (10-inch-) diameter pile sample at which it experienced failure was 1392 kN (313 kips).

Reviewing the current state-of-practice within the framework of the current research with the manufacturers of the selected FRP piles illustrated the need for both laboratory and field axial loading tests to assess the engineering performance of these piles as axial load-bearing piles.

Field Observations Use and Experimental Demonstration Projects

The current state-of-practice related to the engineering use of FRP piles[9,11] indicates that FRP composite piles primarily have been used experimentally for fender piles, waterfront barriers, and bearing piles for light structures.[12-13]

Figure 3 shows fender piles manufactured by Lancaster Composite, Inc., in the U.S. Naval Submarine Base, San Diego, CA. Pier 5000, located in Point Loma at the southern tip of the San Diego Bay, is one of four major piers that serve as home base for several attack submarines.[14]

Figure 3. Photo. Fender piles in the U.S. Naval Submarine Base, San Diego, CA.

Figure 4 shows fender piles manufactured by PPI in U.S. Navy Pier 10 in San Diego, CA. This pier berths U.S. Navy vessels.

Figure 4. Photo. Fendering system in the U.S. Navy Pier 10, San Diego, CA.

Figure 5 shows the Nashville Avenue Marine Terminal at Port of New Orleans, LA. This terminal contains 40.6-cm (16-inch) SEAPILE® piles and a 30.5- by 30.5-cm (12- by 12-inch) SEATIMBER® fendering system that was manufactured by Seaward International in 1996.

Figure 5. Photo. Fendering system, Nashville Avenue Marine Terminal, Port of New Orleans, LA.

Figure 6 shows a floating dock project that consists of piles manufactured by American Ecoboard. The piles are 30.5 cm (12 inches) in diameter and 13.7 m (45 ft) long.

Figure 6. Photo. Floating dock project.

The current practice illustrates the lack of mechanical laboratory test results that would help assess engineering behavior of the FRP composite materials under axial loading, as well as the lack of SLT results and comparisons with dynamic experimental test results. The engineering applications of the FRP composite piles as bearing piles raise the following research and development (R&D) needs.

RESEARCH AND DEVELOPMENT NEEDS

The engineering use of FRP bearing piles requires assessing their field performance, as well as developing and evaluating reliable testing procedures and design methods to assess:

- Drivability and constructability of composite piling.
- Quality control during manufacturing and during pile installation.
- Load-settlement response and axial bearing capacity.
- Soil-pile interaction and load transfer along the installed piling.
- Short-term composite material properties.
- Creep and time effects on the long-term pile performance.
- Physical, mechanical, and chemical material degradation mechanisms.

To address these R&D needs and assess the feasibility of using FRP composite piles as vertical load-bearing piles, a full-scale experiment including dynamic and static load tests on FRP piles was conducted at a site provided by the Port Authority of New York and New Jersey (PANY&NJ) at their Port of Elizabeth facility in New Jersey. Figure 7 shows the Port of Elizabeth demonstration site. The full-scale experiment was conducted with the cooperation and support of the PANY&NJ engineering department and the New York State Department of Transportation (NYSDOT).

Figure 7. Photo. Port of Elizabeth demonstration site.

The scope of this demonstration project included:

- Manufacturing and instrumentation of selected FRP composite piles.
- Field and laboratory soil investigations.
- Laboratory tests on full-scale recycled plastic and composite material samples under axial compression loads.

- Driving and monitoring 11 FRP piles and a reference steel pile at Port of Elizabeth, NJ.
- Performing four full-scale SLTs at Port of Elizabeth, NJ.

To select the piles for this demonstration project, a team of experts prepared a request for qualification and disseminated the request to composite piling manufacturers; these manufacturers were invited to submit their qualifications and products for consideration. The items in the request for qualifications were: contact information, general description of piling system, material properties, drivability, durability, creep, quality assurance/quality control, experience, field records, and specimens. The selected FRP composite piles consisted of recycled plastic reinforced by fiberglass rebar (SEAPILE composite marine piles), recycled plastic reinforced by steel bars, recycled plastic with no reinforcement rebar, recycled plastic with randomly distributed fiberglass fibers (Trimax), and concrete-filled plastic shell manufactured, respectively, by Seaward International Inc., PPI, American Ecoboard, U.S. Plastic Lumber (USPL), and Lancaster Composite, Inc. Figure 8 indicates the locations of the pile manufacturers.

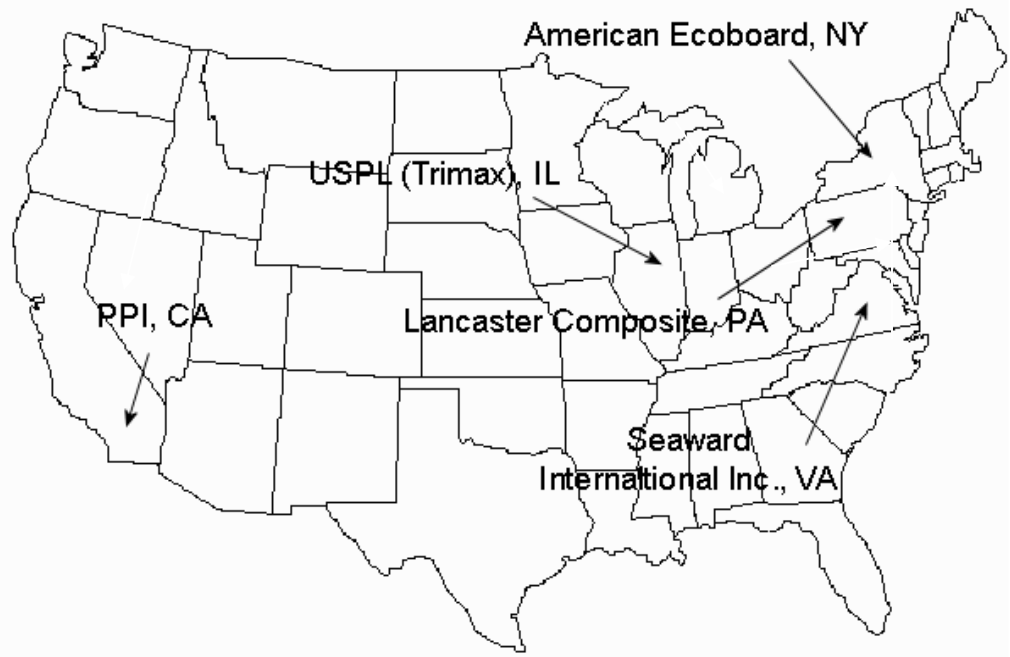

Figure 8. Illustration. Locations of pile manufacturers.

Pile instrumentation was performed at the manufacturing plants and included installing strain gauges at several levels in the piles. The manufacturers delivered these piles to the site, and the installation of the piles was conducted with the full support and cooperation of the manufacturers. All the manufacturers also attended the SLTs.

This research report summarizes the results of this full-scale experiment and the companion laboratory tests.

Chapter 2 presents an engineering analysis approach for establishing the equivalent mechanical properties of the composite material, including elastic modulus for the initial loading quasilinear phase, axial compression strength, inertia moment, and critical buckling load. The composite material used in this study consisted of recycled plastic reinforced by fiberglass rebar (SEAPILE composite marine piles), recycled plastic reinforced by steel bars, and recycled plastic reinforced with randomly distributed fiberglass (Trimax), manufactured by Seaward International Inc., PPI, and USPL, respectively.

Chapter 3 describes the results of the SLTs, along with the instrumentation schemes that were specifically designed for strain measurements in the FRP piles. The experimental results are compared with current design codes and with the methods commonly used for evaluating the ultimate capacity, end bearing capacity, and shaft frictional resistance along the piles. This engineering analysis leads to preliminary recommendations for the design of FRP piles.

In chapter 4, Pile Driving Analyzer® (PDA) and Pile Integrity Tester (PIT) test results were analyzed using the Case Pile Wave Analysis Program (CAPWAP)[1] and the GRL Wave Equation Analysis of Piles program (GRLWEAP)[2] to establish the dynamic properties of the FRP piles. The PDA also was used to evaluate the feasibility of installing FRP piles using standard pile driving equipment. Pile bearing capacities were assessed using the CAPWAP program with the dynamic data measured by the PDA, and the calculated pile capacities were compared with the results of SLTs performed on the four FRP piles.

Chapter 5 summarizes the main conclusions and recommendations of this project.

CHAPTER 2. MECHANICAL SHORT-TERM BEHAVIOR OF FRP COMPOSITE MATERIALS UNDER AXIAL COMPRESSION LOADS

The engineering use of FRP piles on a widespread basis requires developing and assessing reliable testing procedures and data analysis methods to establishing the material properties of the FRP composite piles. The results can be used to determine if these piles offer an alternative for deep foundation construction, especially in waterfront environments and aggressive soils.[15-20] To address these engineering issues and assess the mechanical behavior of these materials under axial compression loads, FRP composite material specimens were tested in the laboratory. The composite material used in this study consisted of recycled plastic reinforced by fiberglass rebar (SEAPILE composite marine piles), recycled plastic reinforced by steel bars, and recycled plastic reinforced with randomly distributed fiberglass (Trimax).

SEAPILE COMPOSITE FRP MATERIAL

In this chapter, the results of the laboratory compression tests performed on full-scale FRP composite material samples are discussed. The composite material used in this study consisted of recycled plastic reinforced by fiberglass rebar (SEAPILE composite marine piles) manufactured by Seaward International, Inc. The tests were performed on both the composite material specimens and each of the component materials, including the fiberglass bars and the recycled plastic.

The authors present an engineering analysis approach for establishing the equivalent mechanical properties of the composite material, including elastic modulus for the initial loading quasilinear phase, axial compression strength, inertia moment, and critical buckling load. The equivalent mechanical properties of the composite material are related to the mechanical properties of the component materials, assuming strain compatibility between the plastic and the fiber reinforcement during the axial compression loading. The results of this analysis illustrate that the main effect of the recycled plastic on the response of the composite material is to increase the buckling resistance. For the tested SEAPILE sample, the recycled plastic appears to prevent buckling of the bars but does not effectively prevent the peripheral disintegration of the fiberglass bars; therefore, it makes only a limited contribution to the axial compression strength of the composite material.

MECHANICAL PROPERTIES OF THE FRP COMPOSITE AND THE COMPONENT MATERIALS

SEAPILE composite marine piles consist of an extruded recycled plastic material reinforced by fiberglass bars (figure 9). The fiberglass rebar are manufactured in a pultrusion process, using fiberglass strands and polyester resin. The recycled plastic is composed mainly of high, medium, and low density polypropylene (HDPE, MDPE, and LDPE). It also contains a small percentage of polypropylene made from post-consumer waste (e.g., blow-molded bottles, plastic barrels, plastic bags, and TV cable jackets) and industrial waste (e.g., scrap pipes, telephone cables, film auto carpets, diaper trim, and auto insulation). The composite pile material consists of an inner core, foam that contains the fiberglass bars, and a skin. The core and the foam are made of

recycled plastic, and the skin is made of a solid polyethylene compounded with pigments, ultraviolet (UV) absorbers, and antioxidants. The skin is relatively smooth, giving a friction coefficient of approximately 0.21 (wet) and 0.22 (dry), when tested in accordance with American Society for Testing and Materials (ASTM) F489.[21,22]

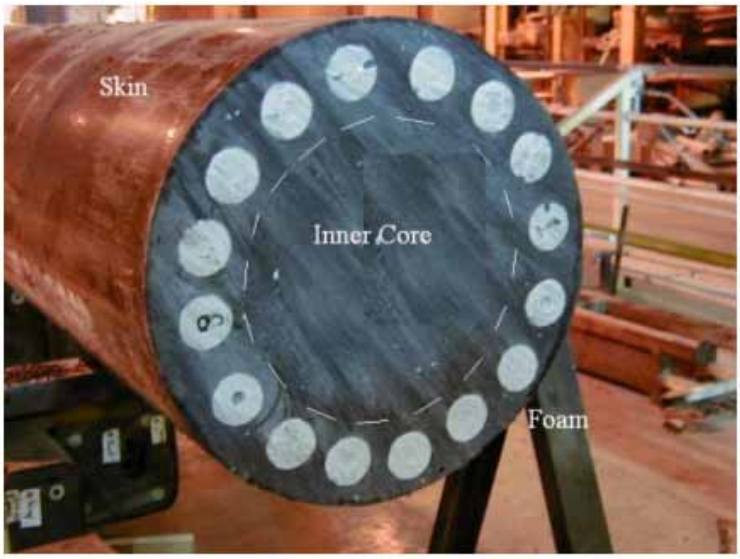

Figure 9. Photo. SEAPILE composite marine piles.

To establish the mechanical properties of the fiberglass bars, two axial compression tests were performed on 4.4-cm- (1.75-inch-) diameter bars. The maximum load reached 591.6 kN (133 kips) and, at this point, the bars displayed a brittle failure. Figure 10 illustrates the stress-strain relationship of the fiberglass bars. Young's modulus of the fiberglass bars is 1.6×10^7 kPa (2,320 ksi), and the maximum stress at failure is 3.63×10^5 kPa (52.6 ksi). Figure 11 shows the bar both before and after parts of it disintegrated upon test completion. It illustrates that the failure mechanism involves peripheral disintegration by peeling fiberglass from the 9-cm- (3.54-inch-) long bar, which did not buckle during the loading. Considering the elastic properties of the bar, its buckling free length was calculated (according to Euler's equation) to be 22.5 cm (8.9 inches) for this failure load.

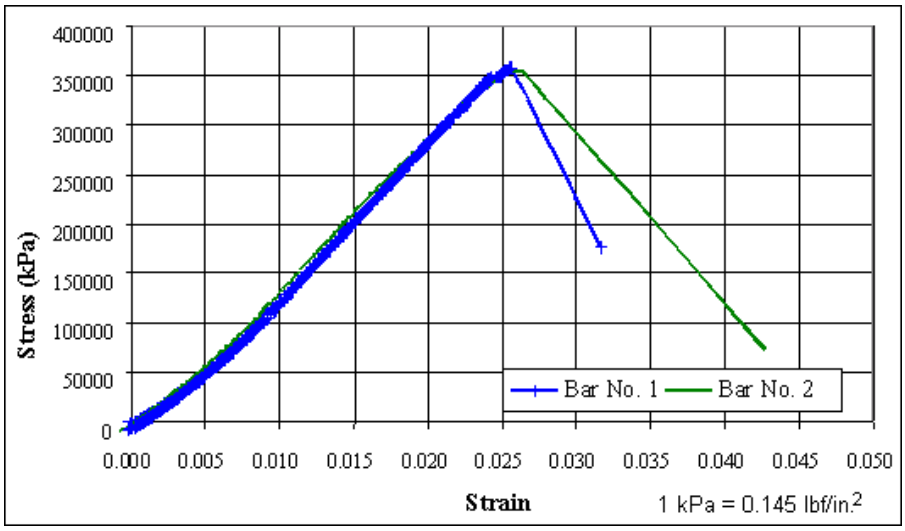

Figure 10. Graph. Stress-strain relationship of 4.4-cm (1.75-inch) fiberglass bars.

Figure 11. Photo. Fiberglass bar before axial compression test and disintegrated fiberglass parts.

Axial compression tests were performed on the recycled plastic foam. The sample's dimensions were 15.2 cm (6 inches) in diameter and 30.4 cm (12 inches) long. Figure 12 shows the stress-strain relationships of the recycled plastic material obtained for strain rates of 0.1 cm (0.04 inch) per minute (min) (0.33 percent/min) and for 0.025 cm (0.01 inch) per min (0.083 percent/min). The results illustrate that the nonlinear response of this recycled plastic material to the axial loading is strain-rate dependent. Young's modulus of the recycled plastic obtained for the linear portion of the stress-strain curves are 3 x 10^5 kilopascals (kPa) (43.5 ksi) and 1.93 x 10^5 kPa (28 ksi), respectively, for the strain rates of 0.33 percent/min and 0.083 percent/min. Figure 13 shows the axial stress versus radial strain relationships obtained for the recycled plastic foam.

The calculated Poisson's ratio is equal to 0.37, and the corresponding shear modulus value for the linear portion of the stress-strain curve is 109,489 kPa (15.9 ksi).

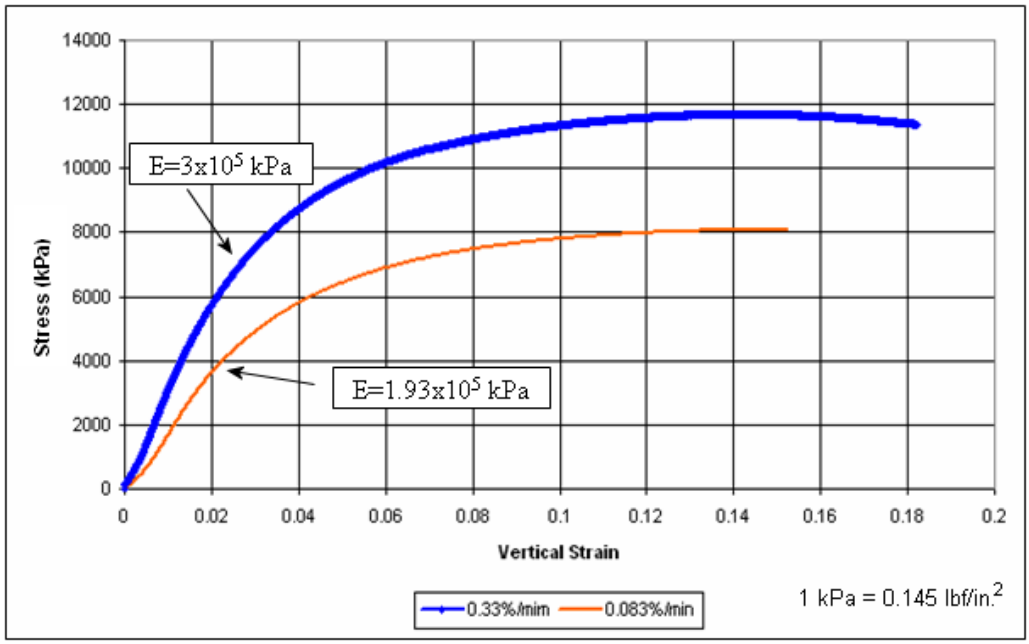

Figure 12. Graph. Stress-vertical strain relationship of SEAPILE pile recycled plastic.

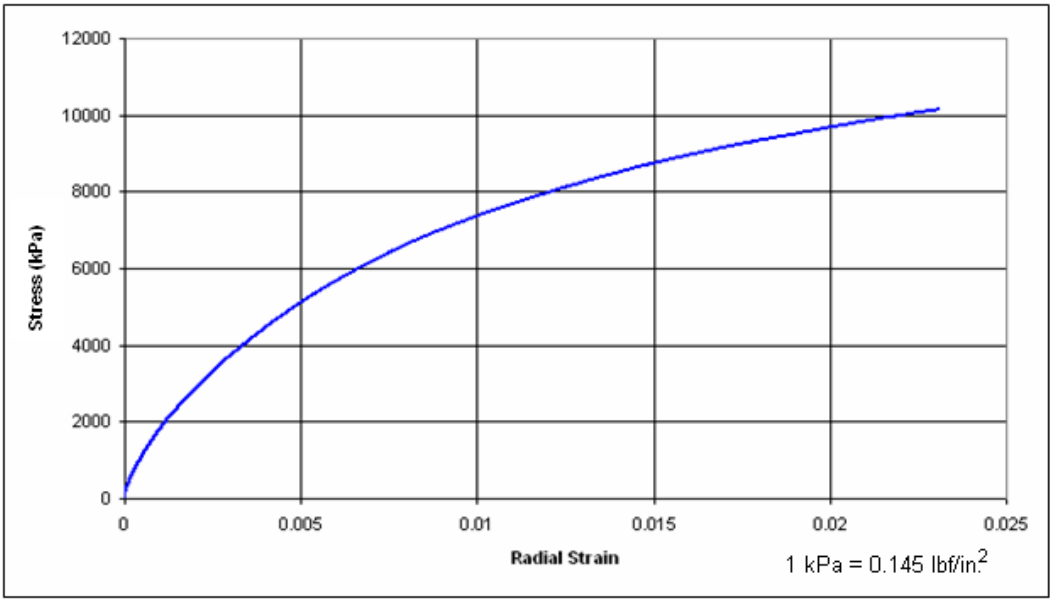

Figure 13. Graph. Stress-radial strain relationship of SEAPILE pile recycled plastic; rate 0.33 percent/min.

To establish the composite material properties, a compression axial test was performed on a SEAPILE pile sample 40.6 cm (16 inches) in diameter and 81 cm (32 inches) long. The sample

contained 16 fiberglass reinforcing rods each 7.6 cm (1.75 inches) in diameter. Because the top end of the sample was not leveled, Hydrostone® grout was placed between the pile upper surface and the loading steel plate. Three Geokon vibrating wire strain gauges were installed in the pile section on the fiberglass rebar, and four additional strain gauges were glued into holes on the outer skin. After the initial seating load was applied, the nominal loading rate was 0.25 mm (0.01 inch) per min.

Figure 14 shows the force-strain relationship obtained for the FRP composite material under the axial compression test. The maximum load reached was 9661 kN (2172 kips), at which point the sample experienced a brittle failure. The Young's modulus of the composite material was 3.38 x 10^6 kPa (490.23 ksi). Figure 15 shows the post-failure, full-scale sample section. It illustrates that the bars did not experience any buckling during loading, and only the upper section of the sample was damaged.

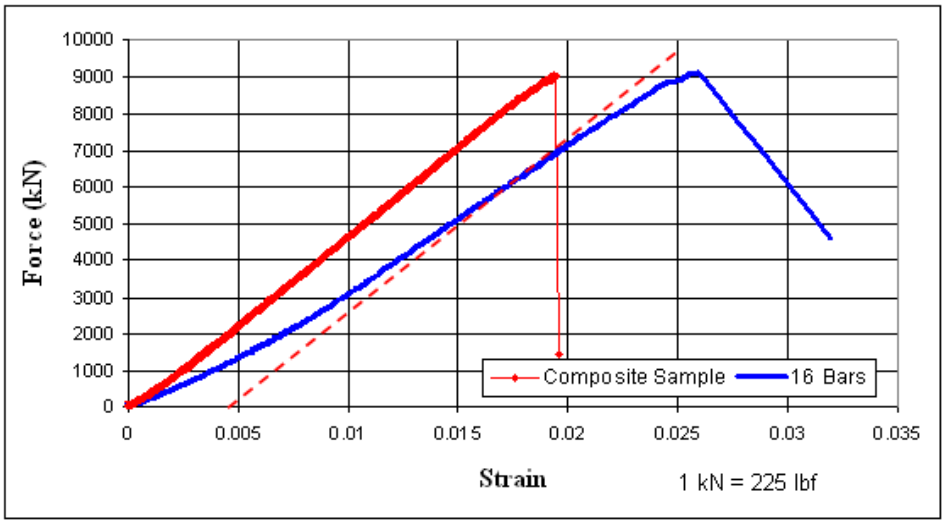

Figure 14. Graph. Force-vertical strain relationship of SEAPILE pile sample.

Figure 15. Graph. SEAPILE pile sample after axial compression test.

ENGINEERING ANALYSIS OF THE AXIAL COMPRESSION TEST ON THE COMPOSITE PILE SAMPLE

Elastic Modulus and Compressive Strength

The main purpose of the engineering analysis is to establish the equivalent mechanical properties of the composite material, including the elastic modulus for the initial loading phase, the axial compression strength, the inertia moment, and the critical buckling load. The equivalent material properties of the composite are related to the mechanical properties of the component materials, assuming strain compatibility between the plastic and the fiber reinforcement during the axial compression loading. The following assumptions were used in this analysis.

For the composite material section, the equilibrium equation under the applied load, F, can be written as in figure 16.

$$F = \sigma_c A_c = n\sigma_b A_b + \sigma_p A_p$$

Figure 16. Equation. Applied load F.

Where:
σ_c = Stress of the total section of the sample.
A_c = Cross-sectional area of the sample.
n = Number of bars in the composite section.
σ_b = Stress of the fiberglass bar.
A_b = Section area of the fiberglass bar.
σ_p = Stress of the plastic.
A_p = Section area of the plastic.

For axial compression, assuming elastic materials and strain compatibility between the plastic and the fiber reinforcement during the axial compression loading implies the relationships in figure 17.

$$E = \frac{\sigma_b}{E_b} = \frac{\sigma_p}{E_p} = \frac{\sigma_c}{E_c}$$

Figure 17. Equation. Young's modulus E.

Where:
E = Young's modulus.
E_b = Young's modulus of the bar.
E_p = Young's modulus of the plastic.
E_c = Young's modulus of the total section of the sample.

Solving the equations in figures 16 and 17 yields the equation in figure 18.

$$\frac{\sigma_c}{\sigma_b} = \frac{E_c}{E_b} = n\frac{A_b}{A} + \frac{E_p}{E_b}\left[1 - \left(\frac{nA_b}{A}\right)\right]$$

Figure 18. Equation. σ_c/σ_b.

By making the following substitutions,

$\alpha = nA_b/A$, where α is defined as the area replacement factor,
$\beta = E_p/E_b$, where β is the relative axial stiffness coefficient,
$A_c = A$, where A_c is the section area of the composite sample,

the equation in figure 18 can be written in the form of the equation in figure 19.

$$\frac{E_c}{E_b} = \alpha + \beta(1 - \alpha)$$

Figure 19. Equation. E_c/E_b.

The equation in figure 19 yields the equivalent Young's modulus of the composite material as a function of the replacement factor α, the relative stiffness coefficient β, and the Young's modulus of the fiberglass bar E_b. For the SEAPILE composite material, equation 4 yields an equivalent Young's modulus value of $E_c = 3.05 \times 10^6$ kPa (442.36 ksi); the difference between this calculated E_c value and the experimental result obtained for the composite sample $E_c = 3.38 \times 10^6$ kPa (490.23 ksi) is less than 10 percent of the experimental value.

The equivalent shear modulus, G_c, of the composite material can be calculated from the theory of elasticity assuming that the FRP composite is an isotropic elastic material. This assumption does not take into account the anisotropy of the composite material induced by the preferential direction of the fiber reinforcement. Accordingly the equivalent shear modulus, G_c can be calculated by the equation in figure 20.

$$G_c = E_c/2(1+\upsilon_c) \qquad \upsilon_c = \upsilon_p$$

Figure 20. Equation. G_c.

Where:
υ_c and υ_p are the Poisson's ratio values of the composite material and its recycled plastic component, respectively.

The equivalent compression strength, R_c, of the composite material is given by the equation in figure 21.

$$R_c/R_b = \alpha + \eta(1-\alpha)$$

Figure 21. Equation. R_c/R_b.

Where:
$\eta = R_p/R_b$, the compression strength ratio of the component materials.
R_p = Compression strength of the fiberglass bar.
R_b = Compression strength of the recycled plastic mobilized at the failure strain of the fiberglass bar (ε = 2.6 percent).

For the SEAPILE composite material, the equation in figure 21 yields an equivalent compression strength $R_c = 7.4 \times 10^4$ kPa (10.73 ksi); the difference between this calculated R_c value and the experimental result obtained for the composite sample, $R_c = 6.8 \times 10^4$ kPa (9.86 ksi), is about 8.8 percent of the experimental value.

The effect of the recycled plastic on the behavior of the composite material can be analyzed considering the failure load factor (FLF), defined as the ratio of the failure load F_c of the composite material to the failure load nF_b, defined as the failure load of the bar multiplied by the number of bars in the composite material. The FLF can be calculated by the equation in figure 22.

$$FLF = \frac{F_c}{nF_b} = \frac{E_c A_c}{E_b n A_b} = 1 + \beta\left[\frac{1}{\alpha} - 1\right]$$

Figure 22. Equation. FLF.

Figure 14 illustrates the experimental relationships between the applied axial load and the axial strain for the group of 16 bars and the composite material. The results show that, at failure by axial compression, the recycled plastic has only a limited effect on the load-bearing capacity of the composite material. The equation in figure 22 yields an FLF of 1.068, which is quite consistent with the experimental results (FLF = 1).

Moment of Inertia

Bending moment, assuming elastic materials and strain compatibility between the plastic and the fiber reinforcement during bending, implies the relationships in figure 23.

$$\frac{M}{y''} = E_c I_c = E_p I_p + E_b \sum I_b * \left(1 - \frac{E_p}{E_b}\right)$$

Figure 23. Equation. Bending moment M.

Where:

M = Bending moment.

y″ = Second derivative of the displacement variation with depth.

ΣI_b = Sum of the moments of inertia of all the fiberglass bars with respect to the axis of symmetry of the composite material section.

I_p = Moment of inertia of the recycled plastic section with respect to the axis of symmetry of the composite material section.

The moment of inertia (I_c) of the composite material can be derived by rearranging the equation in figure 23 to give the equation in figure 24.

$$I_c = \left[\frac{E_b}{E_c}\right]\left[\frac{E_p}{E_b} I_p + \sum I_b * \left(1 - \frac{E_p}{E_b}\right)\right]$$

Figure 24. Equation. Moment of inertia $I_c(1)$.

By substituting β for E_p/E_b, the equation in figure 24 can be rewritten as the equation in figure 25.

$$I_c = \left[\frac{E_b}{E_c}\right]\left[\beta I_b + \sum I_b * (1 - \beta)\right]$$

Figure 25. Equation. Moment of inertia $I_c(2)$.

The relative inertia moment coefficient λ is given by the equation in figure 26.

$$\lambda = I_p / \sum I_b$$

Figure 26. Equation. Relative inertia moment coefficient λ.

Preceding equations can be combined and rearranged to give the equation in figure 27.

$$I_c / \sum I_b = \left[1 + \beta(\lambda - 1)\right] / \left[\alpha + \beta(1 - \alpha)\right]$$

Figure 27. Equation. $I_c/\Sigma I_b$.

Critical Buckling Force

The critical buckling force, P_{cr}, can be calculated according to Euler's equation (figure 27).:

$$P_{cr} = \frac{\pi^2 EI}{l^2}$$

Figure 28. Equation. Critical buckling force P_{cr}.

Where:
E = Young's modulus.
l = Length of the bar.
I = Moment of inertia.

For the fiberglass bar sample (E = 1.6 x 10^7 kPa (2,320.6 ksi); l = 9 cm (3.5 inches); I = 19.16 cm^4 (0.46 $inch^4$)), the equation in figure 28 yields the calculated critical buckling load of P_{cr} = 3,736 kN (839.8 kips). For a given fixed boundary condition at the top and at the bottom of the bar, k = 0.5, P_{cr} = 1,868 kN (419.9 kips). This buckling load exceeds the compression failure load of 591.6 kN (133 kips), causing the bar to collapse by peripheral disintegration.

The equivalent critical buckling load, P_{cr}, of an axially loaded bar confined in a low shear modulus material such as the recycled plastic is given by the equation in figure 29.[23]

$$P_{cr} = \frac{P_{cr}^o}{1 + \frac{P_{cr}^o}{G_c A}}$$

Figure 29. Equation. P_{cr} of an axially loaded bar.

The term P^o_{cr} in figure 29 is the equivalent critical buckling load calculated for the composite material according to Euler's equation (figure 30).

$$P_{cr}^o = \frac{\pi^2 E_c I_c}{l^2}$$

Figure 30. Equation. Equivalent critical buckling load for composite material.

The terms E_c and I_c in figure 30 are the elastic Young's modulus and the moment of inertia of the composite material, respectively.

The effect of the recycled plastic on the buckling failure load of the composite material can be analyzed by considering the critical buckling load factor (BLF), defined as the ratio of the critical buckling load P^c_{cr} of the composite material to the critical buckling load of the bar, multiplied by the number of bars in the composite material ΣP^b_{cr}. The BLF can be calculated by the equation in figure 31.

$$BLF = \frac{P_{cr}^{c}}{\sum P_{cr}^{b}} = \frac{E_c}{E_b}\frac{I_c}{nI_b}\left[\frac{1}{1+\frac{P_{cr}^{o}}{G_c A}}\right]$$

Figure 31. Equation. Critical buckling load factor BLF.

Substituting $\lambda_o = I_c / n\ I_b$ as a relative inertia moment index, the equation in figure 31 can be written as the equation in figure 32.

$$\frac{P_{cr}^{c}}{\sum P_{cr}^{b}} = \lambda_o(\alpha + \beta(1-\alpha))\left[\frac{1}{1+\frac{P_{cr}^{o}}{G_c A}}\right]$$

Figure 32. Equation. Critical buckling load decomposed.

Figure 16 illustrates the variation of the critical buckling load with the length of the sample for the composite material and for the group of fiberglass bars. The critical buckling load of the composite material is calculated according to the equations in figures 29 and 30. The critical buckling load for the group of 16 bars is calculated from the sum of the buckling loads of the individual bars: $\Sigma P^b_{cr} = n*P^b_{cr}$, where the critical buckling load of each bar, P^b_{cr}, is calculated from the equation in figure 28. The results show that the recycled plastic has a significant effect on the critical buckling load.

The failure load of the sample is equal to the smaller load that can cause either buckling or peripheral disintegration of the pile matrix. It was observed that, for the failure load of 9,661 kN (2,172 kips), the composite material sample (40 cm (16 inches) in diameter and 80 cm (32 inches) in height) did not experience any buckling failure (figure 15). As illustrated in figure 33, under a critical buckling load which is equal to the compressive strength of the group of 16 bars, the calculated maximum free length is about 22 cm (8.7 inches), which is significantly smaller than the height of the composite sample. However, the maximum free length of the composite sample calculated from the equation in figure 29 for the composite material reaches about 150 cm (59 inches), illustrating that the recycled plastic appears to prevent buckling of the bars in the composite material. The critical BLF calculated from the equation in figure 31 for the composite sample reaches about 38, indicating the significant effect of the recycled plastic on the buckling resistance of the composite material.

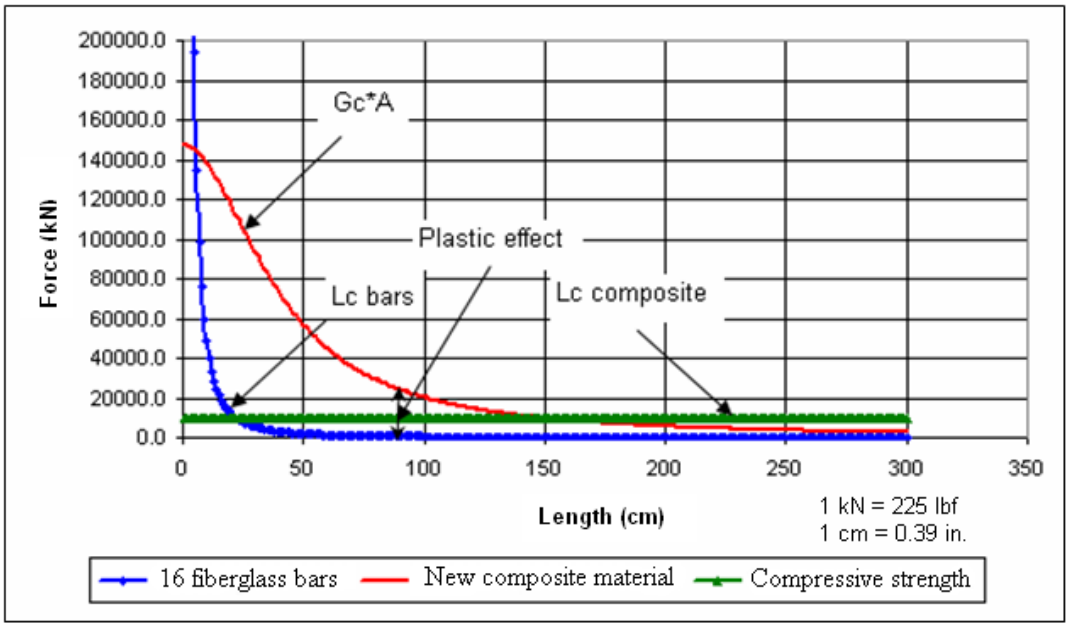

Figure 33. Graph. Buckling force versus length for SEAPILE pile sample and 16 fiberglass bars.

PPI PILES

PPI manufactures recycled plastic piles reinforced by steel bars (figure 34). The company obtains recycled plastic pellets from recycling firms that acquire their plastic from curbside collection and industrial waste. HDPE and LDPE are required to develop a cohesive and durable product. The formulation of the recycled plastic includes a mixture of approximately 30 percent HDPE and 70 percent LDPE. Carbon black material is added to the mix at the rate of 4 percent by weight of plastic to serve as a UV inhibitor. Celogen AZ130® is added at the rate of 0.5 percent by weight of plastic to encourage uniformity of porosity and minimize the size of voids. Calcium carbonate can be added to the mix to make the plastic material heavier when it is necessary to avoid a product that is lighter than water. The outer surface of the recycled plastic yields a material friction coefficient of approximately 0.20 (wet) and 0.22 (dry), when tested in accordance with ASTM F489.[24]

Figure 34. Photo. PPI pile.

To establish the composite material properties, a compression axial test was performed on a PPI pile sample containing 16 steel reinforcing rods of 2.54-cm (1.0-inch) nominal diameter. The sample was 38.7 cm (15.25 inches) in diameter and 80 cm (31.5 inches) long. The results illustrate that this composite material has a behavior similar to that of steel (figure 35) and yields a compressive strength of 45,190 kPa (6.55 ksi). The Young's modulus of the composite material obtained for the linear portion of the stress-strain curve is 7.84 x 10^5 kPa (113.7 ksi).

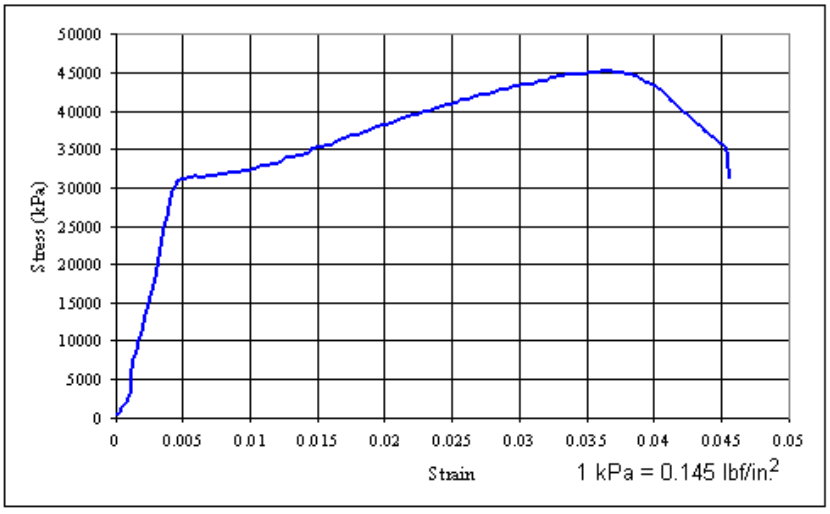

Figure 35. Graph. PPI pile—stress-strain relationship.

TRIMAX STRUCTURAL PLASTIC MATERIAL

Trimax structural plastic lumber material consists of recycled plastic, fiberglass, and selected additives (figure 36). The plastic raw material used in Trimax is derived from post-consumer bottle waste such as milk and detergent bottles. This material is compounded into a consistent, reinforced plastic timber product using reactive compatibilizers, which create a stable plastic/fiber matrix.[25]

Figure 36. Photo. Trimax pile.

Axial Compression Tests on the Trimax Pile Recycled Plastic

Axial compression tests were performed on the Trimax pile recycled plastic. The sample's dimensions were 25.4 cm (10 inches) in diameter and 50.8 cm (20 inches) long. Figure 37 shows the vertical stress-strain relationships obtained for several strain rates. The results illustrate that the nonlinear response of this recycled plastic material to the axial loading is strain-rate dependent. The Young's modulus of this material, obtained for the linear portion of the stress-strain curve at the strain rate of 1.7 mm (0.07 inch) per min (0.33 percent/min), is 370,000 kPa (53.7 ksi). Figure 38 shows the axial compression stress versus radial strain relationships obtained for strain rates of 0.33 percent/min. Poisson's ratio calculated for this strain rate at 1000 kPa (0.145 ksi) is equal to 0.35, and the corresponding shear modulus value for the linear portion of the stress-strain curve is 1.37×10^5 kPa (19.9 ksi).

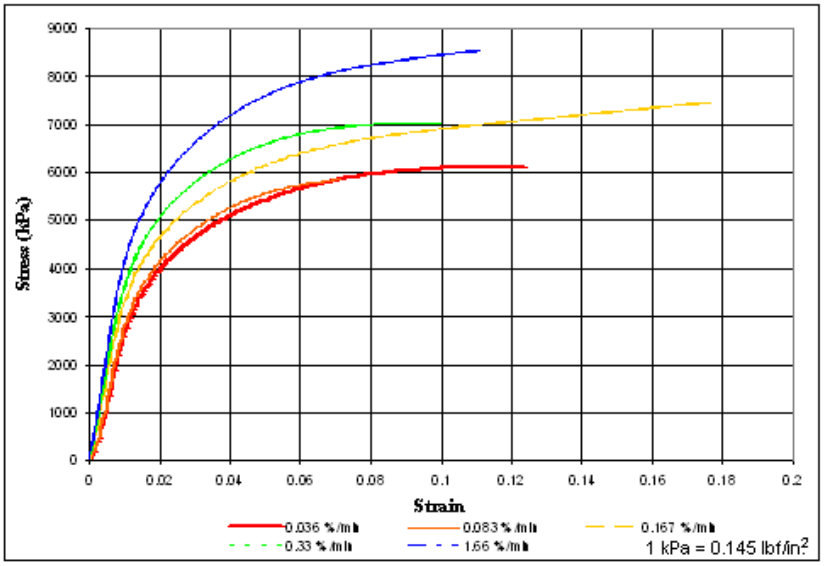

Figure 37. Graph. Trimax pile—vertical stress-strain curves at different rates.

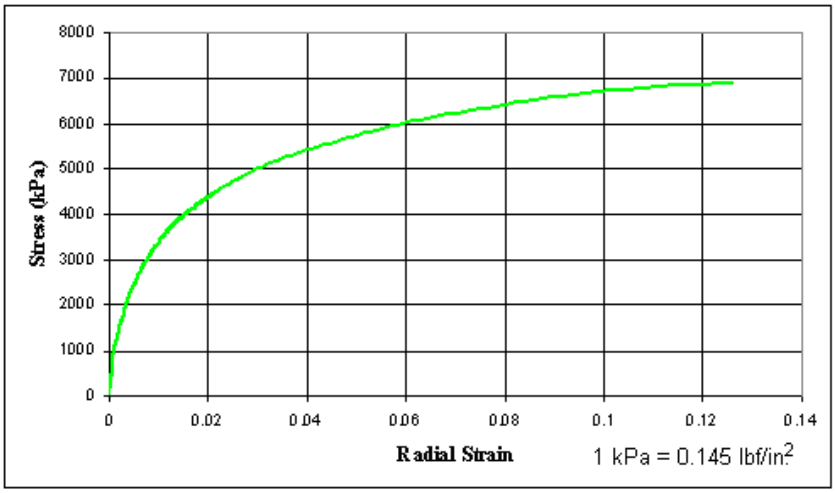

Figure 38. Graph. Trimax pile—vertical stress-lateral strain curve; strain rate 0.33 percent per min.

Table 1 summarizes the comparison between the predicted and experimental values of the SEAPILE composite material properties.

Table 1. Material properties—test results and model calculations.

Material Property	Recycled Plastic	16 Fiberglass Bars	Composite Material Test Results	Model Prediction
Elastic modulus, kPa (ksi)	300,000 (43.5)	1.6×10^7 (2,320)	3.38×10^6 (490.23)	3.05×10^6 (442.36)
Compressive strength, kPa (ksi)	1.169×10^4 (1.69)	3.63×10^5 (51.9)	6.8×10^4 (9.86)	7.4×10^4 (10.73)
Moment of inertia, m^4 ($inch^4$)	1.6×10^{-3} (3,844)	118.98×10^{-6} (285.8)	–	0.77×10^{-3} (1850)
Critical buckling load, kN (kips) (80 cm) sample	–	757 (170)	9661 (2172) (no buckling observed)	29,066 (6,534)

CHAPTER 3. BEHAVIOR OF FRP COMPOSITE PILES UNDER VERTICAL LOADS

The engineering use of FRP piles on a widespread basis requires developing and evaluating reliable testing procedures and design methods that will help evaluate the load-settlement curve of these composite piles and their static bearing capacity. In particular, full-scale loading tests on FRP piles must be conducted to evaluate the behavior of these types of piles under vertical loads. The main objective of the study described in this chapter was to conduct a full-scale experiment (including dynamic and static load tests) on FRP piles, to address these engineering needs, and assess the feasibility of using FRP composite piles as vertical load-bearing piles. The full-scale experiment, described in this chapter, was conducted in a selected site of the Port Authority of New York and New Jersey at Port of Elizabeth, NJ. It included dynamic pile testing and analysis on 11 FRP driven piles and a reference steel pile, as well as SLTs on four FRP composite piles. Figure 39 shows the Port of Elizabeth demonstration site.

In this chapter, the results of SLTs are presented along with the instrumentation schemes that were specifically designed for strain measurements in the FRP piles. The experimental results are compared with current design codes and with the methods commonly used for evaluating the ultimate capacity, end bearing capacity, and shaft frictional resistance along the piles. This engineering analysis leads to preliminary recommendations for the design of FRP piles.

Figure 39. Photo. Port of Elizabeth demonstration site.

PILE MANUFACTURING AND INSTRUMENTATION

The FRP test piles were manufactured and instrumented to allow for the measurement of the load and settlements at the pile top, the displacements of the reaction dead load, and the axial strain at several levels in the pile to obtain the axial force variation with depth along the piles. The pile top settlements were measured by four linear variable differential transformers (LVDTs) (Model 10,000 hollow cylinder apparatus (HCA)), and the dead load displacements were measured by a LVDT (Model 5,000 HCA). Additional digital dial gauge indicators were also used to measure displacements. Vibrating wire and foil strain gauges were used to determine the axial force at several levels in the pile. The foil strain gauges were connected to a National Instruments data acquisition system, and the instrumentation of the pile head and the loading system was connected to a Geokon data acquisition system. The instrumentation and data acquisition systems (figures 40 through 42) allowed for online monitoring during the SLTs of: the pile top displacement versus the applied load; the applied load; and the stresses at different levels in the pile.

The manufacturers calibrated data acquisition with the LVDTs, the load cell, and the strain gauges before performing the field tests. All the strain gauges were installed in the FRP pile during the manufacturing process before the piles were delivered to the site. Pile manufacturing methods and instrumentation details are briefly described in the following paragraphs.

Figure 40. Photo. Equipment used in the in-load tests.

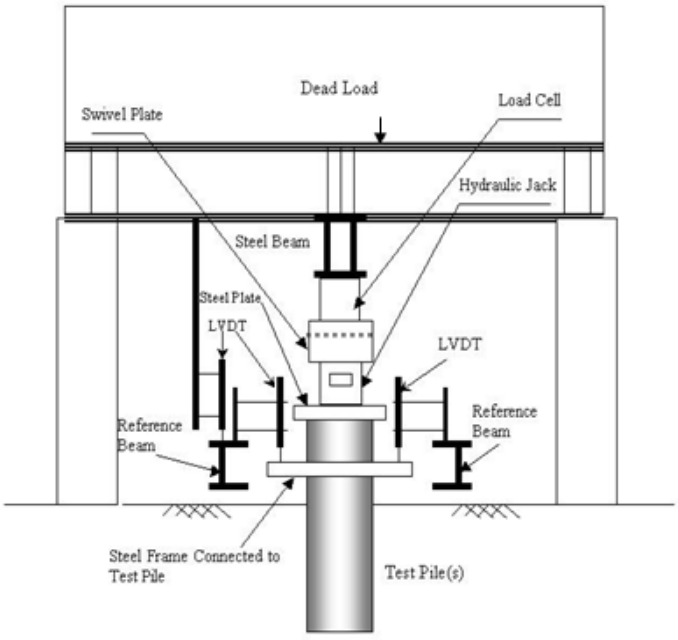

Figure 41. Illustration. Schematic of the equipment used in the in-load tests.

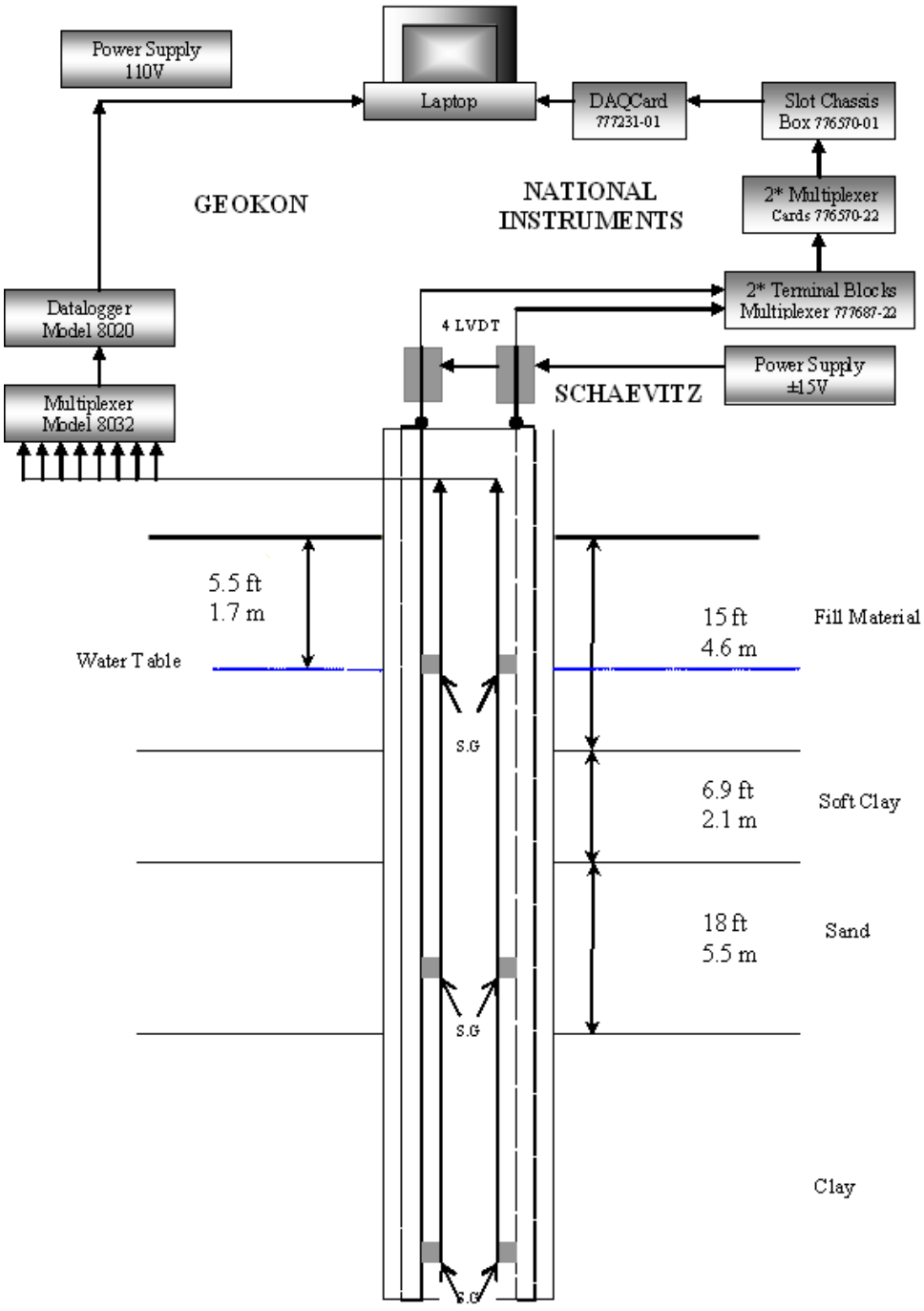

Figure 42. Illustration. Data acquisition system.

Lancaster Composite, Inc.

Lancaster Composite, Inc., piles are composed of a hollow FRP pipe that is filled before installation with an expanding concrete and is coated with a durable corrosion-resistant coating layer (figure 43). The hollow pipe is produced from unsaturated polyester or epoxy reinforced with reinforcement rovings (E-glass) and appropriate filler material to form a rigid structural support member. E-glass is incorporated as continuous rovings and is set in resin under pressure during the fabrication process. Table 2 shows the design material properties.

Table 2. Selected design material properties (published by Lancaster Composite, Inc.).

Material Properties—FRP Shell for 16.5-inch outer diameter	
Young's modulus—axial (tensile) (psi)	2.79×10^6
Tensile strength—axial direction (psi)	50,400
Young's modulus—axial (compression) (psi)	1.9×10^6
Compressive strength—axial direction (psi)	30,000
Tensile strength—hoop direction (psi)	35,000
Elastic modulus—hoop direction (psi)	4.5×10^8
Material Properties—Concrete Core for 16.5-inch outer diameter	
Concrete property (28 days)—f_c prime (psi)	6,000
Expansion—confined permanent positive stress (psi)	25

1 psi (lbf/in^2) = 6.89 kPa
1 inch = 2.54 cm

The precast FRP composite pile (C40) is produced in two stages. The first stage consists of fabricating the hollow FRP tube, which is produced using the continuous filament winding method. The tube is given its final protective coating in the line during the winding process at the last station of the production line. During the second stage of the process, the tube is filled with an expanding cementious material at the plant.

Two vibrating wire strain gauges (model 4200VW) are installed 0.25 m (9.84 inches) from the bottom of the pile. The strain gauges were installed in the piles before the tube was filled with the cementious material. The installation procedure included casting strain gauges in the concrete (figure 43), inserting the strain gauge wires into the 1.9-cm- (0.75-inch-) diameter hollow fiberglass pipe, and locating the pipe in the center of the hollow FRP tube using steel spacers. At the end of the pile manufacturing process, concrete was cast into the FRP tube. To detect any zero drifts, strain readings were taken before strain gauge installation, after casting the concrete, before pile driving, and before performing the SLT.

Table 3 shows compressive laboratory test results performed on two samples that were taken from a concrete pile. The compressive strengths of the concrete after 28 days were 41,693 kPa (6,047 psi) and 43,609 kPa (6,325 psi), which are greater than the manufacturer's strength recommended values, by 0.8 percent and 5.4 percent, respectively.

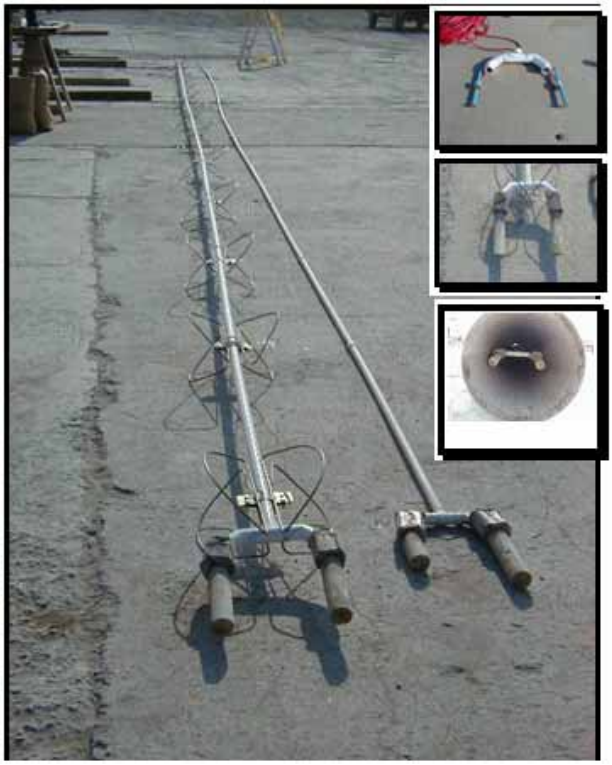

Figure 43. Photo. Strain gauges installation in pile of Lancaster Composite, Inc.

Table 3. Compression strength testing of the concrete.

Material Properties—Concrete Core for 16.5-inch O.D.		
Test Number	**Compression after 7 days, kPa (psi)**	**Compression after 28 days, kPa (psi)**
1	36,756 (5331)	43,609 (6325)
2	35,660 (5172)	41,693 (6047)

1 inch = 2.54 cm

PPI

PPI piles are composed of steel reinforcing bars that are welded to a spiral-reinforcing cage and encapsulated with recycled polyethylene plastic (figure 44). The manufacturing process uses a steel mold pipe and involves a combination of extrusion and injection molding, into which the plastic marine products are cast. Mold pipes for plastic pilings range in diameter from 20.3 cm (8 inches) to 121.9 cm (48 inches). The structural steel cage core is held at the center of the molded pile while the plastic is injected into the mold (figure 44). A centering apparatus is connected to the steel rebar cage so that it can be removed after the pile has been formed. Plastic is then fed into the extruder hopper through a mixing chamber, ensuring mixing with the carbon black material and the Celogen AZ130. The extruder temperature is set at 308 °C (525 °F). Plastic pressures range from 1.38 to 3.45 kPa (200 to 500 psi) throughout the mold while the plastic is being injected. After the extrusion process is complete, the mold is dropped into chilled water for a cooling period of several hours.

Figure 44. Photo. Vibrating and foil strain gauges attached to steel cage in PPI pile.

The strain gauges were installed in the piles at the company site before extruding the plastic material; therefore, the gauges and the cables had to resist high temperatures. Six vibrating wire strain gauges (model 4911-4HTX) were installed in the pile at 0.8 m (2.6 ft), 9.8 m (32.1 ft), and 18 m (59 ft) from the bottom. Two strain gauges were installed at each level. The strain gauges were attached to steel rebar and calibrated. Two additional foil strain gauges (model N2K-06-S076K-45C) were installed 0.8 m (2.6 ft) from the bottom of the pile. The foil strain gauges were attached to the steel rebar and sealed with epoxy glue to avoid moisture penetration. They then were assembled as a half-bridge and connected with the strain gauges located outside of the pile, creating a full Winston bridge. The installation process in the factory included welding the rebar with the strain gauges to the pile's steel reinforcement cage (figure 44). The strain gauges were connected to the data acquisition system to collect data before welding them to the steel cage, before extruding the hot plastic, and after cooling the pile down to detect any drifts of the zero reading. At the Port of Elizabeth, NJ, site, strain readings also were taken before pile driving and conducting the SLT.

SEAPILE Piles

SEAPILE composite marine piles contain fiberglass bars in recycled plastic material (figure 45). The manufacturing process of the SEAPILE composite marine piles consists of extruding the plastic material around the fiberglass bars using a blowing agent to foam to a density of 6.408 kN/m^3 (40 lbf/ft^3) at 217.5 °C (380 °F) and adding a black color for UV protection. The extrusion is followed by cooling the product and cutting to the desired length.

Figure 45. Photo. Vibrating and foil strain gauges attached to SEAPILE composite marine pile.

The strain gauges were installed at the factory after the pile was manufactured and the recycled plastic was cooled. Six vibrating wire strain gauges (model VK-4150)—two at each level—were installed in the pile 1 m (3.3 ft), 9.5 m (31.2 ft), and 18 m (59 ft) from the bottom. Two additional foil strain gauges (model EP-O8-250BF-350) were installed 1 m (3.3 ft) from the bottom of the pile. Each of these foil strain gauges was attached to plastic pieces by heating and sealing, using epoxy glue to avoid moisture penetration. The strain gauges were assembled to create a full Winston bridge. The installation procedure for the gauges included routing two grooves in the plastic material along the pile, providing an access to two rebar, and attaching the strain gauges and covering them by PC7 heavy duty epoxy paste. The wires in the groove were covered using hot, liquefied, recycled plastic.

The strain gauges were connected to the data acquisition system, and data were collected before connecting the gauges to the pile and after covering them with epoxy paste to detect any drift of the zero reading. Onsite strain readings also were taken before pile driving and before performing the SLT.

FIELD TESTING PROGRAM

Full-Scale Experiment

Figure 46 shows the schematic drawing of the Port Elizabeth site, and table 4 provides the testing program details, including pile structure, diameter, length, and the pile driving order. The test pile types included:

- A reference steel closed-end pipe pile, 40.6 cm (16 inches) in diameter with a wall 1.27 cm (0.5 inch) thick; the pile was 20 m (65.6 ft) long and furnished with a 45-degree conical shoe; the pipe pile was manufactured using A252, Grade 2 steel, which has a minimum yield strength of 241,316.5 MPa (35 ksi).

- Two Lancaster Composite, Inc., piles, 41.9 cm (16.5 inches) in diameter and 18.8 m (61.7 ft) long, and a spliced pile with a total length of 29.6 m (97 ft) that was driven to refusal.
- Three PPI piles, 38.7 cm (15.25 inches) in diameter and 19.8 m (65 ft) long; these piles were constructed from solid polyethylene and reinforced with 16 steel reinforcing bars, each 2.54 cm (1 inch) in diameter.
- Three SEAPILE piles, 20 m (65.6 ft) long and 42.5 cm (16.75 inches) in diameter; these piles were solid polyethylene reinforced with 16 fiberglass bars, each 4.4 cm (1.75 inches) in diameter.
- Two American Ecoboard solid polyethylene piles; these piles were delivered in 6.1-m (20-ft) sections and were 41.9 cm (16.5 inches) in diameter; the total length of one pile, after splicing, was 11.8 m (38.75 ft); the splice was made with steel pipe sections connected with bolts through the pile.

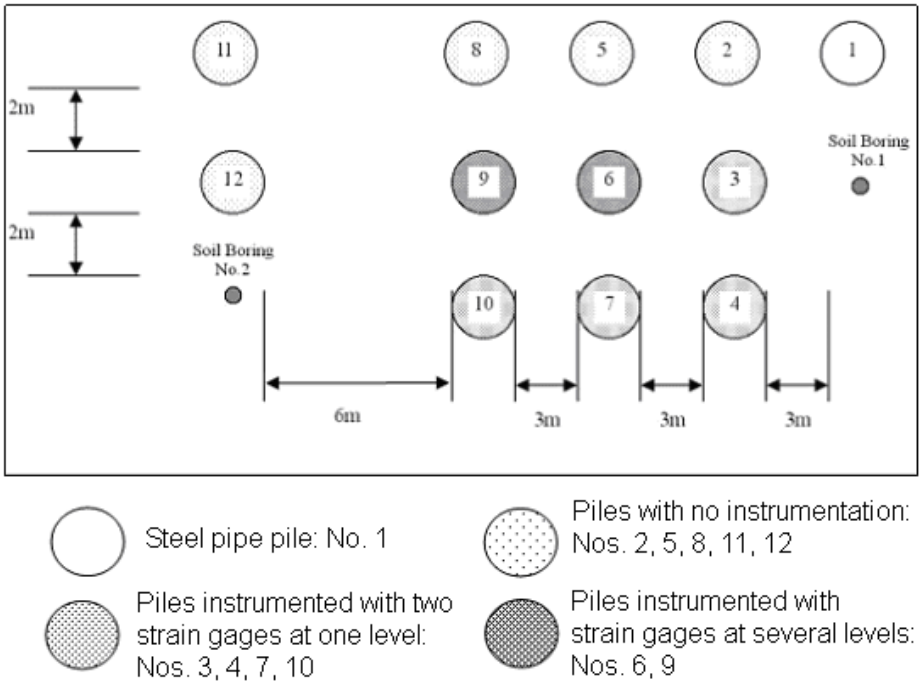

Figure 46. Illustration. Schematic drawing of Port Elizabeth site.

Table 4. Testing program details, Port Elizabeth site.

Pile Type	Pile Structure	Driving Order Number	Ref. Number of Tested (SLT) Piles	Diameter cm (inch)	Length m (ft)	AE[1] kN (kips)
Steel Pile	Steel	1	—	41.9 (16.5)	20 (65.6)	—
Lancaster	Fiberglass cased concrete	2,3,4	3	41.9 (16.5)	18.8 (61.7)	4.050×10^6 (9.1×10^5)
PPI	16 steel bars 2.54 cm (1inch) in diameter in recycled plastic	5,6,7	6	38.7 (15.25)	19.8 (65.0)	0.890×10^6 (2×10^5)
SEAPILE	16 fiberglass bars 4.5 cm (1.75 inches) in diameter in recycled plastic	8,9,10	9	42.5 (16.75)	20 (65.6)	0.745×10^6 (1.67×10^5)
American Ecoboard	Recycled plastic	11,12	12	41.9 (16.5)	6.1 (20) 11.8 (38.8)	—

[1] A is area in square meters; E is Young's modulus in kilopascals, which is kilonewtons per square meter.

GEOTECHNICAL SITE CONDITIONS

Port Elizabeth was constructed over a tidal marsh deposit consisting of soft organic silts, clays, and peats extending from mean high water to a depth of 3 to 9 m (10 to 30 ft). The site was reclaimed by placing fill over the marsh and surcharged to consolidate the compressible soils. The depth of the water table at the site is 1.7 m (5.5 ft) below the surface of the ground. Borings B-1 and B-2 indicated that the moisture content of the organic deposits ranged from 60 percent to 131 percent. The organic deposits are underlaid by silty fine sand. Below these materials are glacial lake deposits that generally range from sandy silt to clay and are sometimes varved. The glacial lake deposit at this site is overconsolidated. The consolidation test performed on a sample that was taken from this layer indicated a preconsolidation load of approximately 23 metric tons (t)/m^2 (4.7 kips/ft^2) and an overburden pressure of approximately 21.5 t/m^2 (4.4 kips/ft^2). The site is underlaid by shale rock. Two soil borings were performed: one near the steel pile, and the other near the American Ecoboard pile (figure 46). Soil laboratory tests show that the soil profiles can be roughly stratified into the layers in table 5.

Table 5. Soil profile and soil properties at Port Elizabeth site.

Depth, m (ft)	Soil Classification	Total Unit Weight, kN/m^3 (lb/ft^3)	Effective Cohesion, kN/m^2 (psf)	Effective Friction Angle, Degrees
0–4.6 (0–15)	SW-SC–Fill material	20 (125)	6 (125)	35
4.6–6.7 (15–22)	OL–Organic clay with peat	14.9 (93)	1 (21)	22
6.7–12.2 (22–40)	SM–Fine sand with silt	20(125)	6 (125)	37
12.2–23.2 (40–76)	CL–Silt and clay	19.4 (121)	1 (21)	23
23.2–25.9 (76–85)	Weathered shale	–	–	–
25.9–29.7 (85–97.5)	Red shale	–	–	–

STATIC LOAD TEST PROCEDURE

Four SLTs were performed on the FRP piles 6 months after they were driven. This procedure allowed for dissipation of the excess pore water pressure that was generated in the clay layers during pile driving. The SLTs on the selected FRP piles were performed according to ASTM D-1143. Figures 47–50 illustrate the settlement-time records obtained during the SLTs. The load at each increment was maintained until the measured settlement was less than 0.001 mm (0.000039 inch). At each stage, an increment of 10 t (22 kips) were applied until the test ended or failure occurred.

Two loading cycles were performed in the SLTs on Lancaster Composite, Inc., and PPI piles. After loading to 100 t (220 kips) at the end of the first cycle, or to the maximum applied load, the piles were unloaded to zero load at 25-t (55-kip) increments.

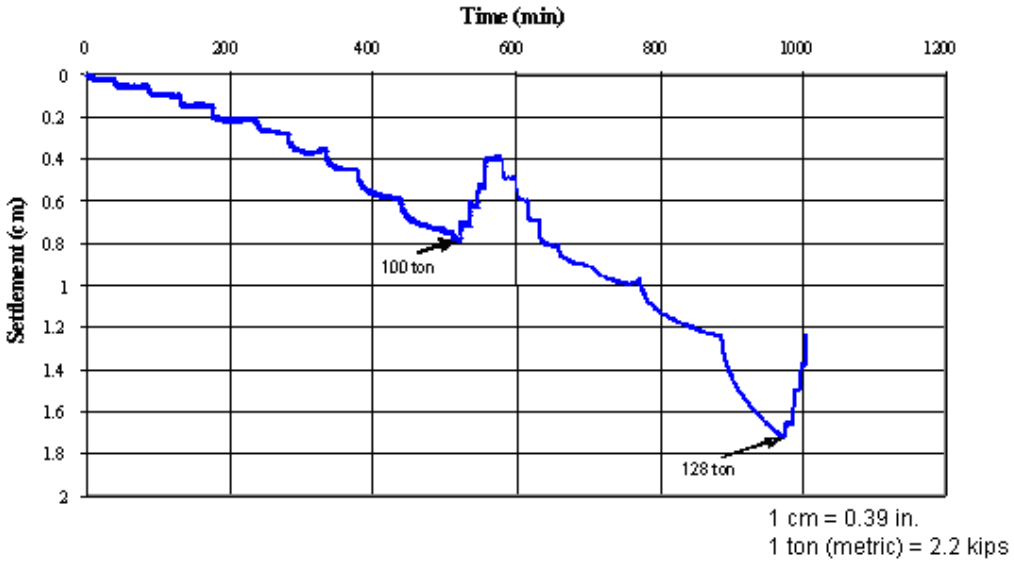

Figure 47. Graph. Lancaster pile—settlement-time relationship.

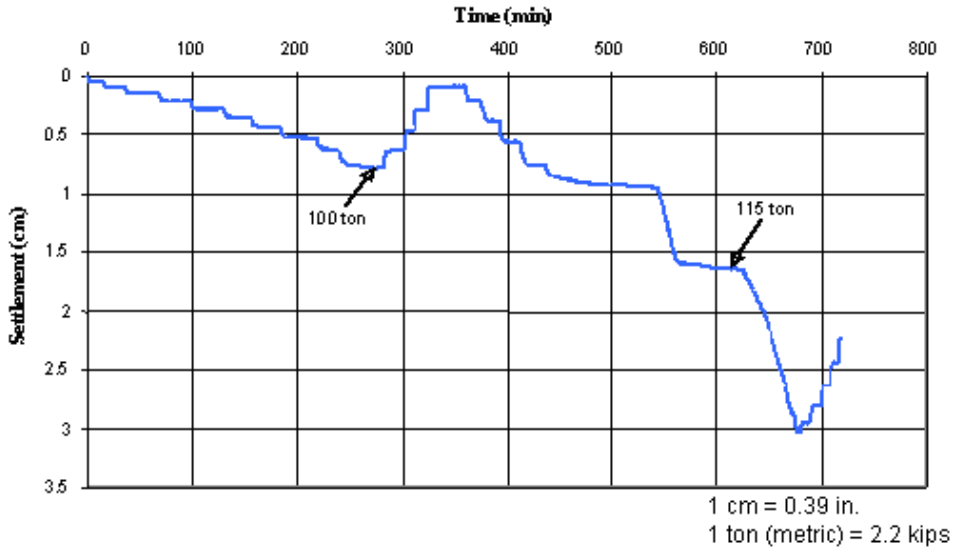

Figure 48. Graph. PPI pile—settlement-time relationship.

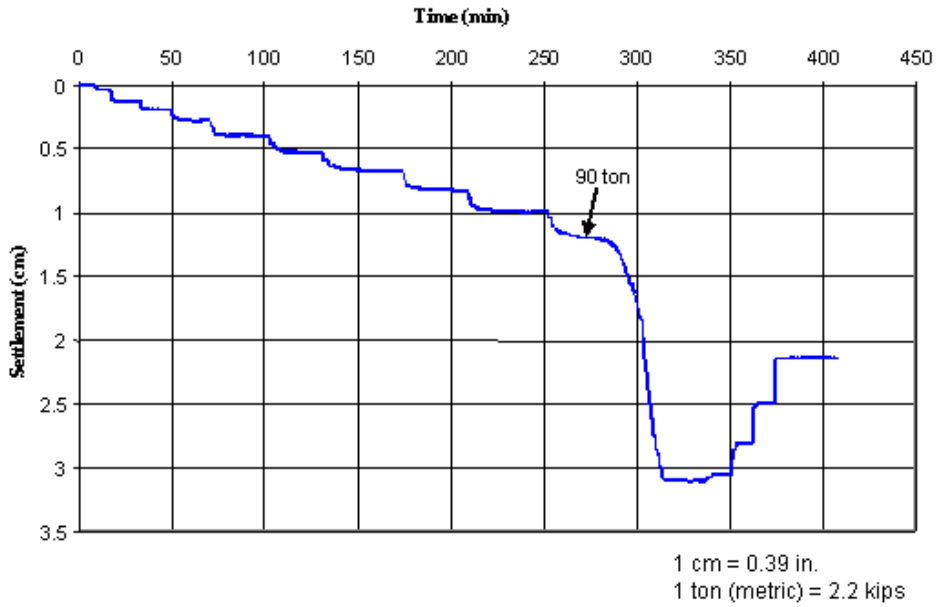

Figure 49. Graph. SEAPILE pile—settlement-time relationship.

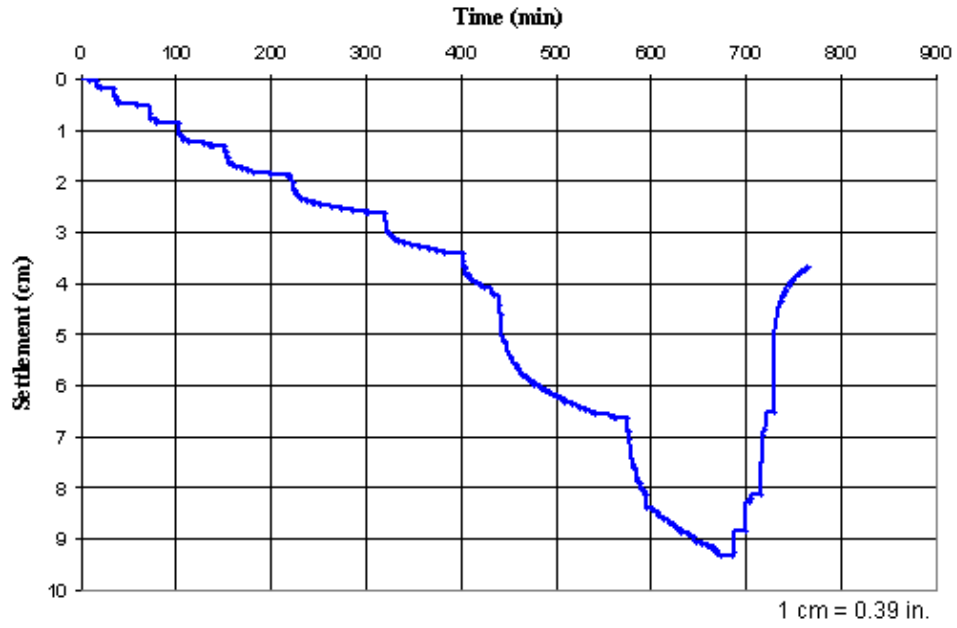

Figure 50. Graph. American Ecoboard pile—settlement-time relationship.

ENGINEERING ANALYSIS OF STATIC LOAD TEST RESULTS

Vertical load-bearing capacity of piles depends mainly on site conditions, soil properties, method of pile installation, pile dimensions, and pile material properties. Full-scale SLTs (ASTM D-1143), analytical methods[26,27,28] based on pile and soil properties obtained from in situ or laboratory tests, and dynamic methods[8] based on pile driving dynamics are generally used to evaluate the static pile capacity. Testing procedures and design methods to determine the FRP composite pile capacities have not yet been established. For the purpose of this study, several analysis methods commonly used to design steel and concrete piles have been considered for evaluating the maximum load, end bearing, and shaft friction distribution along the FRP composite piles.

Ultimate Capacities of FRP Piles

The Davisson Offset Limit Load

The offset limit method proposed by Davisson defines the limit load as the load corresponding to the settlement, S, resulting from the superposition of the settlement S_{el} due to the elastic compression of the pile (taken as a free standing column) and the residual plastic settlement S_{res} due to relative soil pile shear displacement.[26] The total settlement S can be calculated using the empirically derived Davisson's equation (figure 51).

$$S = 0.004(m) + \frac{D(m)}{120} + S_{el}$$

Figure 51. Equation. Settlement, S.

Where:
S_{el} = PL/EA.
S_{el} = The settlement due to the elastic compression of a free standing pile column.
D = Pile diameter (m).
l = Pile length (m).
A = Pile cross section area (m^2).
e = Pile Young's modulus (kPa).
P = Load (kN).

The limit load calculated according to this method is not necessarily the ultimate load. The offset limit load is reached at a certain toe movement, taking into account the stiffness, length, and diameter of the pile. The assumption that the elastic compression of the pile corresponds to that of a free-standing pile column ignores the load transfer along the pile and can, therefore, lead to overestimating the pile head settlement, particularly for a friction pile. Because of the load transfer along the pile, the settlement corresponding to the elastic compression generally does not exceed 50 percent of the elastic settlement for a free-standing column.

Pile data used to calculate the ultimate capacities according to the Davisson offset limit load method for FRP piles are summarized in table 6. The elastic properties of pile materials were determined by laboratory compression tests on full-section composite samples.

Figures 52–55 show the load versus pile head settlement curves measured during the SLTs. As illustrated in these figures, Davisson's limit method is used to establish the limit loads under the following assumptions:

- The settlement due to the elastic compression corresponds to the settlement of an elastic free-standing pile column and can, therefore, be calculated from the equation in figure 51.
- The settlement due to the elastic compression corresponds to the elastic compression of a friction pile, assuming a constant load transfer rate along the pile, and can, therefore, be estimated as 50 percent of the elastic compression of a free-standing pile column.
- The settlement due to the elastic compression corresponds to the pile load movement during an unloading-reloading cycle, and the equivalent pile elastic modulus can, therefore, be derived directly from the slope of the load-settlement curve obtained for the unloading-reloading cycle. This procedure incorporates the field conditions and the effect of the load transfer along the pile.

Comparing the results obtained with the Davisson's procedure for these three assumptions and load-settlement curves obtained from the static loading tests, it can be concluded that for the highly compressible FRP piles, the assumption that the pile elastic compression is equivalent to that of a free-standing column leads to greatly overestimating the pile head settlement. The assumption that an equivalent elastic modulus of the composite pile can be derived from the slope of the load-settlement curve that is defined from an unloading-reloading cycle leads to settlement estimates that appear to be quite consistent with the experimental results. Further, these settlements are also quite close to the settlements, due to the elastic compression calculated for the friction piles, assuming a constant load transfer rate along the pile (i.e., about 50 percent of the elastic compression of a free-standing pile column). For the American Ecoboard pile that was driven to the sand layer, the load-settlement curve did not reach any plunging failure. For this pile, the Davisson's procedure that considers the equivalent elastic modulus derived from the unloading-reloading load-settlement curve yields estimates of the limit load (about 50 t) and pile head settlement (about 6 cm (2.4 inches)), which appear to be consistent with the experimental results.

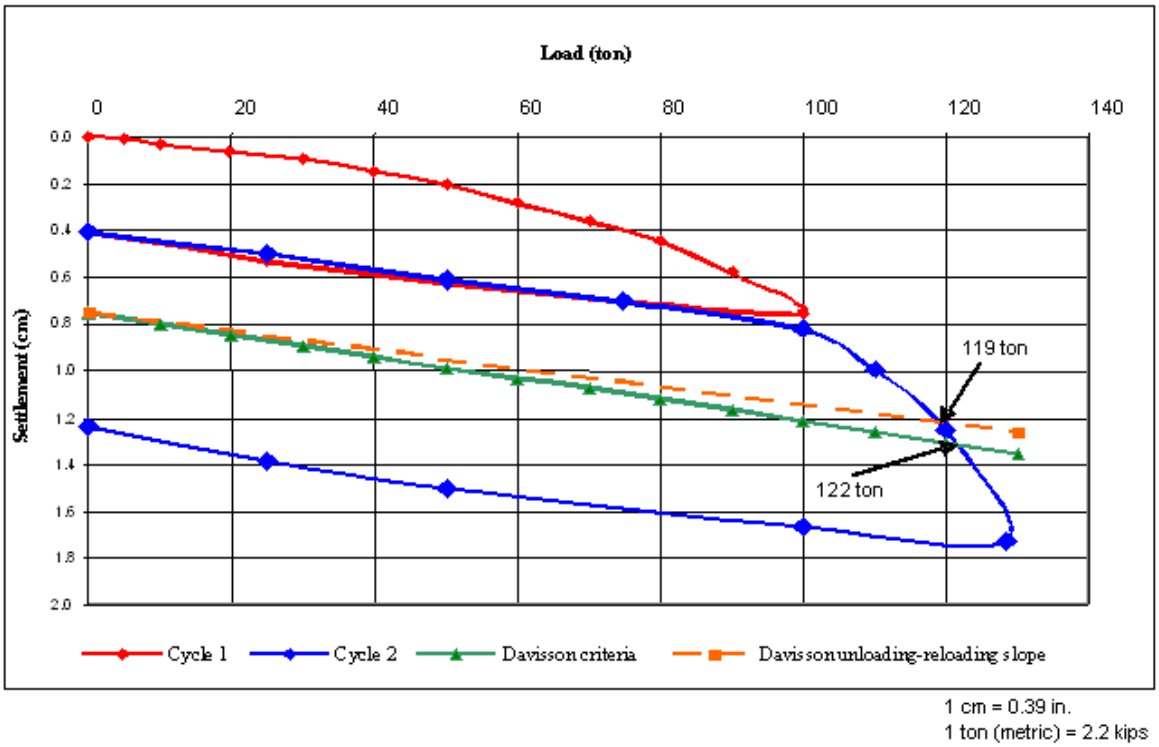

Figure 52. Graph. Lancaster Composite pile—Davisson criteria and measured load-settlement curve.

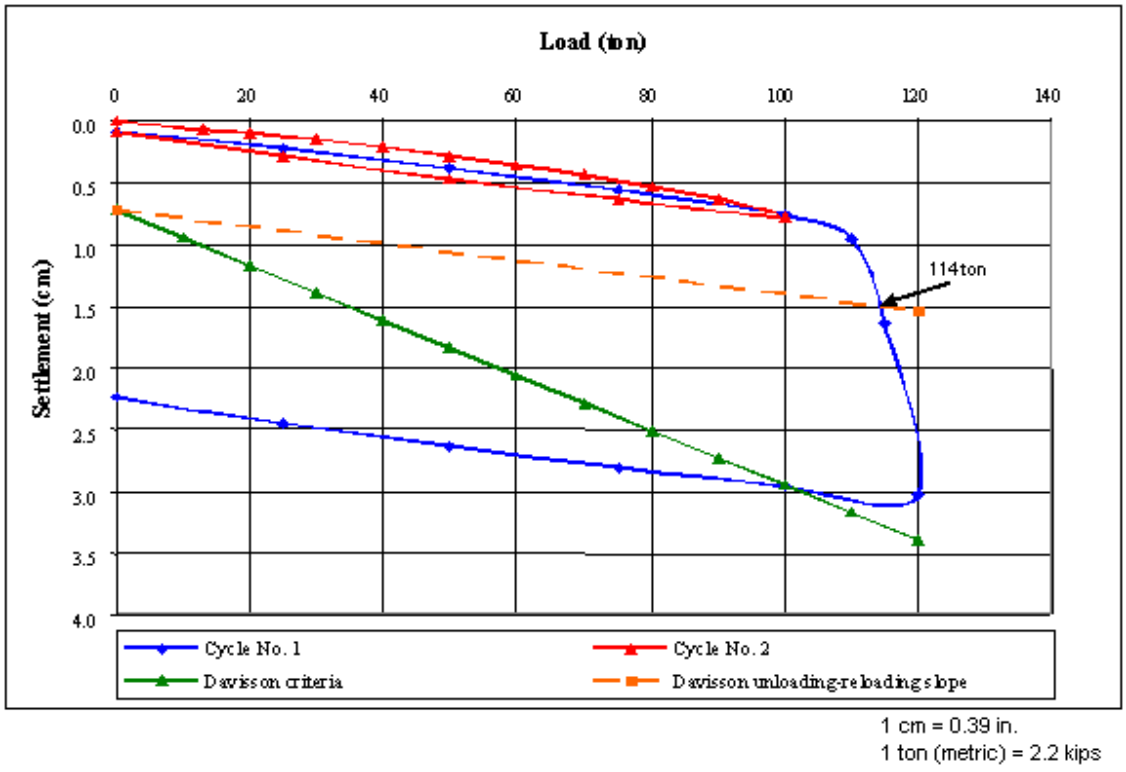

Figure 53. Graph. PPI pile—Davisson criteria and measured load-settlement curve.

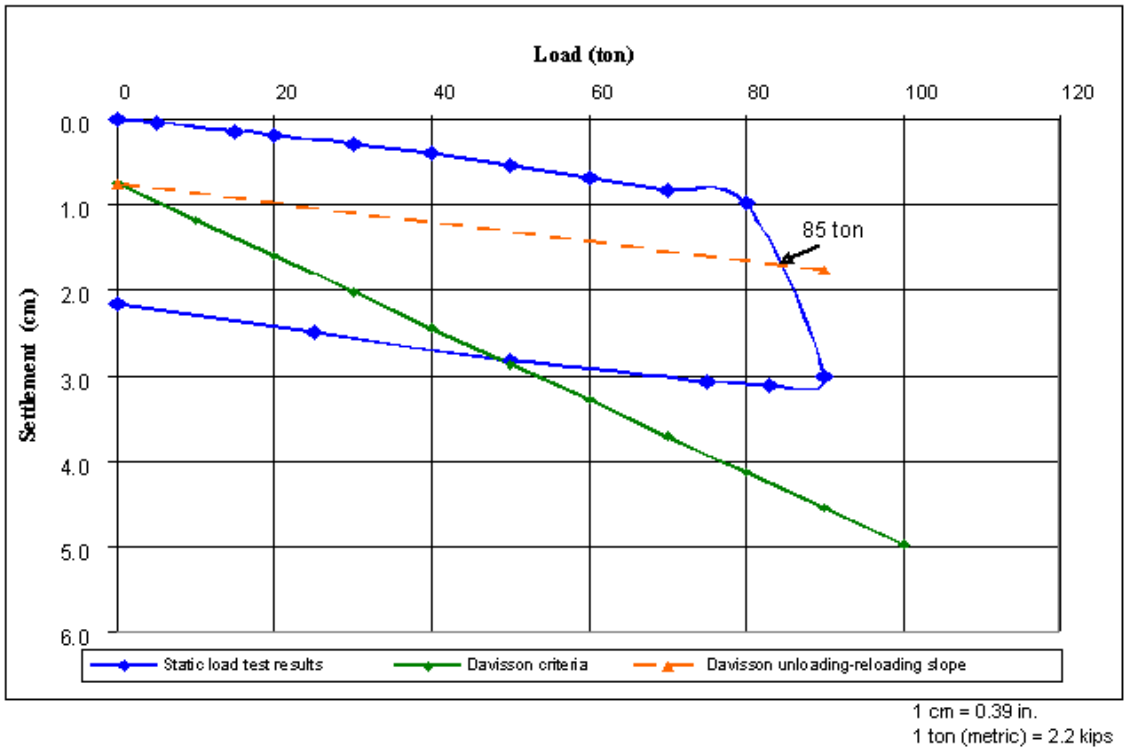

Figure 54. Graph. SEAPILE pile—Davisson criteria and measured load-settlement curve.

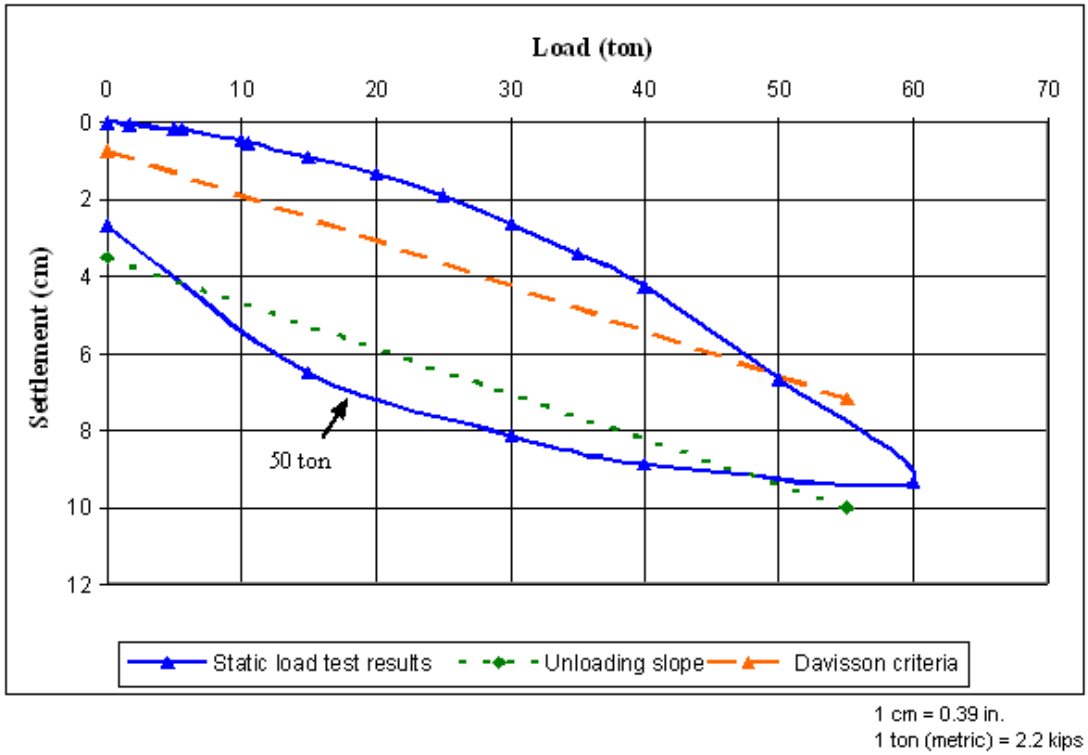

Figure 55. Graph. American Ecoboard pile—Davisson criteria and measured load-settlement curve.

DeBeer Yield Load

The DeBeer ultimate capacity is determined by plotting the load-settlement curve on a log-log scale diagram.[27] As illustrated in figure 56, on the bilinear plot of the load versus settlement, the point of intersection (i.e., change in slope) corresponds to a change in the response of the pile to the applied load before and after the ultimate load has been reached. The load corresponding to this intersection point is defined by DeBeer as the yield load. Figure 56 shows the DeBeer criteria as plotted for the FRP piles. The DeBeer yield loads are 110 t (242 kips) for the Lancaster Composite, Inc., and PPI piles and 80 t (176 kips) for the SEAPILE pile. The yield load for the American Ecoboard pile could not be defined. This pile did not experience a plunging failure during the SLT.

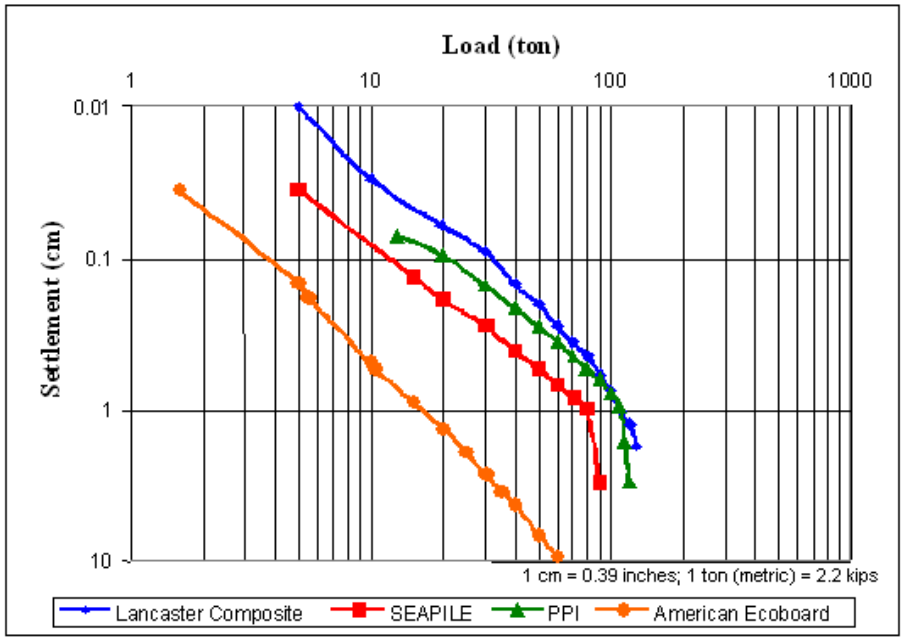

Figure 56. Graph. DeBeer criterion plotted for FRP piles.

Chin-Kondner Method

Chin[28] proposed an application of the Kondner[29] method to determine the failure load. As illustrated in figure 57, the pile top settlement is plotted versus the settlement divided by the applied load, yielding an approximately straight line on a linear scale diagram. The inverse of the slope of this line is defined as the Chin-Kondner failure load. The application of the Chin-Kondner method for the engineering analysis of the SLTs conducted on the FRP piles, illustrated in figure 57, yields the ultimate loads of 161 t (354 kips), 96 t (211 kips), and 125 t (275 kips) for the Lancaster Composite, Inc., SEAPILE, and PPI piles, respectively.

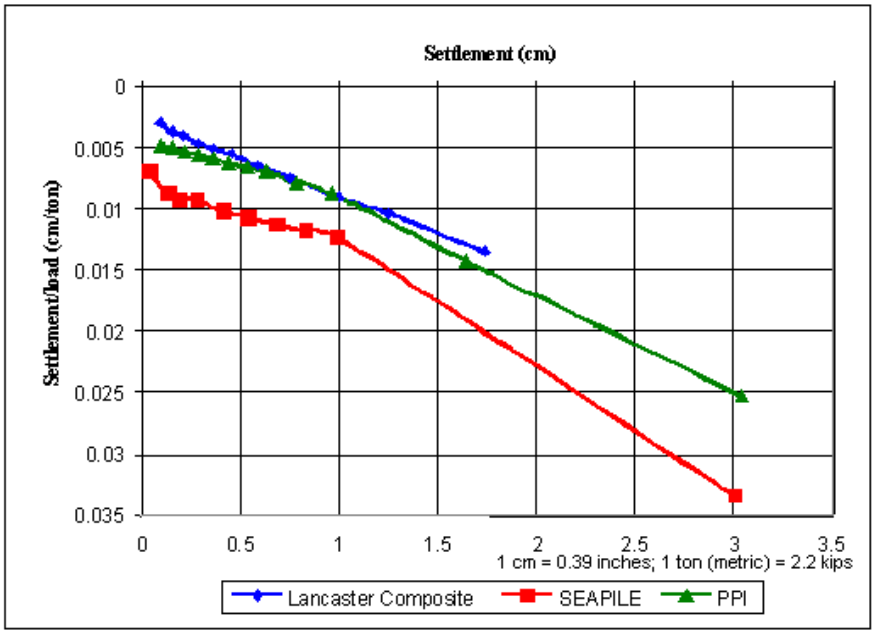

Figure 57. Chin-Kondner method plotted for FRP piles.

Applying the Chin-Kondner method for the American Ecoboard pile, illustrated in figure 58, yields a failure load of approximately 102 t (224 kips).

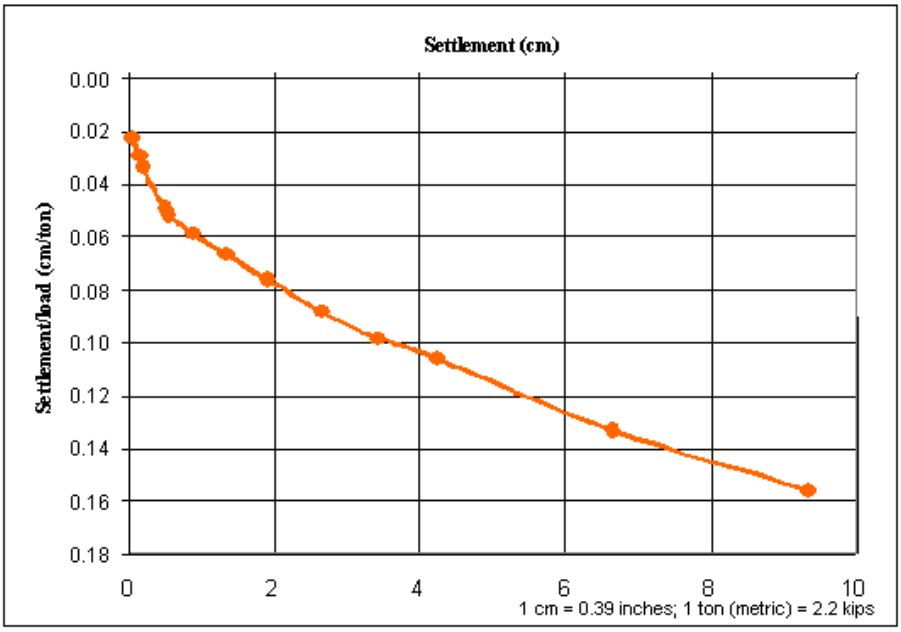

Figure 58. Chin-Kondner method plotted for American Ecoboard pile.

The application of the Chin-Kondner method yields a failure load that is defined as the asymptotic ultimate load of the load-settlement curve. It therefore yields an upper limit for the failure load leading in practice to overestimating the ultimate load.

However, if a distinct plunging ultimate load is not obtained in the test, the pile capacity or ultimate load is determined by considering a specific pile head movement, usually 2 to 10 percent of the diameter of the pile, or a given displacement, often 3.81 cm (1.5 inches). As indicated by Felenius, such definitions do not take into account the elastic shortening of the pile, which can be substantial for composite long piles such as FRP piles.[30]

Table 6. Comparison of measured and calculated ultimate loads.

Pile Manufacturer	Static Load Test Results		Davisson Offset Limit Load		DeBeer Yield Load		Chin-Kondner		Davisson Criteria Un/reloading Slope	
	Load t	Settlement cm	Load t	Settlement cm	Load t	Settlement cm	Load t	Settlement cm	Load t	Settlement cm
Lancaster Composite[1]	128	1.73	122	1.31	110	0.96	161	–	119	1.3
PPI	115	1.64	121	3.40	110	0.96	125	–	114	1.5
SEAPILE	90	1.16	92	4.60	80	0.98	96	–	85	1.8
American Ecoboard[1]	60	9.34	–	–	–	–	102	–	50	6.0

[1] The pile did not experience plunging failure during the static load test. 1 cm = 0.39 inch; 1 t = 2.2 kips

Table 6 summarizes the maximum loads applied during the SLTs and the ultimate loads calculated using the Davisson offset limit load, DeBeer yield load, and the Chin-Kondner methods. Distinct plunging failure occurred during the SLTs on PPI and SEAPILE piles as the applied loads reached 115 and 90 t (253 and 198 kips) and the measured pile top settlements were 1.64 cm (0.65 inch) and 1.16 cm (0.46 inch), respectively. The Lancaster Composite, Inc., pile did not experience a distinct plunging failure, and as the maximum load applied on the pile reached 128 t (282 kips), the measured settlement was 1.73 cm (0.68 inch). The maximum load applied on the American Ecoboard pile was 60 t (132 kips). At this load, the pile top settlement was 9.34 cm (3.7 inches), and no distinct plunging was observed. The pile top settlements of this pile, which contains only recycled plastic with no reinforcement bars, were significantly greater than the settlements measured during the tests on the other FRP piles (figures 52 through 57).

The Davisson's offset limit is intended primarily to analyze test results from driven piles tested according to quick testing methods (ASTM D-1143) and, as indicated by Fellenius, it has gained widespread use with the increasing popularity of wave equation analysis of driven piles and dynamic testing.[31] This method allows the engineer, when proof testing a pile for a certain

allowable load, to determine in advance the maximum allowable movement for this load considering the length and dimensions of the pile.[32] The application of the Davisson's offset limit load method illustrates that for the compressible FRP piles, the effect of load transfer along the piles must be considered in estimating the maximum allowable pile movement. The equivalent elastic modulus of the composite pile derived from the measured pile response to the unloading-reloading cycle leads to settlement estimates that are quite consistent with the experimental results.

The DeBeer yield load method was proposed mainly for slow tests (ASTM D-1143).[33] In general, the loads calculated by this method are considered to be conservative. The calculated loads for the Lancaster Composite, Inc., and PPI piles (110 t (242 kips)), and for the SEAPILE pile, (80 t (176 kips)), are smaller than the maximum load applied on these piles by 14 percent, 4 percent, and 11 percent, respectively. For these calculated loads, the calculated settlements for the Lancaster Composite, Inc., PPI, and SEAPILE piles are smaller than the measured settlements by 44.5 percent, 41.5 percent, and 15.5 percent, respectively.

The Chin-Kondner method is applicable for both quick and slow tests, provided constant time increments are used. As indicated by Fellenius,[30] during a static loading test, the Chin-Kondner method can be used to identify local low resistant zones in the pile, which can be of particular interest for the composite FRP piles.

As an approximate rule, the Chin-Kondner failure load is about 20 to 40 percent greater than the Davisson limit.[30] As shown in table 6, all the loads calculated by the Chin-Kondner method were greater than the maximum load applied on the piles in the field test. The calculated loads for the Lancaster Composite, Inc., PPI, SEAPILE, and American Ecoboard piles, 161, 125, 96, and 102 t (354, 275, 211, and 224 kips), are greater than the Davisson offset limit load by 32 percent, 3 percent, 4 percent, and 30 percent, respectively.

In general, the ultimate loads calculated for FRP piles using the Chin-Kondner method are greater than the maximum loads applied in the field test. The DeBeer yield load method yields conservative loads in comparison to the maximum loads obtained at the SLTs. The Davisson offset limit load method, using the equivalent elastic modulus obtained from the pile response to an unloading-reloading cycle, yields ultimate loads that are within the range of loads obtained with the above-mentioned methods and allowable settlements that are close to the settlements reached with maximum loads applied in the field tests.

Analysis of the End Bearing and Shaft Friction Distribution

Axial load-bearing capacity, end bearing, and shaft friction along the pile can be evaluated using analytical methods based on pile and soil properties obtained from in situ and/or laboratory tests. For the purpose of the SLT engineering analysis, the experimental results were compared with several commonly used methods, including the "alpha" total stress analysis and the "beta" effective stress analysis. A state-of-the-art review on foundations and retaining structures presented by Poulos, et al., (briefly summarized below) relates to axial capacity of piles.[34] An estimate of a pile's ultimate axial load-bearing capacity can be obtained by the superposition of the ultimate shaft capacity, P_{su}, and the ultimate end bearing capacity, P_{bu}. The weight, W_p, of the

pile is subtracted for the compressive ultimate load capacity. For compression, then, the ultimate load capacity, P_{uc}, is given by the equation in figure 5.

$$P_{uc} = \sum f_s C dz + f_b A_b - W_p$$

Figure 59. Equation. Ultimate load capacity P_{uc}.

Where:
f_s = Ultimate shaft friction resistance in compression (over the entire embedded length of the pile shaft).
C = Pile perimeter.
dz = Length of the pile in a specific soil layer or sublayer.
f_b = Ultimate base pressure in compression.
A_b = Cross-sectional area of the pile base.

Alpha Method—Total Stress Analyses for Pile Capacity Evaluation in Clay Soils

Commonly, the alpha method is used to estimate the ultimate shaft friction in compression, f_s, for piles in clay soils. The equation in figure 60 relates the undrained shear strength s_u to f_s.

$$f_s = \alpha s_u$$

Figure 60. Equation. Ultimate shaft friction in compression f_s.

Where:
α = Adhesion factor.

The ultimate end bearing resistance f_b is given by the equation in figure 61.

$$f_b = N_c s_u$$

Figure 61. Equation. Ultimate end bearing resistance f_b.

Where:
N_c = Bearing capacity factor.

Several common approaches used for estimating the adhesion factor α for driven piles are summarized in table 7. Other recommendations for estimating α, for example, in Europe, are given by De Cock.[35] For pile length exceeding about three to four times the diameter, the bearing capacity factor N_c is commonly taken as 9.

A key difficulty in applying the total stress analysis is estimating the undrained shear strength s_u. It is now common to estimate s_u from in situ tests such as field vane tests or cone penetration tests, rather than estimating it from laboratory unconfined compression test data. Values for s_u

can vary considerably, depending on the test type and the method of interpretation. Therefore, it is recommended that local correlations be developed for α in relation to a defined method of measuring s_u.[34]

Table 7. Total stress analysis approaches for estimating f_s.[34]

Pile Type	Remarks	Reference
Driven	$\alpha = 1.0$ ($s_u \leq 25$ kPa) $\alpha = 0.5$ ($s_u \geq 70$ kPa) Interpolate linearly between	API[6]
Driven	$\alpha = 1.0$ ($s_u \leq 25$ kPa) $\alpha = 0.5$ ($s_u \geq 70$ kPa) Linear variation between length factor applies for $L/d \geq 50$	Semple and Rigden[36]
Driven	$\alpha = (s_u/\sigma'_v)^{0.5} (s_u/\sigma'_v)^{-0.5}$ for $(s_u/\sigma_v') \leq 1$ $\alpha = (s_u/\sigma'_v)^{0.5} (s_u/\sigma'_v)^{-0.25}$ for $(s_u/\sigma_v') \geq 1$	Fleming, et al.[37]

Beta Method—Effective Stress Analysis

For any soil type, the beta effective stress analysis may be used for predicting pile capacity. The relationship between f_s and the in situ effective stresses may be expressed by the equation in figure 62.

$$f_s = K_s \sigma'_v \tan \delta$$

Figure 62. Equation. Relationship between f_s and in situ stresses.

Where:
K_s = Lateral stress coefficient.
δ = Pile-soil friction angle.
σ'_v = Effective vertical stress at the level of point under consideration.

A number of researchers have developed methods of estimating the lateral stress coefficient K_s. Table 8 summarizes several approaches, including the commonly used approaches of Burland[38] and Meyerhof.[4]

Table 8. Effective stress analysis approaches for estimating ultimate shaft friction.

Pile Type	Soil Type	Details	Reference
Driven and Bored	Sand	$K_s = A + BN$ where N = SPT (standard penetration test) value A = 0.9 (displacement piles) Or 0.5 (nondisplacement piles) B = 0.02 for all pile types	Go and Olsen[39]
Driven and Bored	Sand	$K_s = K_o\ (K_s/K_o)$ where K_o= at-rest pressure coefficient (K_s/K_o) depends on installation method; range is 0.5 for jetted piles to up to 2 for driven piles	Stas and Kulhawy[40]
Driven	Clay	$K_s = (1 - \sin \phi')\ (OCR)^{0.5}$ where ϕ' = effective angle of friction OCR = overconsolidation ratio; Also, $\delta = \phi'$	Burland[38] Meyerhof[4]

Correlations With Standard Penetration Test (SPT) Data

SPT test result data imply the empirical correlations expressed in figures 63 and 64.

$$f_s = A_N + B_N N$$

Figure 63. Equation. Empirical correlations for shaft friction.

Where:
A_N and B_N = Empirical coefficients.
N = SPT blow count number at the point under consideration.

$$f_b = C_N N_b$$

Figure 64. Equation. Empirical correlation for end bearing resistance.

Where:
C_N = Empirical factor.
N_b = Average SPT blow count within the effective depth of influence below the pile base (typically one to three pile base diameters).

Meyerhof recommended using $A_N = 0$, $B_N = 2$ for displacement piles and 1 for small displacement piles, and $C_N = 0.3$ for driven piles in sand.[41] Limiting values of f_s of about 100 kPa (14.5 psi) were recommended for displacement piles and 50 kPa (7.25 psi) for small displacement piles. Poulos summarized other correlations, which include several soil types for both bored and driven piles.[42] Decourt's recommendations included correlations between f_s and SPT, which take into account both the soil type and the methods of installation.[43] For displacement piles, $A_N = 10$ and $B_N = 2.8$, and for nondisplacement piles, $A_N = 5–6$ and $B_N = 1.4–1.7$. Table 9 shows the values of C_N for estimating the end bearings. Rollins et al.

discussed the correlations for piles in gravel.[44] The correlations with SPT must be treated with caution, as they are inevitably approximate, and are not universally applicable.[34]

Table 9. Factor C_N for base resistance.[43]

Soil Type	Displacement Piles	Nondisplacement Piles
Sand	0.325	0.165
Sandy silt	0.205	0.115
Clayey silt	0.165	0.100
Clay	0.100	0.080

Comparison Between Various Analysis Methods and Test Results

SLT results were compared with several design codes[5-7] and methods commonly used[4] for evaluating the end bearing and shaft friction along the pile. Figures 65, 66, and 67 show the loads versus depth measured in the SLTs for PPI, SEAPILE, and Lancaster Composite, Inc., piles, respectively.

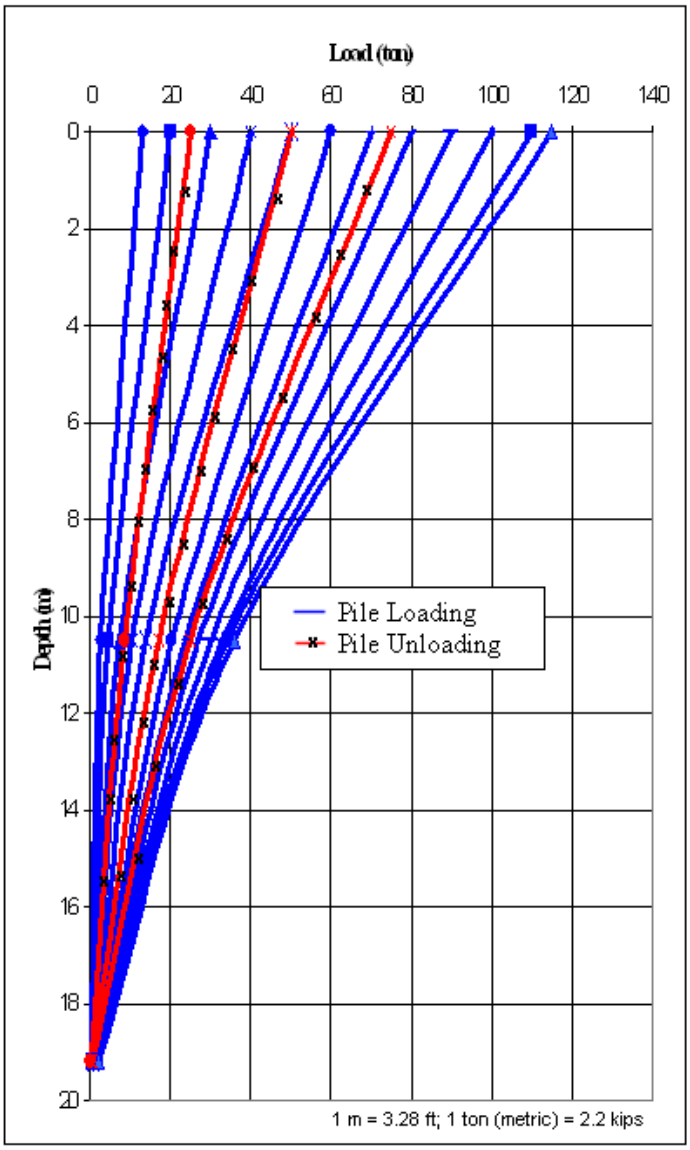

Figure 65. Graph. PPI pile, measured loads versus depth.

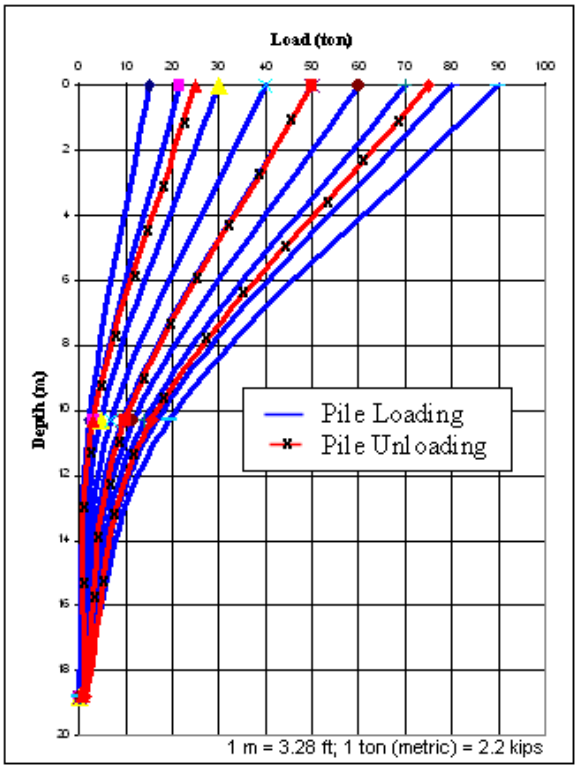

Figure 66. Graph. SEAPILE pile, measured loads versus depth.

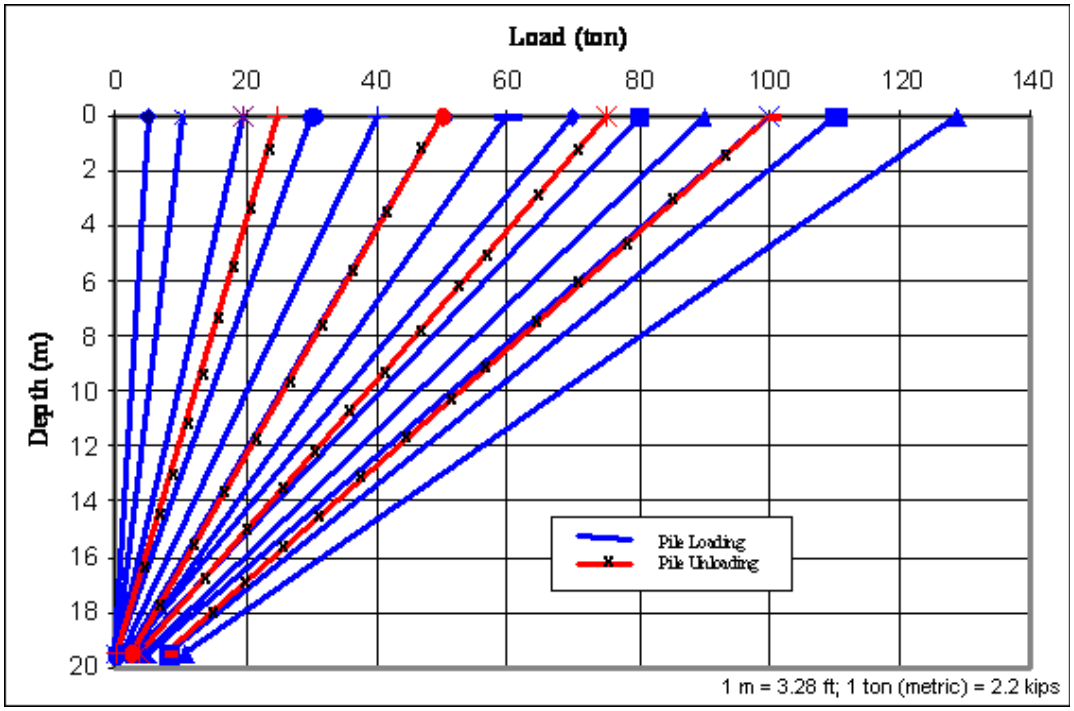

Figure 67. Graph. Lancaster Composite, Inc., pile, measured loads versus depth.

As illustrated in these figures, the axial force distribution measured along the piles indicates that the FRP piles at the Port Elizabeth site were frictional piles, with maximum end bearing capacities, which were equal to 1.6 percent, 1.0 percent, and 8.4 percent of the total applied load for the PPI, SEAPILE, and the Lancaster Composite, Inc. piles, respectively.

Table 10. Comparison between SLT results and several analysis methods and design codes.

	Static Load Test Results			Go and Olsen[39]	Stas and Kulhawy[40]	FHWA [5]	API [6]	Meyerhof [4]	AASHTO [7]
	PPI	SEAPILE	Lancaster Composite						
End bearing capacity, t	1.9	0.9	10.8	–	–	73.5	6.6	75.4	–
Total shaft friction, t	113.1	89.1	117.7	11.3	7.33	49.7	81	4.3	16.4
Shaft friction depth 0 to 10 m, t/m^2	6.0	5.6	–	2.9	2.0	2.4	4.0	4.5	7.3
Shaft friction depth 10 to 20 m, t/m^2	3.15	1.65	–	9.1	5.8	2.6	8.8	6.8	1.2
Shaft friction depth 0 to 20 m, t/m^2	4.5	3.5	4.7	4.5	2.6	4	6.4	5.6	4.2
Total capacity, t	115	90	128.5	–	–	123.2	87.6	79.7	–
End bearing capacity / Total load, %	1.6	1.0	8.4	–	–	59.7	7.5	94.6	–

1 t = 2.2 kips; 1 m = 3.28 ft

Table 10 summarizes the comparison of the average measured shaft friction along the FRP piles and the shaft friction values calculated from several design codes and methods of analysis commonly used. The engineering analysis of the shaft friction distribution takes into consideration two soil layers corresponding to the upper soil layers from 0 to 10 m (32.8 ft), which consists of fill material, a soft clay layer, and a sandy layer, and the lower soil layer from 10 to 20 m (32.8 to 65.6 ft), which consists of a 3-m (9.8-ft) sand layer overlaying a 7-m (23-ft) clay and silt layer. Average values of the shaft friction also are obtained, taking into account the axial force measured at the top and the bottom of the soil. For the PPI and SEAPILE piles, the average shaft friction values obtained at the upper 10-m (32.8-ft) layer were greater than the shaft friction values measured at the lower clay layer. The Burland and Meyerhof methods and the AASHTO code appear to yield the best correlation for shaft friction values in the upper layer. The FHWA code appears to yield the best correlation for the shaft friction values obtained in the lower clay and silt layer.

CHAPTER 4. EVALUATION OF FRP COMPOSITE PILING CAPACITY USING WAVE EQUATION ANALYSIS

The engineering use of FRP piles on a widespread basis presently raises the need to establish testing procedures to determine the dynamic properties of FRP composite materials. In particular, PDA tests and full-scale loading tests on FRP piles must be conducted to establish site correlations for evaluating the use of wave equation analysis in predicting static piling capacity and evaluating pile drivability and integrity. The main objective of the study described in this chapter was to conduct a full-scale experiment including dynamic and static load tests on FRP piles to address these engineering needs.

PDA and PIT test results were analyzed using CAPWAP[1,45-46] and GRLWEAP[47] programs to establish the dynamic properties of the FRP piles. The PDA was also used to evaluate the feasibility of installing FRP piles using standard pile driving equipment. Pile-bearing capacities were assessed using the CAPWAP program with the dynamic data measured by the PDA, and the calculated pile capacities were compared to the results of SLTs performed on the four FRP piles.

TESTING PROGRAM AND SITE OBSERVATIONS

Test Piles and Dynamic Instrumentation

The test piles were driven with an ICE 70 single-acting, variable stroke hydraulic hammer. According to the manufacturer's literature, this hammer has a 31.1-kN (7.0-kip) ram with a maximum rated energy of 28.5 kJ (21 ft-kips) at a maximum stroke of 91.4 cm (3 ft). This hammer has a pump-controlled stroke, and during the initial driving and restrike, the stroke was varied from 30.5 to 91.4 cm (1 to 3 ft). Plywood cushions were used to protect the pile top. In most cases during driving and restriking, the cushion was nominally 24.8 cm (9.75 inches) thick. 15.2-cm- (6-inch-) thick cushions were used to drive the Lancaster piles.

Dynamic measurements of strain and acceleration were taken 91.4 cm to 1.5 m (3 to 5 ft) below the head of the test piles. During initial drive, two strain transducers and two accelerometers were bolted at opposite sides of the pile to monitor strain and acceleration. During redrive, four strain transducers and four accelerometers were attached to the pile. Strain and acceleration signals were conditioned and converted to forces and velocities by the PDA. During driving, the PDA calculated values of the maximum transferred hammer energy and the maximum compression stress at the gauge location, and an estimate of the pile capacity by the Case Method.[8] These results were displayed on the PDA monitor for every blow.

Force and velocity records from the PDA were also displayed on a graphic liquid crystal display (LCD) screen to evaluate data quality, soil resistance distribution, and pile integrity. The force and velocity records were also digitally stored on a disc for subsequent laboratory analysis.

Site Observations on Drivability and Durability During Pile Installation

Figures 68 through 71 show the FRP piles before and after driving. Site observations on drivability and durability during installation of the test piles are summarized below.

The steel pile was driven with the lowest blow counts (36 blows/m (11 blows/ft)) and the highest transfer energy of 23.1 kJ (17 ft-kips); this pile, however, was driven without a plywood pile cushion and with a helmet specifically designed for steel pipe piles. Adding 15.2 to 24.8 cm (6 to 9.75 inches) of pile cushion may explain some of the energy losses and increased blow counts observed with the other piles.

Among the FRP piles, the SEAPILE pile was driven with the lowest blow counts (62 to 118 blows/m (19 to 36 blows/ft)), and showed relatively high transfer energies of 13.6 to 17.6 kJ (10 to 13 ft-kips) at the end of driving. The pile cushion for these piles showed very little degradation after driving.

The PPI piles were driven with blow counts ranging between 1 to 1.4 blows/mm (27 to 37 blows/inch), and transfer energies at the gauge location of 8.1 to 10.8 kJ (6 to 8 ft-kips), significantly lower than those obtained for the SEAPILE and Lancaster Composite, Inc., piles. After driving, it was observed that the PPI piles experienced severe pile top degradation; the plastic matrix covering the rebar had melted and some pieces of the steel rebar had sheared off. The heat and pile top damage could have been the reason for the losses in the transfer energy. After driving, the upper foot of each PPI pile was removed, and no damage or separation between bars and the plastic material was observed.

Figure 68. Photo. PPI pile.

Figure 69. Photo. SEAPILE pile.

Figure 70. Photo. Lancaster Composite, Inc., pile.

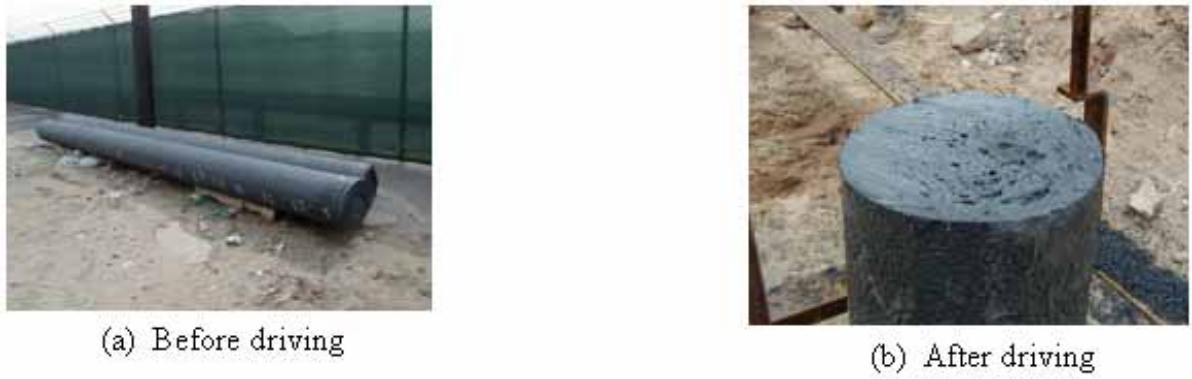

Figure 71. Photo. American Ecoboard pile.

At the end of installation (EOI), the Lancaster Composite, Inc., piles had blow counts ranging from 154 to 305 blows/m (47 to 93 blows/ft), with calculated transfer energy values of 12.2 to 17.6 kJ (9 to 13 ft-kips) at the end of drive. It should be noted that to reduce the estimated tension stresses, the Lancaster Composite, Inc., SLT pile was driven with a reduced stroke of

61.0 cm (2 ft) for the last few feet of penetration; this driving process resulted in a higher blow count of 305.1 blows/m (93 blows/ft). By the EOI of these piles, it was observed that the pile cushion had experienced initial burning.

The Lancaster Composite, Inc., pile that was driven to refusal (almost 0.4 blows/mm (10 blows/ inch)) into the weathered shale at the depth of 26.5 m (87 ft) below grade was spliced. Driving resistance ranged from 164 to 299 blows/m (50 to 91 blows/ft) for a penetration of 18.8 to 26.5 m (60 to 87 ft).

The American Ecoboard piles were driven into the upper sand layer at approximately 9.1 m (30 ft) below the ground surface. They were spliced at the depth of 6 m (19.7 ft). After splicing, the American Ecoboard dynamic testing results evidenced a toe signal, which indicated that the stress wave propagated through the splice. A significant impedance increase followed by a sharp decrease was observed at the splice location. This wave reflection is likely to be the result of the additional steel bolts and sleeve, as well as of a slight gap between the two sections.

DYNAMIC PROPERTIES OF THE FRP COMPOSITE PILE MATERIALS

Methods for Evaluating Dynamic Properties

Before dynamic testing, several material properties at the gauge location have to be determined. These data include the pile length, cross-sectional area, specific weight, wave speed, and elastic modulus. Testing procedures to establish the dynamic elastic modulus of FRP composite piles have not yet been established or evaluated. For the purpose of this study, the dynamic testing procedures commonly used for steel and concrete piles have been followed to evaluate the dynamic properties of the composite piles, including:

- PIT—low-strain integrity testing (ASTM D5882).[48]
- PDA testing—high strain (ASTM D4945).[49]
- PDA testing—considering the initial portion of the high-strain records (ASTM D4945).[49]

These testing procedures are briefly summarized below.

Pile Integrity Tester (PIT)

Before initial installation, low-strain integrity testing was performed with a PIT. The PIT testing (ASTM D5882) consists of attaching a small accelerometer to the pile top sample and using a small handheld hammer to lightly impact the pile sample top. This impact induces a low-strain stress wave in the pile, which travels to the pile toe and reflects back toward the pile top. With the length of the pile sample known, a wave speed, c, can be calculated from the time measured between the impact and the toe response. The wave speed can, in turn, be used with a known material density, ρ, to calculate the low-strain dynamic modulus using the relationship in figure 72.

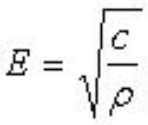

Figure 72. Equation. Dynamic modulus E.

PDA Testing—High Strain

PDA testing yields wave speed following a procedure similar to that used for low-strain PIT tests. For a specified length of the pile, the time between impact and toe response can be used to estimate an overall wave speed. The dynamic modulus, E, can be determined using the equation in figure 72.

PDA Testing—Initial Portion of the High-Strain Records

This method involves the initial portion of the high-strain records and the expected proportionality between measured strain and wave speed. Assuming that for low strains, the FRP piles behave as a linear elastic material and no changes in resistance or pile properties occur during the pile installation for the initial part of the high-strain record, this assumption implies that the wave speed is directly proportional to the measured strain and can, therefore, be calculated from the equation in figure 73.

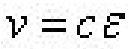

Figure 73. Equation. Pile particle speed v.

Where:
v = Pile particle speed calculated from the acceleration record.
ε = Measured strain.
c = Material wave speed.

The dynamic modulus, E, then can be determined using the equation in figure 72.

Dynamic Properties—Test Results

PIT tests were performed before driving on American Ecoboard, Lancaster Composite, Inc., PPI, and SEAPILE full-scale piles. For the FRP piles, the foam (i.e., outer layer) is stiffer than the core (i.e., inner layer). Therefore, for the American Ecoboard piles, the PIT tests were conducted on the outer layer, and for the SEAPILE and PPI piles, tests were conducted on the fiberglass bars and the reinforced foam, respectively.

In a linearly elastic pile material, such as steel or concrete, the wave speed determined from the proportionality condition (figure 73) is equal to the overall wave speed calculated from the PDA results. In the case of FRP piles, however, the overall wave speeds obtained with PIT, c_l, PDA, c_h, and the proportional wave speed, c_p, values were consistently different. Table 11 summarizes these results.

Table 11. Elastic modulus of FRP piles estimated from PIT and PDA tests.

Pile Type	Specific Weight[1]	Low Strain (PIT)		High Strain (PDA)			
	kN/m^3 (lb/ft^3)	Measured Wave Speed (Test I) c_l, m/s (ft/s)	Estimated Elastic Mod.E_l, kPa (ksi)	Proportional Wave Speed (Test II) c_p, m/s (ft/s)	Estimated Elastic Mod. E_p, kPa (ksi)	Overall Wave Speed (Test III) c_h, m/s (ft/s)	Estimated Elastic Mod. E_h, kPa (ksi)
American Ecoboard	7.9 (50)	1524 (5000)	1.86 x 10^6 (270)	1828.8 (6000)	2.68 x 10^6 (388)	1371.6 (4500)	1.50 x 10^6 (218)
Lancaster Composite	22.0 (140)	4114.8 (13500)	37.94 x 10^6 (5503)	4175.76 (13700)	39.07 x 10^6 (5667)	4023.36 (13200)	36.27 x 10^6 (5261)
PPI	8.0 (51)	3505.2 (11500)	10.03 x 10^6 (1455)	3810 (12500)	11.85 x 10^6 (1719)	3322.32 (10900)	9.01 x 10^6 (1307)
SEAPILE	8.5 (54)	2743.2 (9000)	6.50 x 10^6 (943)	3048 (10000)	8.03 x 10^6 (1165)	2529.84 (8300)	5.53 x 10^6 (802)

[1] Reported by the manufacturers.

DYNAMIC PILE TESTING DATA ANALYSIS

The PDA data analysis was conducted to obtain the dynamic properties, including Smith damping and soil quake, and evaluate the load-set response and the static bearing capacity of the FRP piles. The dynamic analysis involved:

- Case method analysis (PDA)—for onsite measurement of the transfer energy and evaluation of the driving system performance, pile stresses, structural integrity, and static capacity.
- CAPWAP analysis—using the force and velocity data recorded in the field to obtain the dynamic properties, including Smith damping and soil quake, and to evaluate the load-set pile response.
- GRLWEAP—using CAPWAP analysis results to evaluate the dynamic Young's modulus of each FRP composite pile.

The dynamic analysis results were compared to the results of SLTs performed on four FRP piles.

Case Method Analysis (PDA)

During the PDA testing, the Case Method is used to interpret the measured dynamic data to assess the hammer and driving system performance, determine pile head compression stresses, evaluate structural integrity, and estimate the static pile capacity. Table 12 summarizes the PDA dynamic test results, including the maximum measured pile top strain, maximum compressive stress, maximum estimated tensile stress, transfer energy to pile, hammer operating rate, and the pile capacities calculated by the case method and by CAPWAP analysis. The maximum compressive and tensile stresses were calculated using the dynamic elastic modulus obtained

with the PDA testing, considering the wave speed-strain proportionality condition of the initial portion of the high-strain records.

CAPWAP Analysis

The CAPWAP Version 2000-1 was used with the data recorded in the field to evaluate the ultimate pile capacity of the tested piles. CAPWAP analyses compute soil resistance forces and their approximate distribution using the velocity and speed data recorded in the field during the dynamic pile testing. The CAPWAP results include an evaluation of the soil resistance distribution, soil quake and damping factors, and a simulated static load-set graph. The static load-set simulation is based upon the CAPWAP calculated static resistance parameters and the elastic compression characteristics of the pile. For each pile, the three elastic modulus values calculated from PDA and PIT tests as reported in table 11 were considered. The CAPWAP analyses using the elastic modules calculated from PDA testing and considering the initial portion of the high-strain records (1) yielded the most reasonable energy values for the ICE 70 hammer and (2) predicted load-set curves that yielded the best correlation with SLT results. CAPWAP static capacities calculated using the dynamic elastic modulus values are reported in table 13.

Table 12. PDA results.

Pile Designation	Test Date	Pile Penetration,[1] m (ft)	Blow Count,[1] blows/m (blows/ft)	Average Maximum Measured Strain (με)	Average Maximum Compressive Stress,[2] kPa (ksi)	Maximum Estimate Tensile Stress,[3] kPa (ksi)	Average Transfer Energy,[2] kJ (ft-kips)	Hammer Rate, blows/ min	Case Method Capacity,[4] kN (kips)	CAPWAP Estimated Capacity, kips	Remarks[5]
Steel Reference	11/14/01	18.9 (62)	36.1 (11)	714	147,547.8 (21.4)	NA	23.1(17)	47	413.7 (93)	489.3 (110)	EOI
	5/24/02	18.6 (61)	0.31 b/mm (8/inch)	499	103,421.4 (15.0)	NA	13.6 (10)	45	1267.7 (285)	1156.5 (260)	BOR
Ecoboard	5/22/02	8.8 (29)	98.4 (30)	1540	4,136.9 (0.6)	689.5 (0.1)	12.2 (9)	76	435.9 (98)	382.5 (86)	EOI, Section 2; 9.75-inch cushion
Lancaster 1	11/14/01	17.7 (58)	210.0 (64)	392	151,684.7 (2.2)	3447.5 (0.5)	14.9 (11)	50	186.8 (42)	–	ID, Section 1; 9.75-inch cushion
	11/14/01	26.5 (87)	298.6 (91)	523	199,948.0 (2.9)	5516 (0.8)	17.6 (13)	49	1450 (326)	–	EOI, Section 2; 7.5-inch cushion
	5/24/02	26.2 (86)	1.5 b/mm (77/ 0.5 inch)	448	16,547.4 (2.5)	4137 (0.6)	16.3 (12)	43	2375.2 (534)	2090.6 (470)	EOR
Lancaster 4	11/15/01	17.7 (58)	154.2 (47)	377	14,479.0 (2.1)	5516 (0.8)	12.2 (9)	52	346.9 (78)	–	EOI; 6-inch cushion
	5/24/02	17.1 (56)	0.96 b/mm (25/inch)	324	12411 (1.8)	1379 (0.2)	9.5 (7)	52	1072 (241)	–	BOR
Lancaster 3 (SLT)	11/15/01	17.7 (58)	154.2 (93)	399	15858.5 (2.3)	8274 (1.2)	13.6 (10)	56	480.4 (108)	516 (116)	EOI; 6-inch cushion; 2-ft stroke
	5/24/02	17.1 (56)	1.20 b/mm (31 / inch)	309	11721.5 (1.7)	1379 (0.2)	9.5 (7)	44	1049.7 (236)	1000.8 (225)	BOR
PPI 5	11/15/01	19.2 (63)	121.4 (37)	436	5171.25 (0.75)	2068.5 (0.3)	9.5 (7)	49	453.7 (102)	–	EOI; 9.75-inch cushion
	5/23/02	17.7 (58)	0.94 b/mm (24 / inch)	514	6205.5 (0.9)	689.5 (0.1)	6.8 (5)	45	756.2 (170)	–	BOR
PPI 7	11/15/01	19.05 (62.5)	111.5 (34)	535	6205.5 (0.9)	2068.5 (0.3)	10.9 (8)	48	484.8 (109)	–	EOI; 9.75-inch cushion
	5/23/02	17.7 (58)	0.82 b/mm (21 / inch)	529	6205.5 (0.9)	1379 (0.2)	6.8 (5)	44	791.7 (178)	–	BOR
PPI 6 (SLT)	11/15/01	18.6 (61)	88.6 (27)	373	4137 (0.6)	2068.5 (0.3)	8.1 (6)	47	387 (87)	409.2 (92)	EOI; 9.75-inch cushion
	5/24/02	17.7 (58)	0.86 b/mm (22 / inch)	654	7584.5 (1.1)	1379 (0.2)	10.9 (8)	44	938.5 (211)	978.6 (220)	BOR
Seaward 8	11/16/01	18.6 (61)	78.7 (24)	875	6895 (1.0)	2758 (0.4)	13.6 (10)	57	382.5 (86)	–	EOI; 9.75-inch cushion
	5/22/02	17.7 (58)	0.86 b/mm (22 / inch)	858	6895 (1.0)	1379 (0.2)	12.2 (9)	56	885.2 (199)	–	BOR
Seaward 10	11/16/01	18.6 (61)	62.3 (19)	855	6895 (1.0)	2758 (0.4)	17.6 (13)	54	516 (116)	–	EOI; 9.75-inch cushion
	5/22-23/02	17.7 (58)	0.39 b/mm (10 / inch)	926	7584.5 (1.1)	1379 (0.2)	16.3 (12)	43	978.6 (220)	–	BOR
Seaward 9 (SLT)	11/16/01	18.7 (61.3)	118.1 (36)	758	6205.5 (0.9)	2758 (0.4)	12.2 (9)	57	516 (116)	520.4 (117)	EOI; 9.75-inch cushion
	5/23/2002	17.7 (58)	0.51 b/mm (13 / inch)	1074	8274 (1.2)	1379(0.2)	14.9 (11)	45	978.6 (220)	1067.5 (240)	BOR– Original CW

[1] Pile penetrations from ground surface for initial installation and bottom of excavation for restrike. 1 inch = 2.54 cm, 1 ft = 0.305 m
[2] Measured at the location of the transducers.
[3] Maximum tension stress estimated over all blows.
[4] Using RX9 (maximum case method with Jc = 0.90) equation.
[5] Unless otherwise noted, 3-ft hammer stroke.
BOR—Beginning of redrive.
EOI—End of installation.

CAPWAP analyses were performed on the records obtained for both the EOI and the beginning of restrike (BOR) of each SLT pile, the steel reference pile, and the Lancaster Composite, Inc., pile (No. 1), which was driven to refusal. The results are summarized in table 13.

Table 13. CAPWAP program calculation results.

Pile Designation	Penetration Depth in Soil, m (ft)	Driving Resistance, blows/set	CAPWAP							Remarks
			Static Capacity Estimate			Smith Damping		Soil Quakes		
			Shaft, kN (kips)	Toe, kN (kips)	Total, kN (kips)	Shaft, s/m (s/ft)	Toe, s/m (s/ft)	Shaft, mm (inch)	Toe, mm (inch)	
Steel Pile	18.9 (62)	11/ft	369.2 (83)	120.1 (27)	489.3 (110)	0.26 (0.08)	0.16 (0.05)	2.8 (0.11)	26.9 (1.06)	EOI
	18.3 (60)	8/inch	1049.7 (236)	106.8 (24)	1156.5 (260)	0.69 (0.21)	0.66 (0.2)	2.3 (0.09)	6.9 (0.27)	BOR
American Ecoboard (SLT)	8.8 (29)	30/ft	102.3 (23)	280.2 (63)	382.5 (86)	0.95 (0.29)	1.05 (0.32)	2.8 (0.11)	16.0 (0.63)	EOI; after splicing
Lancaster 1	25.9 (85)	77/0.5 inch	702.8 (158)	1387.8 (312)	2090.6 (470)	0.66 (0.2)	1.05 (0.32)	2.5 (0.10)	1.27 (0.05)	EOR; pile driven to refusal
Lancaster 3 (SLT)	17.7 (58)	93/ft	240.2 (54)	275.8 (62)	516 (116)	0.66 (0.2)	0.1 (0.03)	3.0 (0.12)	18.3 (0.72)	EOI
	18.3 (60)	32/inch	836.2 (188)	164.6 (37)	1000.8 (225)	1.12 (0.34)	1.25 (0.38)	2.0 (0.08)	3.8 (0.15)	BOR
PPI 6 (SLT)	18.6 (61)	27/ft	329.2 (74)	80.1 (18)	409.2 (92)	0.39 (0.12)	0.69 (0.21)	3.6 (0.14)	16 (0.63)	EOI
	17.7 (58)	22/inch	818.4 (184)	160.1 (36)	978.6 (220)	0.75 (0.23)	1.28 (0.39)	3.3 (0.13)	3.8 (0.15)	BOR
Seaward 9 (SLT)	18.7 (61.3)	36/ft	400.3 (90)	120.1 (27)	520.4 (117)	0.66 (0.2)	0.79 (0.24)	2.3 (0.09)	15.5 (0.61)	EOI
	17.4 (57)	130	969.7 (218)	97.9 (22)	1067.5 (240)	0.98 (0.3)	1.25 (0.38)	2.5 (0.10)	2.8 (0.11)	BOR
	17.4 (57)	130	809.5 (182)	84.5 (19)	889.6 (200)	0.89 (0.27)	1.45 (0.45)	2.5 (0.10)	2.0 (0.08)	BOR; revised with SLT

BOR—Beginning of restrike.
EOI—End of installation.
EOR—End of redrive.

Table 14 shows the quake and damping values recommended by the consulting firm GRL Engineers, Inc., for various types of soils and piles.

Table 14. Quake and damping values recommended by GRL.

	Soil Type	Pile Type or Size	Quake mm (in)	Damping Factors/m (s/ft)
Shaft Quake	All soil types	All Types	2.5 (0.10)	–
Toe Quake	All soil types, soft rock	Open ended pipes	2.5 (0.10)	–
	In dry soils, or in very dense or hard soils	Displacement piles of diameter D or width D	D/120	–
	In submerged soils or in loose or soft soils	Displacement Piles of diameter D or width D	D/60	–
Shaft Damping	Noncohesive soils	–	–	0.16 (0.05)
	Cohesive soils	–	–	0.65 (0.20)
Toe Damping	In all soil types	–	–	0.50 (0.15)

Comparison of the CAPWAP analysis results reported in table 13 and the GRL recommendations summarized in table 14 leads to the following conclusions:

- The recommended soil shaft quake values appear to be consistent with the CAPWAP results obtained at the beginning of restriking for all the piles tested, with the exception of the PPI piles. The soil quake values obtained for the PPI piles are about 30 percent greater than those recommended by GRL. As soil shaft quake values are generally assumed to be independent of the pile type, the values obtained for PPI piles are most probably affected by local damages at the pile head observed during the pile driving.
- For the soil type of the site, submerged soils, recommendations yield soil toe quake values of D/60 = 6.85 mm (0.27 inch), where D is the pile diameter. This value agrees with the CAPWAP analysis results obtained at the beginning of restriking for the reference steel pile. The soil toe quake values obtained for the Lancaster Composite, Inc., PPI, and SEAPILE piles are significantly lower (about 45 percent) than the values recommended by GRL.
- Comparing the values of the soil toe quake obtained for all the test piles at the EOI with those obtained at the BOR, the dissipation of excess pore water pressure generated during pile driving resulted in a significant decrease (up to 80 percent) of the soil toe quake values.
- The Smith shaft damping values recommended by GRL for the soil profile at this test site, which consists of cohesive and noncohesive soil layers, are within the range of 0.16 to 0.65 second (s)/m (0.05 to 0.20 s/ft). These values appear to be consistent with the CAPWAP results obtained at the EOI for all the piles tested. It should, however, be noted that the Smith shaft damping values obtained at the EOI for the FRP piles are about 250 percent greater than those obtained for the reference steel pile.
- For all soil types, GRL recommendations yield a toe damping value of 0.49 s/m (0.15 s/ft). This value is consistent with the CAPWAP analysis results obtained at the beginning of restriking for the reference steel pile, indicating a toe damping value of

0.65 s/m (0.2 s/ft). The toe damping values obtained for the American Ecoboard, Lancaster Composite, Inc., PPI, and SEAPILE piles are consistently greater (about 250 percent) than the values recommended by GRL.

- Comparing the values obtained for all the test piles at EOI with those obtained at the BOR, the dissipation of excess pore water pressure generated during pile driving resulted in a significant increase (up to about 100 percent) of the shaft and toe Smith damping.

GRLWEAP Analysis

To evaluate the dynamic testing procedures used to obtain the dynamic elastic modulus of the FRP piles (i.e., PIT, the PDA testing—high-strain record, and the PDA testing considering the proportionality condition), a parametric study was conducted using the GRLWEAP Version 2002-1 program. GRLWEAP computes the number of blows per foot and the energy at the pile top. The parametric study consisted of calculating, for each FRP pile, the transfer energy obtained by PDA, the static capacity calculated by CAPWAP, and the number of blows per foot using the different elastic modulus values obtained with these testing procedures (table 15). The calculated transfer energy was compared to the PDA results, and the calculated blow counts were compared to the measured number of blows per inch at the beginning of restriking of each pile. CAPWAP results, including ultimate pile capacity, soil quake, and toe and shaft damping are used as GRLWEAP input data (table 13).

Table 15. Comparison of GRLWEAP results with measured elastic modulus, number of blows, and energy.

Pile Manufacturer	Measured Elastic Modulus, kPa (ksi)		Measured Number of Blows, blows/m (blows/ft)	Calculated Number of Blows (GRLWEAP), kN/m (kips/ft)	Measured Energy (PDA), kN/m (kips/ft)	Calculated Energy (GRLWEAP), kN/m (kips/ft)
SEAPILE	PIT—low strain	6.5×10^6 (943)	515.1 (157)	18427.2 (1263)	160.5 (11)	145.9 (10)
	PDA—high strain	5.5×10^6 (802)		4537.5 (311)		145.9 (10)
	PDA—early portion of high-strain records	8×10^6 (1165)		2290.6 (157)		145.9 (10)
PPI	PIT—low strain	10×10^6 (1455)	872.7 (266)	21899.6 (1501)	116.7 (8)	116.7 (8)
	PDA—high strain	9×10^6 (1307)		7893.2 (541)		116.7 (8)
	PDA—early portion of high-strain records	11.9×10^6 (1719)		3881 (266)		116.7 (8)
American Ecoboard	PIT—low strain	1.9×10^6 (270)	98.4 (30)	525.2 (36)	131.3 (9)	189.7 (13)
	PDA - high strain	1.5×10^6 (218)		481.5 (33)		189.7 (13)
	PDA—early portion of high-strain records	2.7×10^6 (388)		437.7 (30)		189.7 (43)

The results of this parametric study (figures 74, 75, and 76) illustrate (for the same transfer energy level) the effect of the elastic modulus on the number of blows per foot for the American Ecoboard, PPI, and SEAPILE piles. The GRLWEAP calculations show that the elastic modulus obtained from PDA testing—considering the proportionality condition for the initial portion of the high-strain records—yields the best agreement between (1) the calculated values of the transfer energy level and the energy measured by PDA and (2) the calculated blow count and the measured field records. Figure 74 shows that for the American Ecoboard pile, the effect of Young's modulus on the blow count was relatively small. This may be because Young's modulus values measured by PDA and PIT tests for the American Ecoboard pile were relatively small, compared to those obtained for the PPI and SEAPILE pile materials.

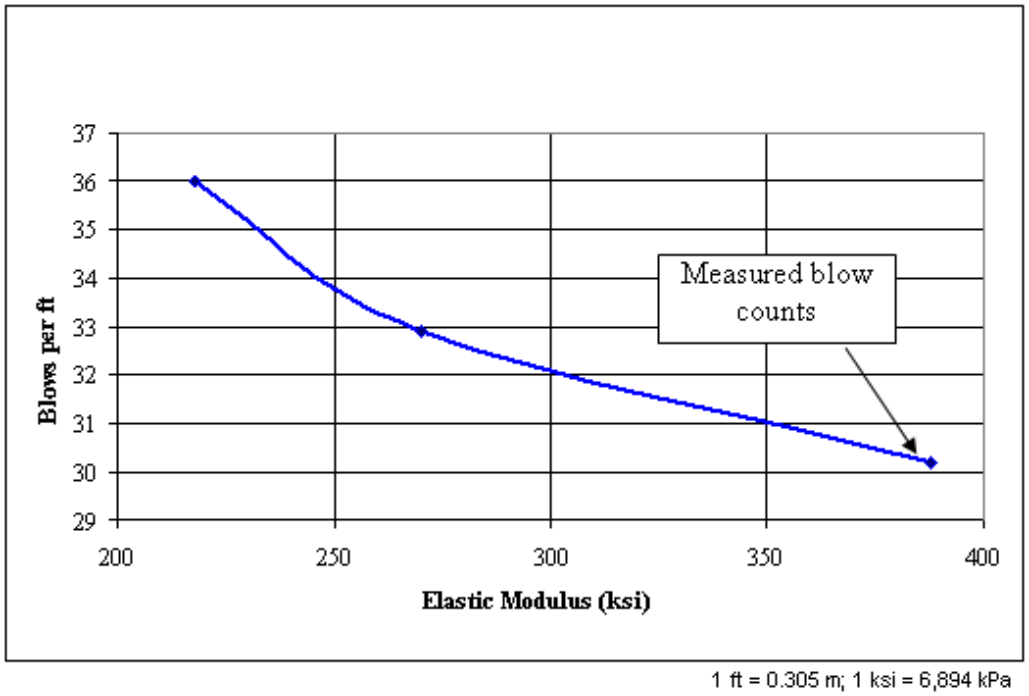

Figure 74. Graph. American Ecoboard pile—blows per foot versus elastic modulus.

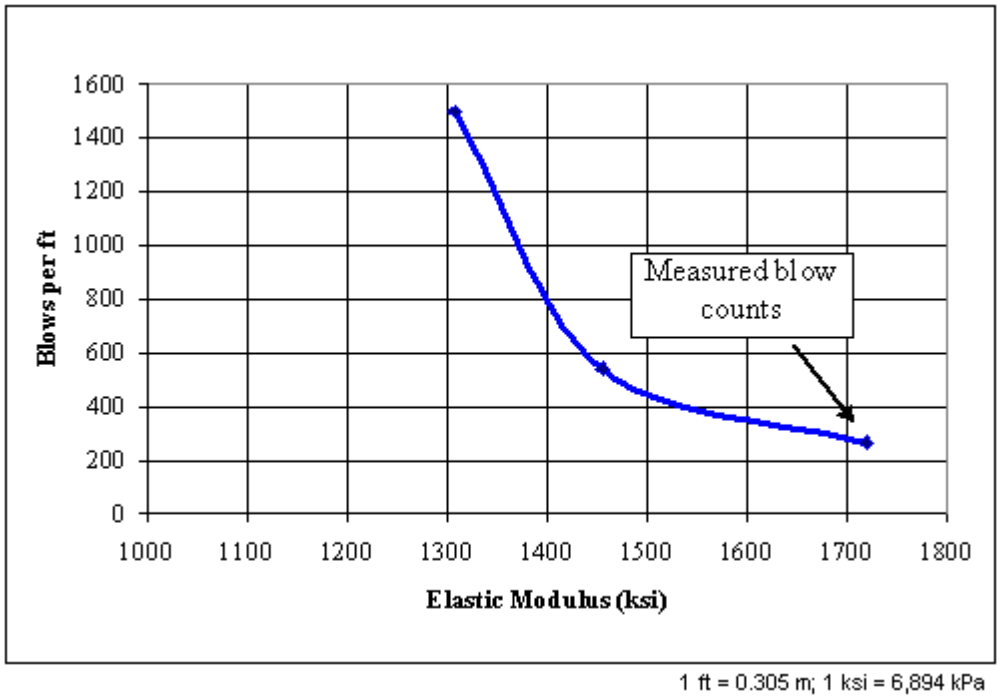

Figure 75. Graph. PPI pile—blows per foot versus elastic modulus.

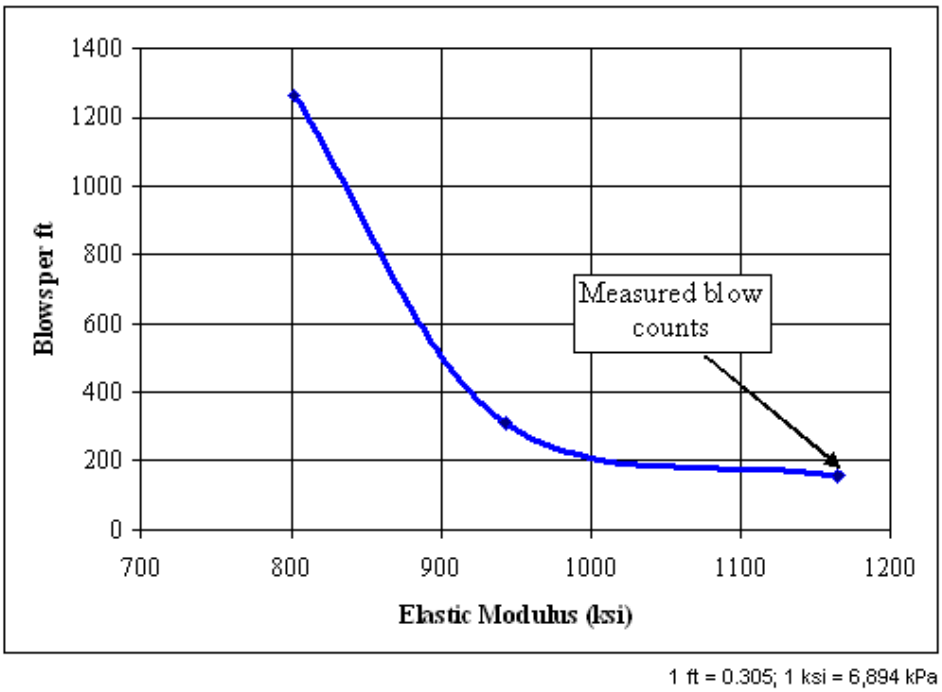

Figure 76. Graph. SEAPILE pile—blows per foot versus elastic modulus.

In general, materials exhibit stiffer behavior as the rate of loading increases. Thus, when comparing dynamic test results with those obtained from static laboratory or field load tests, the dynamic modulus are generally greater than the static elastic modulus.

In table 16, the dynamic elastic modulus, calculated from PDA testing—early portion of the high-strain records, are compared with static elastic modulus for steel and FRP piles, including the PPI and SEAPILE piles, obtained from laboratory compression tests. For steel, which is a rigid material compared to the FRP materials, the difference between static and dynamic modulus is 3 percent. The ratio of dynamic-to-static elastic modulus for FRP materials is 1.64 and 2.38 for the PPI plastic with steel bars and SEAPILE plastic with fiberglass bars, respectively.

Table 16. Comparison, static and dynamic elastic modulus of SEAPILE, PPI, and steel piles.

Pile Manufacturer	Static Elastic Modulus, kPa (ksi)	Dynamic Elastic Modulus, kPa (ksi)	Dynamic Elastic Modulus/ Static Elastic Modulus
SEAPILE	3.38×10^6 (490)	8.03×10^6 (1165)	2.38
PPI	7.22×10^6 (1048)	1.185×10^7 (1719)	1.64
Steel	1.999×10^8 (29000)	2.068×10^8 (30000)	1.03

STATIC LOAD TEST RESULTS—CORRELATIONS WITH CAPWAP ANALYSIS

Pile Capacity and Setup

One of the main objectives of the field demonstration project was to evaluate the dynamic method currently used for predicting the load-set response and ultimate static capacity of FRP piles. To simulate the field conditions as consistently as possible, the static load results were used to evaluate the maximum ratio of the toe bearing capacity to the shaft resistance as an input data for the CAPWAP analysis. The CAPWAP analysis results for the total static capacity, the shaft resistance, and the toe bearing capacity for all the test piles at the EOI and BOR are indicated in table 13.

The PDA and CAPWAP analysis results summarized in tables 12 and 13 show that all the piles experienced a long-term increase in pile capacity from the EOI to the BOR. The capacity gains ranged from 311.4 to 854.1 kN (70 to 192 kips) for the piles installed to 17.7-m (58-ft) penetrations. For most of the tested piles, the measured setup factor, defined as a ratio of the BOR to EOI capacities, is in excess of 2.0. For all the SLT piles, the CAPWAP capacities ranged from 938.6 to 1,267.7 kN (211 to 285 kips) during the BOR and from 186.8 to 556.0 kN (42 to 125 kips) at the EOI.

In general, the CAPWAP analysis showed that at the BOR for the piles driven to penetrations of 17.7 m (58 ft), most of the ultimate capacity was due to the shaft resistance, which ranged from 827.4 to 1,049.8 kN (184 to 236 kips). The toe resistance ranged from 97.9 to 164.6 kN (22 to 37 kips). For the American Ecoboard pile, which was driven to a penetration depth of 8.8 m (29 ft), the analysis yielded a shaft resistance of 102.3 kN (23 kips) and a toe resistance of 280.2 kN

(63 kips). The Lancaster Composite, Inc., pile, which was driven to refusal at a depth of 26.5 m (87 ft), had a mobilized ultimate capacity of 2,090.7 kN (470 kips) at the end of redrive, with 1,387.8 kN (312 kips) in toe resistance.

Correlations of CAPWAP Analysis With Static Load Test Results

Figures 78 through 81 illustrate the comparison between the load-set curves calculated by the CAPWAP program for the BOR and the SLT results for the Lancaster Composite, Inc., PPI, SEAPILE, and American Ecoboard piles. Table 17 summarizes the main experimental and dynamic analysis results, including the maximum applied or ultimate loads and the corresponding pile top settlements. These settlements are also compared with the elastic settlements of the piles due to their elastic compression, which are calculated assuming that the Lancaster Composite, Inc., PPI, and SEAPILE piles are frictional piles. For frictional piles, assuming a constant load transfer rate along the pile, the settlement due to the elastic compression, $S_{elastic}$, can be approximately calculated by the equation in figure 77.

$$S_{elastic} = \frac{P_{max}}{EA} * \frac{L}{2}$$

Figure 77. Equation. $S_{elastic}$.

Where:
P_{max} = Maximum applied or ultimate load.
E = Elastic modulus of the pile.
A = Pile section area.
L = Pile length.

The elastic modulus values indicated in table 17 were obtained from laboratory static compression tests conducted on FRP pile samples, taking into consideration the initial quasilinear portion of the stress-strain curves.

Table 17. Comparison between CAPWAP analysis and static load test results.

Pile Manufacturer	CAPWAP		Static Load Test		EA, kN (kips)	$S_{elastic}$, mm (inches)
	P_{max}, kN (kips)	S_{limit}, mm (inches)	P_{max}, kN (kips)	S_{limit}, mm (inches)		
Lancaster Composite (end of first loading cycle)	1000 (224.8)	5 (0.2)	1000 (224.8)	7.5 (0.3)	4.1 x 10^6 (0.9 x 10^6)	2.3 (0.1)
PPI	980 (220.3)	12 (0.5)	1100 (247.3)	9.6 (0.4)	0.9 x 10^6 (0.2 x 10^6)	11 (0.4)
SEAPILE	900 (202.3)	15 (0.6)	800 (179.8)	9.8 (0.4)	0.745 x 10^6 (1.67 x 10^5)	16.8 (0.7)
American Ecoboard	382 (85.9)	30 (1.2)	600 (134.9)	93.0 (3.6)	–	–
			400 (89.9)	40 (1.6)		

The comparison between the CAPWAP analysis and the SLT results for the FRP piles leads to the following observations.

For the Lancaster Composite, Inc., SLT pile, the CAPWAP analysis yields a load-set curve, which is quite consistent with the results of the first static load cycle. However, it leads to underestimating the total bearing capacity of the pile reached in the second load cycle. The difference between the CAPWAP analysis and the SLT results is likely due to the very high blow counts observed during the restrike (approximately 1 blow/mm (32 blows/inch)). With such low sets, the pile displacement under the dynamic load appears to be too small to fully mobilize the soil resistance and to obtain reliable measurements of the velocity and the force waves as input data for the CAPWAP analysis.

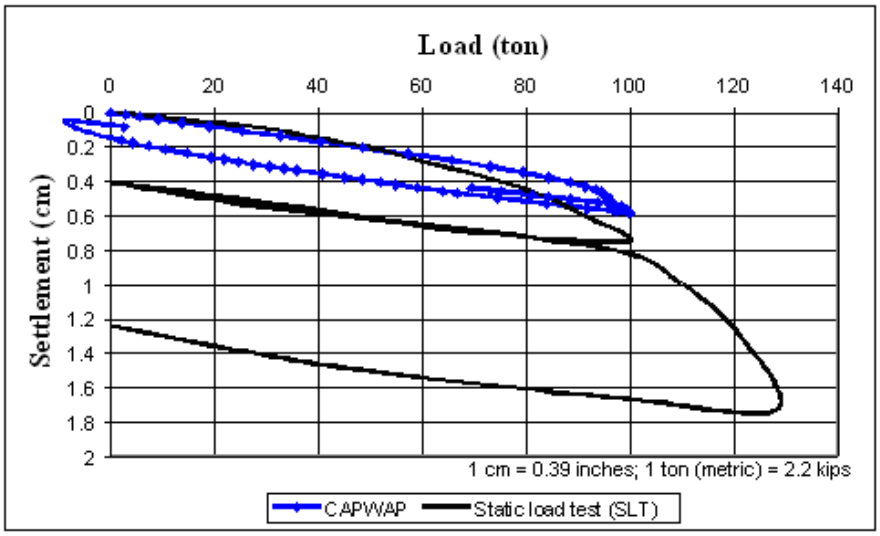

Figure 78. Graph. SLT and CAPWAP analysis—Lancaster Composite, Inc., pile.

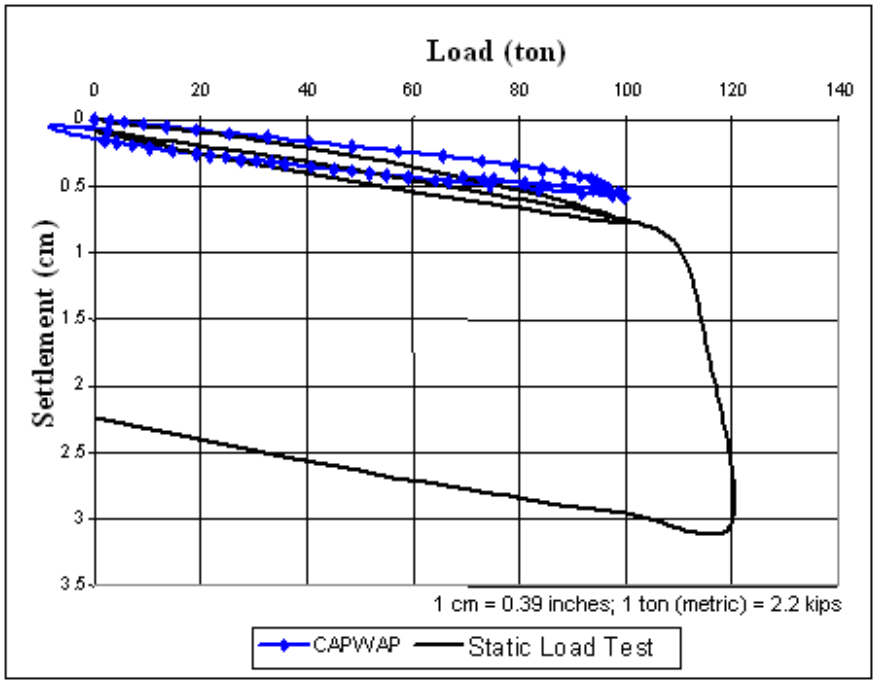

Figure 79. Graph. SLT and CAPWAP analysis—PPI pile.

For the PPI SLT pile, the CAPWAP analysis yields an ultimate capacity that corresponds to about 90 percent of the plunging failure load observed during the SLT. The predicted limit settlement at failure is about 25 percent higher than the measured settlement, indicating that the CAPWAP analysis underestimates the stiffness of the pile response to static loading. The calculated elastic settlement due to pile compression is quite close to the limit settlement calculated by CAPWAP and slightly exceeds the experimental value. This seems to indicate that for the PPI pile, due to its low stiffness compared with the Lancaster Composite, Inc., pile, the settlement at failure is mainly the result of the elastic compression of the pile during loading.

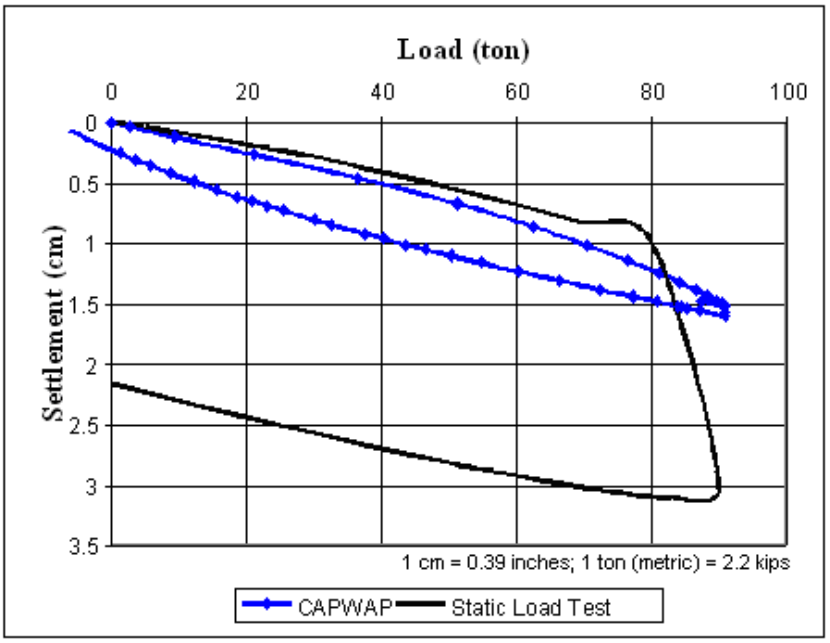

Figure 80. Graph. SLT and CAPWAP analysis—SEAPILE pile.

For the SEAPILE SLT pile, the CAPWAP analysis yields an ultimate capacity that corresponds to about 112.5 percent of the plunging failure load observed during the SLT. Similar to the PPI pile, the predicted limit settlement at failure is higher (about 25 percent under the experimental ultimate load) than the experimental settlement, indicating that the CAPWAP analysis underestimates the stiffness of the pile response to static loading. Consistent with the results obtained for the PPI pile, the calculated elastic settlement due to pile compression is quite close to the limit settlement calculated by CAPWAP and exceeds the experimental value. This seems to confirm that for the SEAPILE and PPI tested piles, the settlement at failure is mainly the result of the elastic compression of the pile during loading.

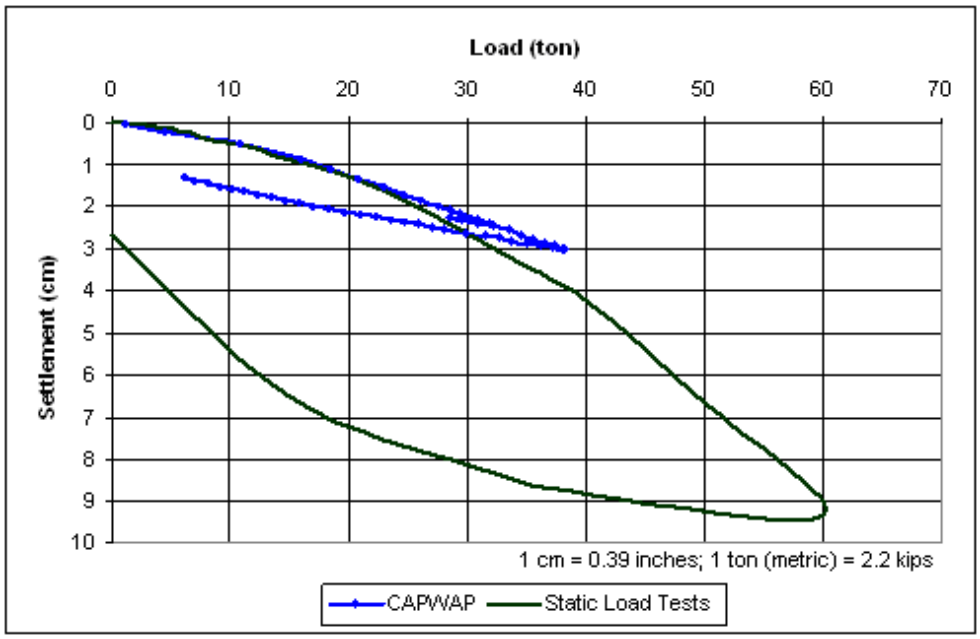

Figure 81. Graph. SLT and CAPWAP analysis—American Ecoboard pile.

For the American Ecoboard SLT pile, the CAPWAP analysis showed a good correlation with the SLT up to 2 cm (0.8 inch) settlement at a load of 25 t (5.6 kips). CAPWAP analysis to predict the behavior of piles during SLTs is limited to settlements that do not exceed approximately 5 cm (2 inches). This might explain the difference between the SLT behavior and CAPWAP prediction curve for the low stiffness American Ecoboard pile, which reached a settlement of 96 mm (3.8 inches) under the static loading of 600 kN (134.9 kips). In addition, the American Ecoboard pile was driven to the sandy layer to assess its behavior primarily as an end bearing pile. The experimental results illustrated that no distinct plunging occurred under the applied static loading. As indicated in table 13, for this pile, the CAPWAP analysis predicted a ratio of end bearing to shaft resistance of 270 percent, which is substantially higher than that predicted for all the FRP piles driven to the clay layer at the depth of about 20 m (65.6 ft).

Pile Tension and Tensile Stress During Driving

In situ evaluation of the integrity of FRP piles during driving requires: (1) reliable data monitoring for determining the compression and tension stresses in the pile, and (2) development of appropriate design criteria for the allowable dynamic stresses in the composite pile material and its basic components.

Figures 84 through 87 show typical pile stress versus penetration depth profiles obtained for the Lancaster Composite, Inc., PPI, SEAPILE, and American Ecoboard piles from the field PDA testing. The dynamic elastic modulus used for this analysis was determined from the proportional condition of the initial portion of the high-strain records. The results show that the calculated tensile stresses did not exceed 6,894.8 kPa (1 ksi); calculated compressive stresses at the pile top ranged from 4,136.9 to 15,857.9 kPa (0.6 to 2.3 ksi) during the driving of all FRP piles.

The design criteria for allowable compression and tension stresses in the FRP piles were primarily developed considering the equation of the axial force equilibrium for the composite material and assuming no delamination between its basic components (figure 82).

$$F = A^t \sigma^t = \sigma^r_{allowable} A^r + \sigma^p_{allowable} A^p$$

Figure 82. Equation. Applied axial force F.

Where:

F = The applied axial force.
A^t = Total pile cross section area.
A^r = Total cross section area of the reinforcement.
A^p = Total cross section area of the plastic or concrete materials.
σ^t = Equivalent axial stress, tension or compression, acting on the pile section.
$\sigma^r_{allowable}$ = Allowable axial stress, tension or compression, acting in the pile reinforcements.
$\sigma^p_{allowable}$ = Allowable axial stress, tension or compression, acting in the plastic material or the concrete for the Lancaster Composite, Inc., pile.

The equation in figure 82 can be solved for the equivalent allowable axial stress in the composite pile section (figure 83).

$$\sigma^t = \sigma^r_{allowable} \frac{A^r}{A^t} + \sigma^p_{allowable} \frac{A^p}{A^t}$$

Figure 83. Equation. Equivalent axial stress σ^t.

Table 18 summarizes the main criteria used for establishing the allowable stresses for the FRP pile installation. It also shows, for each pile, the actual stresses measured by PDA during pile driving.

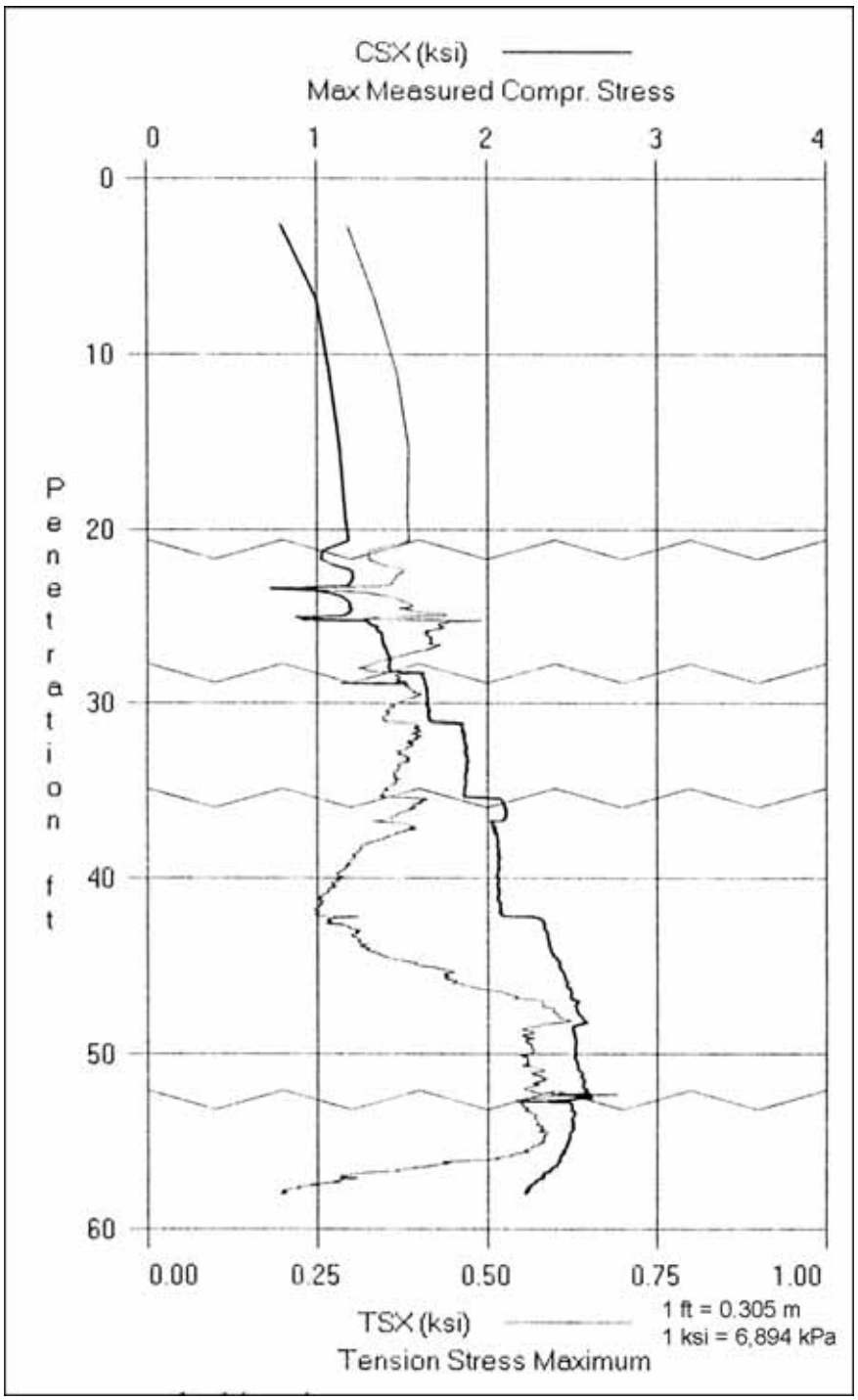

Figure 84. Graph. Stress versus penetration depth for Lancaster Composite, Inc., SLT pile.

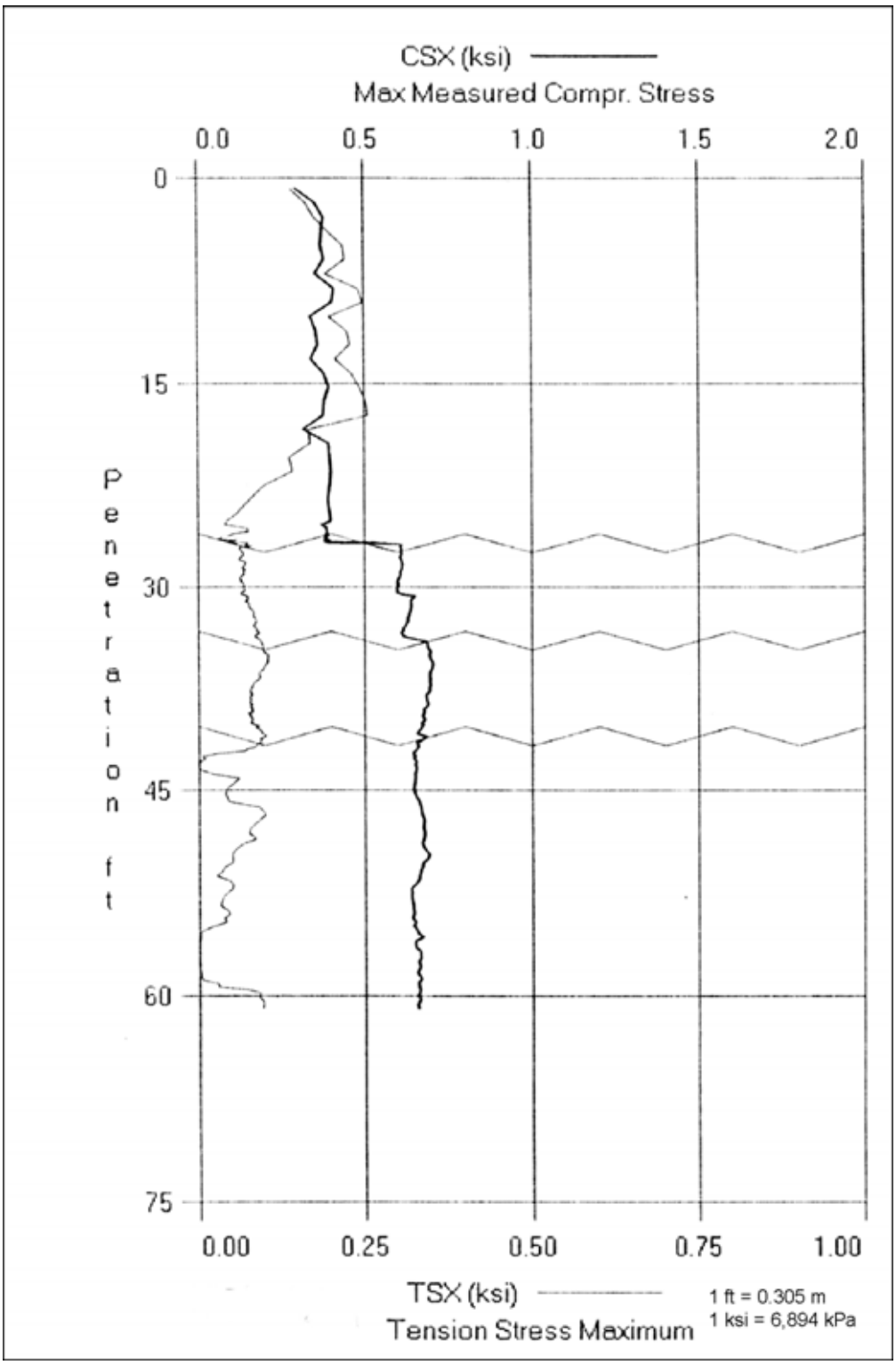

Figure 85. Graph. Stress versus penetration depth for PPI SLT pile.

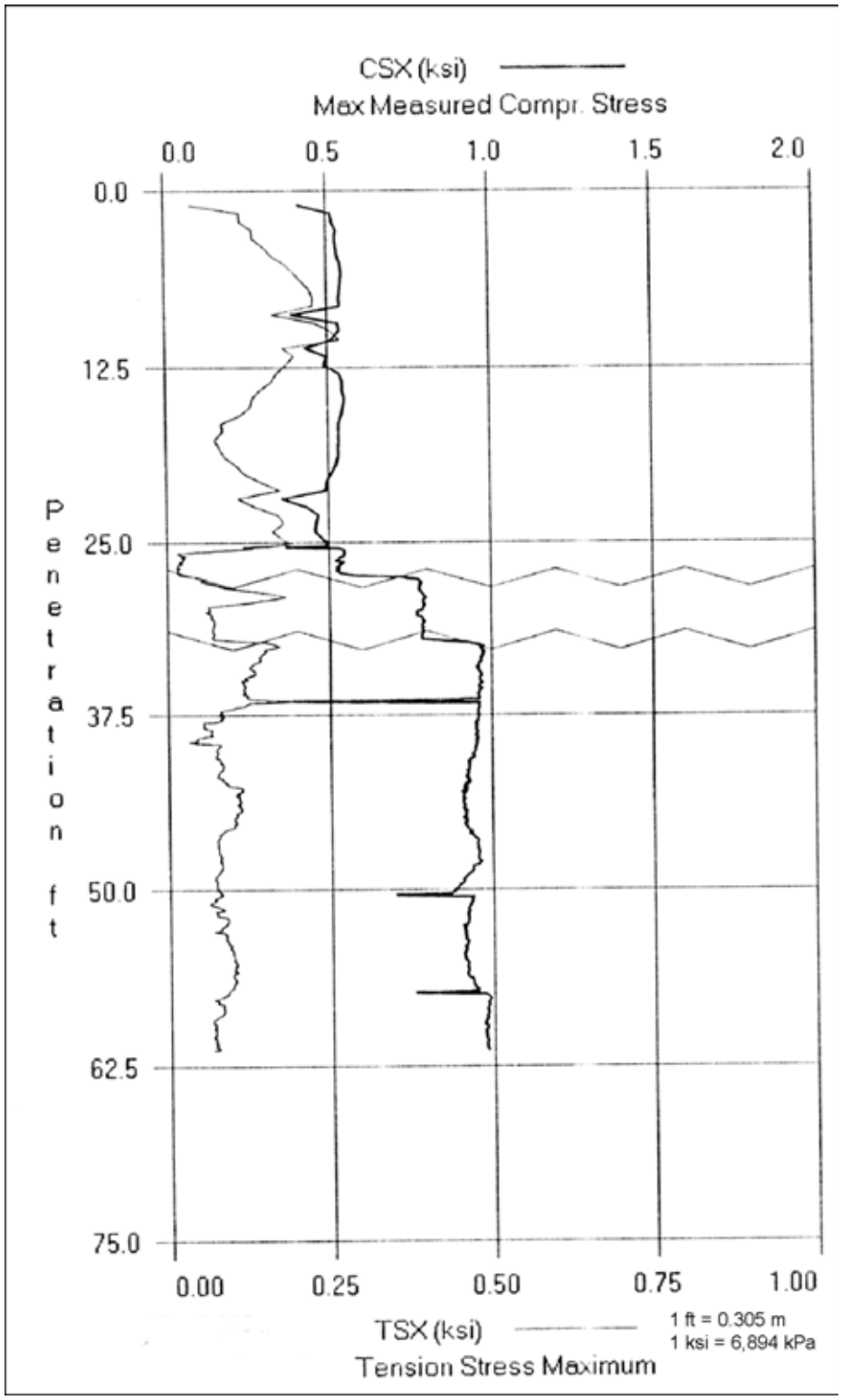

Figure 86. Graph. Stress versus penetration depth for SEAPILE SLT pile.

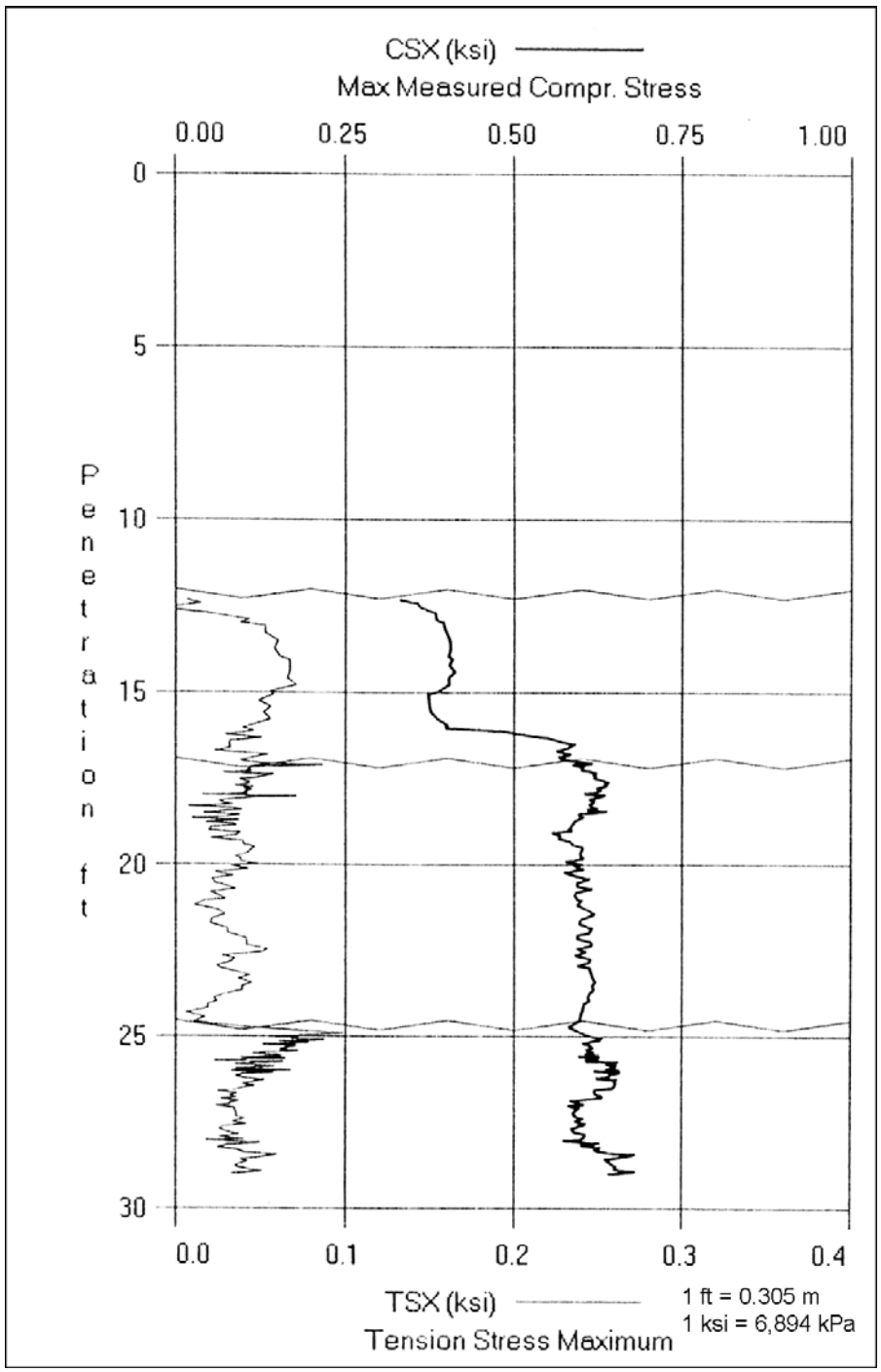

Figure 87. Graph. Stress versus penetration depth for American Ecoboard splice SLT pile.

Table 18. Measured and allowable stresses for FRP piles.

Type of Stress	Lancaster Composite	Lancaster Composite; Driven to the Bedrock Layer	Seaward International	PPI	American Ecoboard	Steel Pile
Compressive stress, kPa (ksi)	85% of the concrete compressive strength	85% of the concrete compressive strength	$\sigma^m_{allowable}$=0 A^r/A^t=0.175 σ^r=1.81x10^5 (26)	$\sigma^m_{allowable}$=0 A^r/A^t=0.011 σ^r=2.89x10^5 (42)	–	90% of yield strength for steel piles
Tension stress	$\sigma^m_{allowable}$=0 A^r/A^t=0.036 σ^r=3.47x10^5 (50.3)	$\sigma^m_{allowable}$=0 A^r/A^t=0.036 σ^r=3.47x10^5 (50.3)	$\sigma^m_{allowable}$=0 A^r/A^t=0.175 σ^r= NA	$\sigma^m_{allowable}$=0 A^r/A^t=0.011 σ^r=2.89x10^5 (42)	–	90% of yield strength for steel piles
Allowable compressive stress, kPa (ksi)	37233 (5.4)	37233 (5.4)	31027.5 (4.5)	3171.7 (0.46)	NA	–
Allowable tension stress, kPa (ksi)	12617.9 (1.83)	12617.9 (1.83)	NA	3171.7 (0.46)	NA	–
Maximum measured compressive stress, kPa (ksi)	15858.5 (2.3)	19995.5 (2.9)	8274 (1.2)	7584.5 (1.1)	4895.5 (0.71)	183407 (26.6)
Maximum measured tension stress, kPa (ksi)	7998.2 (1.16)	5791.8 (0.84)	2827 (0.41)	2206.4 (0.32)	689.5 (0.1)	9790.9 (1.42)
Maximum measured compressive stress during restrike, kPa (ksi)	14824.3 (2.15)	16548 (2.4)	8549.8 (1.24)	8205.1 (1.19)	–	238567 (34.6)
Maximum measured tension stress during restrike, kPa (ksi)	1448 (0.21)	4137 (0.60)	3378.6 (0.49)	(0.18)	–	(9.2)

During pile driving, the measured compression and tension stresses did not exceed the allowable stresses, except for PPI pile. During and after pile driving and restriking of PPI and SEAPILE piles, no damage or separation between the bars and the recycled plastic material was observed, except at the upper foot of each PPI pile. In the case of the Lancaster Composite, Inc., piles, no damage or separation between the concrete and the FRP shell piles was observed (figures 68 through 71). Following these site observations, in the absence of experimental data, the maximum stresses obtained for the FRP piles can be used to establish allowable tension and compression stresses for pile driving.

CHAPTER 5. CONCLUSIONS AND RECOMMENDATIONS

The main purpose of this project was to address the need for a feasibility assessment of FRP composite-bearing piles for highway and related facilities substructures, replacing traditional materials such as timber, concrete, or steel, specifically in the construction of waterfront structures in hostile marine environments. The engineering use of FRP composite-bearing piles raised the need to investigate their field performance and to develop and evaluate reliable testing procedures and design methods to assess:

- Mechanical short-term behavior of FRP composite materials under axial compression loads.
- Behavior of FRP composite piles under vertical loads.
- Evaluation of FRP composite piling capacity, drivability, and constructability.

This project report summarizes the results of the full-scale experiment conducted at Port Elizabeth, NJ, and the companion laboratory tests. The main conclusions are summarized below.

MECHANICAL SHORT-TERM BEHAVIOR OF FRP COMPOSITE MATERIALS UNDER AXIAL COMPRESSION LOADS

Chapter 2 presented an engineering analysis approach for establishing the equivalent mechanical properties of the composite material, including elastic modulus for the initial loading quasilinear phase, axial compression strength, inertia moment, and critical buckling load. The conclusions of this chapter were as follows:

- The laboratory axial compression tests conducted in this study on the SEAPILE composite sample and its component materials (the fiberglass bars and the recycled plastic), illustrated that the recycled plastic has a significant effect on the composite material stability regarding buckling. However, due to its low stiffness and compressive strength compared with the reinforcing fiberglass bars, the recycled plastic does not appear to effectively prevent the peripheral disintegration of the fiberglass bars and, therefore, has a limited contribution to the axial compression strength of the composite material. No delamination between the rebar and the plastic was observed during the axial compression loading.
- The experimental results obtained for the SEAPILE composite materials illustrated that the nonlinear response of the recycled plastic to the axial loading is strain-rate dependent. However, because the quasilinear response of the fiberglass bars to the axial loading does not seem to be strain-rate dependent, the strain-rate effect on the mechanical behavior of the SEAPILE composite is expected to be relatively small.
- A composite material model has been developed for establishing the equivalent mechanical properties of the SEAPILE composite material, including elastic modulus for the initial quasilinear loading phase, axial compression strength, moment of inertia, and critical buckling load. The equivalent material properties of the composite are related to the mechanical properties of the component materials, assuming strain compatibility

between the plastic and the fiber reinforcement bars during the axial compression loading.

- As illustrated in table 1, which summarizes the comparison between the predicted and experimental values of the SEAPILE composite material properties, the proposed model appears to predict the experimental results of the axial loading tests on the composite material sample fairly well. Further, this model seems to provide an effective framework for analyzing the effect of the recycled plastic on the mechanical behavior of the FRP composite.
- Further research is required to better understand the failure mechanisms involved in the SEAPILE composite material. Both laboratory and full-scale loading tests are required to provide a relevant database to evaluate and develop reliable design methods for the engineering applications of composite construction materials in load-bearing piles that are used for waterfront and highway structures.
- A compression axial test was performed on a 38.7-cm- (15.25-inch-) diameter, 80-cm- (31.5-inch-) long PPI pile sample containing 16 steel reinforcing rods of 2.54-cm (1.0-inch) nominal diameter to establish the composite material properties. The test results on the PPI sample showed that this material has a behavior similar to that of steel.
- Axial compression tests were performed on the Trimax pile recycled plastic at several strain rates. The dimensions of the sample were 25.4 cm (10 inches) in diameter and 50.8 cm (20 inches) long. The test results showed that the nonlinear response of the Trimax material to the axial loading is strain-rate dependent. The Young's modulus of this material obtained for the linear portion of the stress-strain curve at the strain rate of 1.7 mm (0.07 inch) per min (0.33 percent/min) is 370,000 kPa (53.7 ksi). Poisson's ratio calculated for this strain rate at 1000 kPa (0.145 ksi) is equal to 0.35, and the corresponding shear modulus value for the linear portion of the stress-strain curve is 1.37×10^5 kPa (19.9 ksi).

BEHAVIOR OF FRP COMPOSITE PILES UNDER VERTICAL LOADS

The testing program included four SLTs on instrumented piles, which were driven in the selected site at Port Elizabeth, NJ. In chapter 3, the experimental results were compared with the methods commonly used for evaluating the ultimate capacity, end bearing capacity, and shaft frictional resistance along the piles. This engineering analysis led to the following conclusions:

- The full-scale experiment confirmed that the FRP composite piles can be used effectively as load-bearing piles and represent an alternative for deep foundation construction, especially in waterfront environments and aggressive soils.
- Distinct plunging failure occurred during the SLTs on PPI and SEAPILE piles as the applied loads reached 115 and 90 t (253 and 198 kips) and the measured pile top settlements were 1.64 cm (0.65 inch) and 1.16 cm (0.46 inch), respectively.
- The Lancaster Composite, Inc., pile did not experience a distinct plunging failure, and the maximum load applied on the pile reached 128 t (282 kips) with a measured settlement of 1.73 cm (0.68 inch).
- The maximum load applied on the American Ecoboard pile, which was driven to the sandy layer, was 60 t (132 kips). At this load, the pile top settlement was 9.34 cm (3.7 inches), and no distinct plunging failure was observed. The pile top settlements of

this pile, which contained only recycled plastic with no reinforcement bars, were significantly greater than the settlements measured during the tests on the other FRP piles.

- Several methods commonly used for evaluating the ultimate capacity were compared with the SLT results. In general, the loads calculated for FRP piles using the Chin-Kondner method are greater than the maximum loads that were applied at the field test. The DeBeer yield load method yields conservative loads compared to the maximum loads applied at the SLTs. The Davisson offset limit load method, using an equivalent elastic modulus that is experimentally derived from the quasilinear load-settlement relationship of the unloading-reloading cycle, yields limit loads that are within the range of loads obtained with the above-mentioned methods and settlement estimates that are consistent with the field test results.
- The experimental results are compared with several codes[5-7] and analytical methods[4,39-40] commonly used for evaluating the shaft friction and end bearing capacity of the piles. The maximum end bearing capacities measured at the Port Elizabeth site were relatively small in comparison to the applied loads, indicating that the piles were frictional piles. The American Petroleum Institute (API) method yields end bearing capacities that are significantly lower than the FHWA and Meyerhof methods, and are in fairly good agreement with the end bearing capacity measured in the field tests.
- Several methods commonly used for evaluating the shaft friction along the piles were compared with the experimental results. Burland and Meyerhof's methods and the AASHTO code yield shaft friction values that are in good agreement with the average shaft friction measured on the PPI and SEAPILE piles in the upper soil (fill and sand) layer. The FHWA method yields the best correlation for the shaft friction values obtained in the lower silt and clayey soil layer.
- The engineering use of FRP piles on a widespread basis requires developing and evaluating design methods through extensive comparison of predictions with reliable data measured during full-scale loading tests. For this purpose, the FRP piles were instrumented by strain gauges that were specifically designed for strain measurements in these piles. This instrumentation allowed measuring the shaft friction distribution along the piles and the end bearing capacities in the saturated soils of the selected site during the SLTs on the FRP piles.
- This full-scale experiment demonstrated the feasibility of effectively using FRP piles as vertical load piles. However, because soil-pile interaction depends largely on prevailing soil profile and site conditions, further full-scale testing in different soil profiles is required to establish a reliable database for developing and evaluating codes and methods of analysis for designing FRP piles.

EVALUATION OF FRP COMPOSITE PILING CAPACITY, DRIVABILITY, AND CONSTRUCTABILITY

In chapter 4, the authors described the full-scale experiment, the dynamic pile testing results, and the engineering analysis of the SLTs on the FRP piles. The main objectives of this demonstration project were to:

- Assess the drivability and durability of FRP piles during installation using PDA.

- Evaluate the currently available dynamic testing methods for establishing the dynamic properties of FRP piles and the dynamic soil-pile interface parameters during driving.
- Evaluate the dynamic methods currently used in predicting the load-set response and ultimate static capacity of FRP piles and, more specifically, the correlations between CAPWAP analysis and SLT results.
- Develop appropriate design criteria for the allowable dynamic stresses in the composite pile material and its basic components during pile driving.
- Obtain dynamic data records of the FRP pile driving that, in the absence of design criteria and field data for these piles, can be used to establish allowable tension and compression stresses for performing dynamic analyses and evaluating drivability and integrity during driving.

The engineering analysis of the dynamic pile testing results and the SLTs led to several conclusions.

Drivability and Integrity During Driving

- PDA during pile driving and restriking of the PPI and SEAPILE piles showed no damage or separation between the bars and the recycled plastic material, except at the upper foot of each PPI pile. Similarly, in the case of the Lancaster Composite, Inc., piles, no damage or separation between the concrete and the FRP shell piles was observed.
- The PDA and CAPWAP analysis results showed that all the piles experienced a long-term increase in pile capacity from the EOI to the BOR. For most of the tested piles, the measured setup factor, defined as a ratio between the BOR and EOI capacities, was in excess of 2.0. The dissipation of excess pore water pressure generated during pile driving resulted in a significant increase, up to about 100 percent, of the shaft and toe Smith damping.

Evaluation of Dynamic Testing Methods

- The dynamic testing procedures commonly used for steel and concrete piles (i.e., PIT, PDA testing—high-strain, and PDA testing—early portion of the high-strain records) were conducted to evaluate the dynamic properties of the composite piles. The parametric study conducted with CAPWAP and GRLWEAP showed that the elastic modulus obtained from PDA testing—early portion of the high-strain records yields the best correlations between (1) the calculated values of the transfer energy level and the energy measured by PDA, and (2) the calculated blow count and the measured field records.

CAPWAP Analysis

- Comparison between the GRL recommendations and the dynamic soil properties obtained from the CAPWAP analysis leads to the following results:
    - The soil shaft quake values recommended by GRL appear to be consistent with the CAPWAP results obtained for all the piles tested with the exception of the PPI piles.

- The soil toe quake values obtained for the FRP test piles are significantly lower (about 45 percent) than the values recommended by GRL.
- The toe damping values obtained for the FRP test piles are consistently greater (about 250 percent) than the values recommended by GRLl.
- The shaft Smith damping values recommended by GRL appear to be consistent with the CAPWAP results obtained for all the piles tested.

- For all SLT piles, CAPWAP capacities ranged from 938.6 to 1,267.7 kN (211 to 285 kips) during the BOR. In general, CAPWAP analysis showed most of the ultimate capacity came from shaft resistance when the piles were driven to penetrations of 17.7 m (58 ft).

Correlations Between CAPWAP Analysis and Static Load Tests

- The CAPWAP analysis yielded load-set curves and ultimate capacities, which correspond fairly well to the SLT results.
- For the SEAPILE and PPI piles, the CAPWAP analysis seemed to indicate that the settlement at failure was close to elastic compression settlement during loading.
- For the low stiffness American Ecoboard pile that was driven to the sandy layer, the settlement, reaching 96 mm (3.7 inches) under a 60-t (132-kips) load, appeared to be due mainly to the elastic compression. The CAPWAP analysis was limited to the settlement range of about 20 mm (0.78 inch). For this range, it seemed to be quite consistent with SLT results.

Design Criteria and Allowable Stresses

- Design criteria for allowable compression and tension stresses in the FRP piles were developed considering the equation of the axial force equilibrium for the composite material and assuming no delamination between its basic components.
- During pile driving, with the exception of the PPI piles, the measured compression and tension stresses did not exceed the allowable stresses. In the absence of design criteria and field data for FRP plies, the maximum stresses obtained for these piles in the site observations can be used to establish allowable tension and compression stresses for pile driving.

R&D NEEDS ASSESSMENT

The dynamic and static loading tests on instrumented FRP piles conducted in this project demonstrated that these piles can be used as an alternative engineering solution for deep foundations. However, their widespread use will require further site testing and full-scale experiments to establish a relevant performance database to develop and evaluate reliable testing procedures and design methods.

The time-dependent stress-deformation behavior of composite recycled plastic materials is of concern, because the FRP piles may undergo an excessive deformation due to an applied sustained loading. The engineering use of FRP piles on a widespread basis requires developing

and evaluating reliable testing procedures and design methods to determine the long-term behavior of these composite piles.

Further, research is now required to evaluate the effect of environmental conditions (i.e., soil confinement, groundwater, etc.) on the long-term behavior of recycled plastic composite materials as well as the combined effects of chemical and mechanical degradation processes. Both laboratory and full-scale loading tests are required to provide a relevant database to develop and evaluate the assessment of the long-term performance of composite, time-dependent FRP piles and to determine the limit creep load for their engineering use in waterfront and highway structures.

REFERENCES

1. Likins, G., Rausche, F., Thendean, G., and Svinkin, M., 1996, "CAPWAP Correlation Studies," STRESSWAY '96 Conference, Orlando, FL, pp. 11-13.

2. Rausche, F., Goble, G., and Likins, G., 1992, "Investigation of Dynamic Soil Resistance on Piles Using GRLWEAP," *Proceedings of the Fourth International Conference on the Application of Stress-Wave Theory to Piles*, The Netherlands, pp. 137-142.

3. Craig R.F., 1987, *Soil Mechanics*, Van Nostrand Reinhold Co. Ltd., Molly Millars Lane, Wokingham, Berkshire, England.

4. Meyerhof G.G., 1976, "Bearing Capacity and Settlement of Pile Foundations," *Journal of the Geotechnical Engineering Division*, American Society of Civil Engineers (ASCE), pp. 195-228

5. Federal Highway Administration, 1998, *Design and Construction of Driven Pile Foundations*, Publication No. FHWA-HI-97-013, Washington, DC, revised November 1998.

6. American Petroleum Institute, 1984, *Recommended Practice for Planning, Designing, and Constructing Fixed Offshore Platforms*, API RP2A, 14th edition, Dallas, TX .

7. American Association of State Highway and Transportation Officials, 1997, *Standard Specifications for Highway Bridges*, Washington, DC.

8. Likins, G., Rausche, F., and Hussein, M., 1990, "Introduction to the Dynamics of Pile Testing," *Geotechnical News*, Vol. 8, No. 4, pp. 21-24.

9. Iskander, M. and Stachula, A., 1999, "FRP Composite Polymer Piling: An Alternative to Timber Piling for Waterfront Applications," *Geotechnical News*, Vol. 17, No. 4, pp. 27-31.

10. Stokes, F., 1996, *Axial Compression Tests on Lancaster Composite Piles* (test report), Fritz Engineering Laboratory at Lehigh University, Lehigh, PA.

11. Iskander M., and Hassan, M., 1998, "State of the Practice Review: FRP Composite Piling," *Journal of Composites for Construction*, ASCE, August, Vol. 2, No. 3, pp. 116-120.

12. Horeczko, G., 1995, "Marine Application of Recycled Plastics," *Proceedings, XIII Structural Congress, Restructuring America and Beyond*, Ed. M. Sanayei, ASCE, Reston, VA, Vol. 1, pp. 834–837.

13. Busel, J., 1995, *FRP Composites in Construction Applications, A Profile in Progress*, SPI Composites Institute, New York, NY.

14. Lancaster Composite, Inc., 2003, Engineers and Manufacturers of Composite Piles, http://www.lancastercomposite.com.

15. Lampo, R., 1995, "Recycled Plastics as an Engineering Material," *Proceedings, XIII Structural Congress, Restructuring America and Beyond*, Ed. M. Sanayei, ASCE, Reston, VA, Vol. 1, pp. 815-818.

16. Lampo, R., Nosker, T., Barno, D., Busel, J., Maher, A., Dutta, P., and Odello, R., 1998, *Development and Demonstration of FRP Composite Fender, Loading-Bearing and Sheet Piling Systems*, U.S. Army Corps of Engineers, Construction Engineering Research Laboratories, Champaign, IL.

17. Bognacki, C. and Gill, R., 1997, *1995-1997 Marine Borer Report*, Materials Engineering Division, Engineering Department, Port Authority of New York and New Jersey.

18. American Water Works Association (AWWA), 2001, *Rehabilitation of Water Mains*, Manual 28, Denver, CO.

19. Zlokovitz, R. and Juran, I., 2001, *Trenchless Technologies for the Reconstruction of New York City's Water Mains* (project report), New York City Department of Design and Construction, New York, NY.

20. Christopher, B., Gill, S., Giroud, J.P., Schlosser, F., Juran, I., Mitchell, J.K., and Dunncliff, J., 1989, *Design and Construction Guidelines for Reinforced Soil Structures*, Federal Highway Administration, Publication No. FHWA-RD-89-063, Washington, DC.

21. American Society for Testing and Materials (ASTM), 1996, "Test Method for Static Coefficient of Friction of Shoe Sole and Heel Materials as Measured by the James Machine," F489-96, ASTM International, West Conshohocken, PA.

22. Seaward International, Inc., 2000, *SEAPILE^{TM} Composite Marine Piling Technical Manual*, Seaward International, Inc., Clearbrook, VA.

23. Bazant, Z.P., and Cedolin, L., 1991, *Stability of Structures—Elastic, Inelastic, Fracture and Damage Theories*, Oxford University Press, New York, NY.

24. Plastic Piles, Inc. (PPI), 2001, *Technical Manual and Product Information*, Plastic Piles, Inc., Rialto, CA.

25. U.S. Plastic Lumber (USPL), 2001, *Trimax Structural Plastic Lumber—Product Information and Test Report*, USPL, Ltd, Auburn, MA.

26. Davisson, M.T., 1972, "High Capacity Piles," *Proceedings of Lecture Series on Innovations in Foundation Construction*, ASCE, Illinois Section, Chicago, IL, March 22, pp. 81-112.

27. DeBeer, E.E., 1968, "Proefondervindlijke Bijdrage Tot de Studie Van Het Grensdraag Vermogen Van Zand onder Funderingen Op Staal," *Tijdshift der Openbar Verken van Belgie*, No. 6, 1967, and Nos. 4-6, 1968.

28. Chin, F.K., 1970, "Estimation of the Ultimate Load of Piles Not Carried to Failure," *Proceedings of the Second Southeast Asian Conference on Soil Engineering*, Singapore, pp. 81-90.

29. Kondner, R.L., 1963, "Hyperbolic Stress-Strain Response: Cohesive Soils," ASCE, *Journal for Soil Mechanics and Foundation Engineering*, Vol. 89, SM-1, pp. 115-143.

30. Fellenius, B.H., 1975, "Test Loading of Piles: Methods, Interpretation, and New Proof Testing Procedure," *Journal of the Geotechnical Engineering Division*, ASCE, Vol. 101, GT9, pp. 855-869.

31. Fellenius, B.H., 1980, "The Analysis of Results from Routine Pile Loading Tests," *Ground Engineering*, Vol. 13, No. 6, London, UK, pp. 19-31.

32. Deep Foundation Institute, 1995, *Guidelines for the Interpretation and Analysis of the Static Loading Test*, Continuing Education Committee, first edition, Ottawa, Ontario, Canada, pp. 10-41.

33. ASTM, 1994, *Standard Test Method for Piles Under Static Axial Compression Load*, D1143-81 (Reapproved 1994), ASTM International, West Conshohocken, PA.

34. Poulos, M.G., Carter, J.P., and Small, J.C., 2001, "Foundation and Retaining Structures—Research and Practice, Theme Lecture" *Proceedings of the 15th International Conference on Soil Mechanics and Geotechnical Engineering*, Istanbul, Turkey, pp. 2527-2606.

35. De Cock, F., 1998, "Design of Axially Loaded Bored Piles—European Codes, Practice and Experience," *Deep Foundations on Bored and Auger Piles*, van Impe and Haegeman (eds.), A.A. Balkema, Rotterdam, The Netherlands, pp. 63-74.

36. Semple, R.M., and Rigden, W.J., 1984, "Shaft Capacity of Driven Piles in Clay," *Analysis and Design of Pile Foundations*, ASCE, Washington, DC, pp. 59-79.

37. Fleming, W.G.K., Weltman, A.J., Randolph, M.F., and Elson, W.K., 1985, *Piling Engineering*, Surrey University Press/Halsted Press, New York, NY.

38. Burland, J.B., 1973, "Shaft Friction on Piles in Clay—A Simple Fundamental Approach," *Ground Engeering*, Vol. 6, No. 3, pp. 30-42.

39. Go, V., and Olsen, R.E., 1993, "Axial Load Capacity of Untapered Piles in Sand," *Proceedings of the 11th Southeast Asian Geotechnical Conference*, Singapore, pp. 517-521.

40. Stas, C.V., and Kulhawy, F.H., 1984, *Critical Evaluation of Design Methods for Foundations Under Axial Uplift and Compression Loading*, Report EL-3771, Electric Power Research Institute, Palo Alto, CA.

41. Meyerhof, G.G., 1956, "Penetration Tests and Bearing Capacity of Cohesionless Soils," *Journal of the Soil Mechanics and Foundation Division*, ASCE, Vol. 82, SM-1, pp. 1-19.

42. Poulos, H.G., 1989, "Pile Behaviour—Theory and Application," *Géotechnique*, Vol. 39, No. 3, pp. 365-415.

43. Decourt, L., 1995, *Prediction of Load-Settlement Relationships for Foundations on the Basis of the SPT-T*, Leonardo Zeevaert Conference, National Autonomous University of Mexico, Mexico, pp. 85-104.

44. Rollins, K.M., Clayton, R.J., and Mikesell, R.C., 1997, "Ultimate Side Friction of Drilled Shafts in Gravels," *Proceedings of the 14th International Conference on Soil Mechanics and Foundations*, Hamburg, Germany, Vol. 2, pp. 1021-1024.

45. Goble, Rausche, Likins, and Associates, Inc., 2001, *An Introduction into Dynamic Pile Testing Methods*, Cleveland, OH.

46. Pile Dynamics, Inc., 2000, Case Pile Wave Analysis Program (CAPWAP), Version 2000-1, *CAPWAP for Windows® Manual*, Cleveland, OH.

47. Pile Dynamics, Inc., 1999, *Pile Driving Analyzer Windows Version (PDA-W) Manual*, Cleveland, OH.

48. ASTM, 2000, *Standard Test Method for Low-Strain Integrity Testing of Piles*, D5882-00, ASTM International, West Conshohocken, PA.

49. ASTM, 2000, *Standard Test Method for High-Strain Dynamic Testing of Piles*, D4945-00, ASTM International, West Conshohocken, PA.

BIBLIOGRAPHY

GRL Engineering, Inc., 2002, *Polymer Pile Driving Research Project Port Newark, New Jersey*, Cleveland, OH.

Hansen, J.B., 1963, "Discussion on Hyperbolic Stress-Strain Response, Cohesive Soils," *Journal for Soil Mechanics and Foundation Engineering*, ASCE, Vol. 89, SM-4, pp. 241–242.

HRDI-06/08-06(1M)E